SYNTHESIS AND EVALUATION OF NOVEL ANTHRACENE ACRYLAMIDES AND IMINES AS G-QUADRUPLEX LIGANDS FOR THE TREATMENT OF CANCER

THESIS

submitted for the degree of

DOCTOR OF PHILOSOPHY

in

Chemistry

at

Kingston University London

by

Tomris Coban

School of Life Sciences, Pharmacy and Chemistry,

Kingston University, Penrhyn Road,

Kingston-upon-Thames, Surrey, KT1 2EE.

November 2020

DECLARATION

This thesis entitled Synthesis and Evaluation of Novel Anthracene Bisacrylamides as G-quadruplex Ligands for The Treatment of Cancer is based upon work conducted by the author in the School of Life Sciences, Pharmacy and Chemistry at Kingston University London between **October 2016 and January 2020**. All of the work described herein is original unless otherwise acknowledged in the text or by references. None of the work has been submitted for another degree in this or any other universities.

_____

Tomris Coban

Acknowledgments

Firstly, I would like to thank my parents for supporting me emotionally and financially during my time away from home throughout the last 5 years. I am truly grateful for their constant and unfaltering love during the highs and lows of my PhD. I couldn't imagine achieving the things I have achieved without their touch on my life from subtle messages when I am down to daily calls to keep me motivated.

My main guidance has been from my exceptional supervisor and mentor Dr. Adam Le Gresley who took a shot on me and put his trust that I could achieve in his research group. I am so thankful for his continued confidence in me and my work. He has also become like a second father figure for me through being in my corner during hard times and doing more than I could have wished for from a supervisor be it academically or personally. I must also acknowledge my second supervisor Dr. Sianne Schwikkard who taught me new things and instilled me with the confidence to excel and develop myself. Her constant positive demeanour allowed me to speak with her informally and gave confidence when questioning the routes of my PhD which allowed for critical decisions to be made. Her fast feedback and advice during the writing of my thesis is deeply appreciated considering the time required.

My sister Munevver Serdarogullari, who is always there for me through thick and thin whenever I need her. She is my other half and special person in my life who is the greatest gift in my life. Having a best friend from birth has always made me feel special and made my life easier in the dark times. Thank you, sister.

Another main and special person who I would like to thank is, Cameron Robertson. Who has been such an amazing and caring partner. I wouldn't be able to finish up this PhD thesis without his encouragement, even though many times I wanted to give up. His trust, love and presence by my side is the best gift he could give me. He has been my rock and home away from home.

A final small thank you to Miles Benardout for feedback and advice on multimedia elements of my thesis, friendship and good heartedness.

All that remains is to thank Kingston University for providing equipment, admin and training support during my Master's and PhD.

Abstract

G-quadruplex ligands, which can intercalate the G-quadruplex structures, have been studied as a strategy for indirect inhibition of telomerase activity, alongside targeting other G-quadruplexes found in other genes, including oncogenes. The scope of G-quadruplex ligands as cancer targeting drugs is particularly high as there more than 350000 DNA sequences within the human genome that can be targeted. In light of this, several small molecules have been introduced, which can induce and stabilise G-quadruplexes, which are classified as new drug agents for cancer therapy. This thesis looks at the synthesis of suitably functionalised polyaromatic compounds to achieve this stabilisation. Deoxyribonucleic acid (DNA) in our cells contains the instructions for all aspects of life, from cell division to immune responses. The discoveries and structural determination of DNA, leading to the human genome project, provides a great resource for genetic understanding. The pairing of nuclear bases is typically represented as Watson-Crick. When DNA is chemically changed, disruption to cell processes occurs. Cancer is one outcome of this damage, where DNA is damaged to a point where cell cycle control is incapacitated. One key aspect of cancer is that cells lose the ability to undergo apoptosis. Telomeres are integral structures present in the DNA of eukaryotic cells. They consist of regions of DNA motifs that are repeated throughout the structure. These conserved motifs contain an abundance of Guanine in sequences of 3-4 repeat units. These Guanine units make up the Guanine tetrad structures that allow the telomere to function as genomic stabiliser and protective agent against DNA damage or cross chromosome fusion such that all telomeres have a single stranded Guanine motif overhang at the 3' end of the chromosome. Telomere length will usually dictate the lifespan of a cell, however in cancer cells we see this mechanism for programmed cell death, hijacked by the expression of telomerase, which extends telomere length and inhibits programmed cell death. The well-established principle behind the development of G quadruplex ligands is that inhibition of telomerase, which isn't expressed in healthy cells, can selectively facilitate apoptosis of cancerous cells. G-quadruplexes are structures that have shown the potential as therapeutic targets through

their propensity to associate with themselves and structures that are similar which will intercalate. Because of this, small molecules that intercalate within the structure and stabilise them within DNA have targeted G-quadruplexes. This stabilised DNA G-quadruplex structure will then inhibit the division of the cell through prevention of unwrapping and recognition of regulation regions and telomeric regions, which are normally cleaved off .

In this research we aimed to make a number of G-quadruplex ligands to specifically target this inhibition and show activity against the HeLa cancer cell line. Throughout the research we synthesised several G-quadruplex ligands with different synthetic methodologies. Our success with these ligands was mainly achieved with imine couplings and these compounds showed cytotoxicity to HeLa cells. Compounds that showed cytotoxicity were further analysed for drug G-quadruplex interaction by 1D, 1H NMR titration experiments. Five of the compounds that showed cytotoxic effect demonstrated drug G-quadruplex interactions.

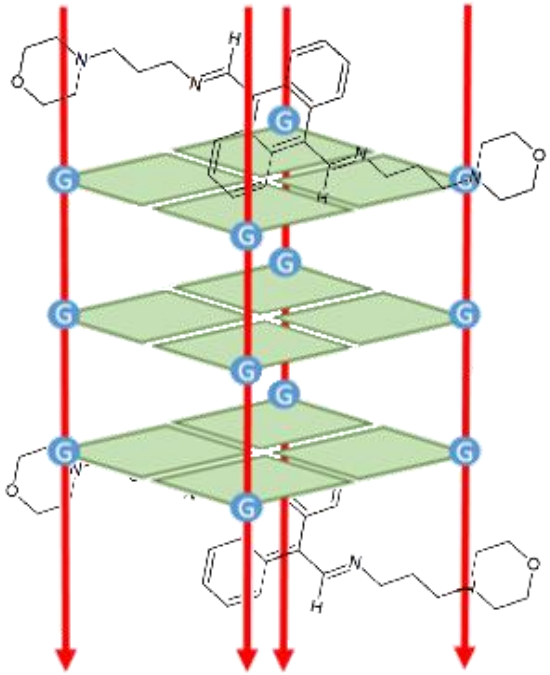

Abbreviations

°C	degree Celsius
δ	chemical shift in parts per million
ΔH	enthalpy change
ΔG_0	Gibbs free energy change
A549	adenocarcinomic human alveolar basal epithelial cells
ALT	alternative lengthening of telomeres
BCL-2	B-cell lymphoma 2
BMH-21	RNA polymerase I inhibitor
BMSG-SH-3	12 tetra-substituted naphthalene diimide
bp	base pairs
br	broad
BRACO-19	3, 6, 9-tri-substituted acridine; 9-[4-(N, N-dimethylamino) phenylamino]-3, 6-bis (3-pyrrolodinopropionamido) acridine
CD	circular dichroism
c-Kit	receptor tyrosine kinase protein
d	doublet
DCM	dichloromethane
dd	doublet of doublets
DIBAL	diisobutylaluminium hydride
DIPEA	N,N-diisopropylethylamine
DMEM	Dulbecco Modified Eagle's Medium
DMF	dimethyl formamide
DMS	dimethyl sulfate
DMSO	dimethyl sulfoxide
DPPP	1,3-Bis(diphenylphosphino)propane
ds	double-stranded
EDCI	1-(3-dimethylaminopropyl)-3-ethylcarbodiimide hydrochloride
eq	equivalent
Et_3N	triethylamine
EtOAc	ethyl acetate
G	guanine
G4P	G4 formation potentials
G4(s)	G-quadruplex(es)
G-G	guanine-guanine
G-overhang	guanine-rich overhang

G-tetrad	guanine-tetrad
G-tract	guanine-tract
G-C	guanine- cysteine
GISTs	gastrointestinal stromal tumours
HATU	1-[Bis(dimethylamino)methylene]-1H-1,2,3-triazolo[4,5-b]pyridinium-3-oxide hexafluorophospate
HIF1α	hypoxia-inducible factor 1
HIV	human immunodeficiency virus
HR MS	high resolution mass spectrometry
HSV-1	herpes simplex virus-1
IC_{50}	half maximal inhibitory concentration
IR	infra-red
m	multiplet
Me	methyl
MeOH	methanol
MMQ3	quinacridine
mRNA	messenger RNA
MYC	c-MYC, V-myc myelocytomatosis viral oncogene homolog
m/z	mass to charge ratio
NDI	naphthalene diimide
NMR	nuclear magnetic resonance
NOESY	nuclear overhauser effect spectroscopy
PDGF-A	platelet-derived growth factor subunit A
Phen-DC3	trifluoromethanesulfonate
PIPER	N,N'-bis[2-(1-piperidino)- ethyl]-3,4,9,10-perylenetetracarboxylic diimide
POT1	protection of Telomeres 1
ppm	parts per million
q	quartet
QSAR	quantitative structure-activity relationship
R_f	retention factor
RHPS4	pentacyclic acridine
RNA	ribonucleic acid
rt	room temperature
SD	standard deviation
SEM	standard error of mean
ss	single-stranded
TRAP	telomeric repeat amplification assay

TERT	telomerase reverse transcriptase
THF	tetrahydrofuran
TLC	thin layer chromatography
Tm	melting temperature
TMPyP4	5,10,15,20-tetrakis-(N-methyl-4-pyridyl)porphine
TRF2	telomeric repeat-binding factor 2
UV-Vis	ultraviolet-visible
UXF1138L	uterus carcinoma cell line
VEGF	vascular endothelial growth factor

Table of Contents

List of Figures

List of Tables

Chapter 1 – Introduction

Normal development and growth of organisms is dependent on appropriate and regulated cell division. The term homeostasis is used where in normal cells this describes the regulation between cell growth, division and the rate at which cells enter apoptosis or stay in senescence. In cancer cells, the regulatory elements which dictate this homeostasis is hijacked and leads primarily to cells growing and dividing out of control with a loss of ability to enter apoptosis (1). The definition of when cells becomes cancerous is when the rules of cell division are not followed by the affected cell, which also leads to the increased chances of further genetic mutation and further loss of regulation. This loss of regulation makes the cells that are affected grow and push out on tissues around them with no restriction in cell growth elicited by messages from exterior tissues (1).

Healthy cells have several mechanisms that try to prevent damage or mutation in gene coding sequences present in the DNA. Most of these are built into the genome itself such as the presence of introns, which act as non-encoding DNA. Therefore, when a mutation does occur, this makes no difference (silent mutation). Alongside this, the way DNA is transcribed and translated means that when a mutation occurs in the coding region (exon), then a missense or nonsense mutation will occur. Either this is where an amino acid will be changed, or a stop message will be received respectively. However, one of the most important properties of the genome, which mitigates damage to DNA, is the presence of genomic structures on the end of chromosomes called telomeres. In healthy cells, the telomeres act as life span determinants for the cell as with each replication 50-200 base pairs are removed from the telomeric region (2). As the telomeres get shorter, the cell will eventually enter apoptosis when the non-telomeric DNA starts to shorten during cell replication. We see that the regulation of cell growth and life span of the cell maintained by the length of the telomeric region within the healthy cells with an absence of co-regulators or maintenance enzymes. The point where the cells stop dividing and enter a senescent state is call the Hayflick limit with apoptosis shortly afterwards (3).

The shortening of telomeres and the DNA is seen in most healthy cells but there are exceptions in stem cells and germline cells. This characteristic is in cancer cells, as telomeres do not shorten with continued and unregulated cell division and is a senescence state (4). In cancer cells the key component that maintains the length of telomeres during cell division is an enzyme called telomerase and its activity is also used as a biomarker for cancer diagnosis (5) (6). Telomeres have G-quadruplex structures present within them and are in transcription regulation genes, specifically seen in genes that when overly expressed are markers of cancer, if these structures are stabilised or blocked then over expression can be inhibited.

1.1 Discovery of G-quadruplex structures

G-quadruplexes (G4) became biologically relevant in the 1980s mostly based on the seminal work undertaken by Dr. Elizabeth Blackburn which showed telomeric DNA forms non-Watson-Crick guanine-guanine base-paired intramolecular DNA structures. This discovery led to increased research interest and initiated interest in the field of G-quadruplex research. Previously, the idea of G-quadruplexes was suggested by Bang in 1910 through work with guanylic acid (7), however the structure was only evidenced in the 1950s and 1960s where the G-quadruplex structure was observed through X-ray diffraction and optical properties. Since these discoveries the formation of G-quadruplexes *in vitro*, *in cellulo* and *in vivo* has been successfully performed. This allows for the identification of possible sequences in the human genome that could form G-quadruplexes.

1.1.1 G-quadruplex formation

G-quadruplexes are nucleic acid, secondary structures that consist of three or four (tetramolecular) single strands. These four- stranded structures differ from the typical duplex model of DNA. G-quadruplex DNA structures comprise of stacked G-tetrads, square-planar phases of four guanines, associated by cyclic Hoogesteen hydrogen bonding (termed G-quartets or G-tetrads), as an alternative to the Watson-Crick hydrogen binding in a B-DNA duplex. The guanine bonds within a G-tetrad possess either a *syn* or *anti*

glycosidic conformation. These conformations are adopted in a G-strand-directional way, with the tetrad guanines attaching through parallel G-strands, therefore embracing the same glycosidic compliance; those from antiparallel G-strands obtain the inverse. These G-quadruplexes can be modified with one, two (8), or four-G-rich strands and are shown in Figure 1. Despite the unusual discovery of guanine-rich DNA solutions forming gelatinous aggregates in 1910 (9), it wasn't until 1962 that their composition was determined after Gellert *et al.* using crystallographic methods, suggested that these gel aggregates were formed from planar guanine tetramers, resulting in stacks of cyclic (tetrametric) arrangements (9).

The configuration of these tetramolecular structures and their stabilities are associated with monovalent cations, especially with K^+ and Na^+ that form bonds with the eight electronegative oxygen molecules (Figure 1) of the adjoining stacked G-quartets (10) (11). Since K^+ and Na^+ are the primary cations *in-vivo*, G-quadruplex generation is preferred under physiological conditions. A Guanine-rich DNA sequence may embrace distinctive structures within the occurrence of various cations. The K^+ ion conformation is thought to be more biologically and naturally applicable, due to its higher intracellular absorption (~140 mM) in comparison with the Na^+ ion (5–15 mM). The actual position of cations between G-tetrads depends on the properties of these ions: Na^+ particles are detected in a wide variety of geometries, K^+ particles are constantly equidistant within every tetramolecular pattern. Generally, K^+ ions are favoured over Na^+ as K^+ has a superior coordination with eight guanine oxygen as well as considerably decreased dehydration energy (11). The subsequent discovery of guanine-rich sequences, builds an understanding of the fundamental, underlying repetitive motif of telomeric DNA observed at the end point of all eukaryotic chromosomes (12)(13).

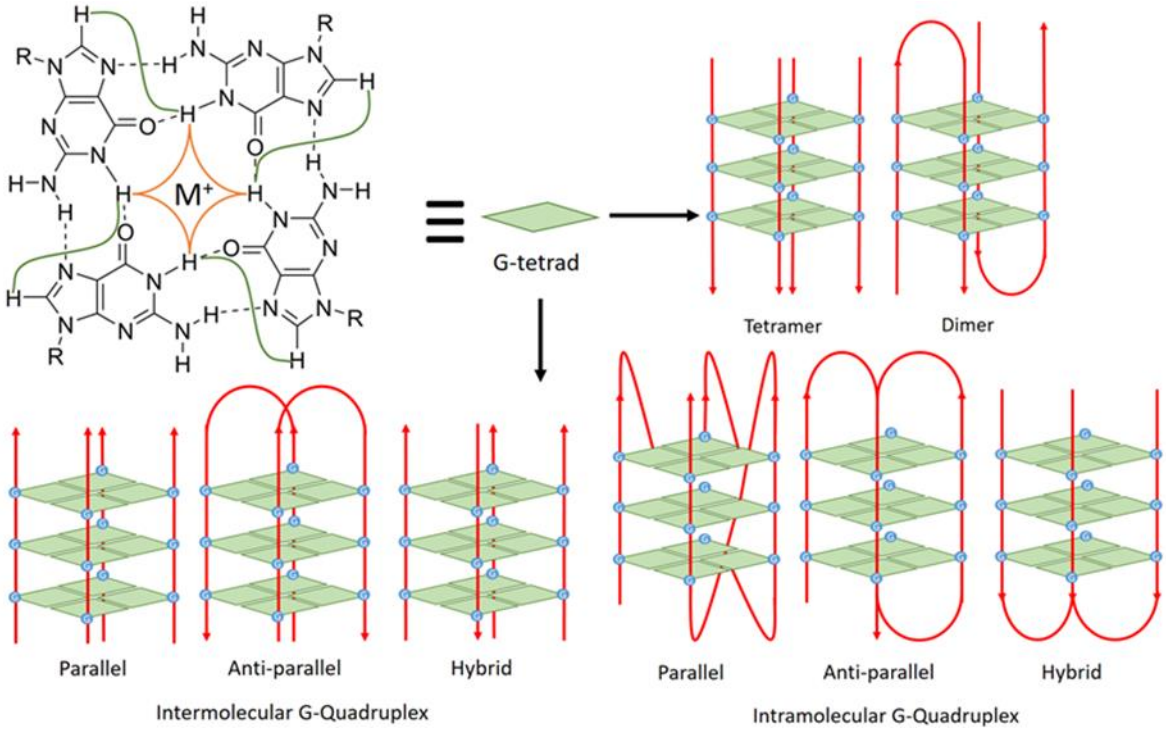

Figure 1 Illustration of G-quadruplex structures from simple square-planar arrangement of four guanines connected by Hoogsteen hydrogen bonding shown by dotted lines followed by the tetrameric and dimeric G-quadruplex structures. The blue dots in the intermolecular G-quadruplex structures and intramolecular G-quadruplex structures represent cations (K+ or Na+). That stabilize G-quadruplexes by coordinating with the electronegative carbonyl oxygen atoms of adjacent G-tetrads. Reproduced from Yang, D., & Okamoto, K. (2010). Structural insights into G-quadruplexes: towards new anticancer drugs. Future medicinal chemistry, 2(4), 619-646.(14).

G-quadruplexes can embrace a diverse variety of structures and topologies, when compared to duplex nucleic acids that exhibit relative uniformity. Various G-quadruplexes have been observed and confirmed by biophysical techniques, particularly by CD (Circular Dichroism Fluorescent assays) and IR spectroscopy (Infrared spectroscopy).

Every G-quadruplex shares a common key element that consists of stacked G-quartets within the core of their structures; this includes interior core ion channels as well as four grooves that can occupy varying dimensions (Figure 1). The diversity within the varying dimensions occurs due to a number of different circumstances. These include:

(1) inconsistencies and variabilities of the loop length and the arrangement of sequences,

(2) sequence variances of the length of G-tracts where in most cases they are non-equivalent and,

(3) the influences and impacts of monovalent ions within the centre of the channel.

Little interest was given to G-quadruplexes up until the early 1990's. From the 1990's NMR (14) and X-ray crystallographic techniques (14) elucidated the nature of G-quartets leading to greater interest in the area of G-quadruplex research.

Considerable interest has been shown in intramolecular G-quadruplexes that are formed from single-stranded DNA. G-quadruplexes have been the subject of considerable investigation, in no small part due to their ability to form telomeres at the ends of DNA strands and within oncogene promoter sequences seen in Figure 1. In 1985, Blackburn *et al.* made researchers aware of both the presence and importance of telomeres and how they are associated with cancer (15). From that point onwards, numerous approaches have been developed and evaluated in order to achieve a clinical application. Researchers have attempted to reach clinical anti-cancer goals in terms of human telomere reverse transcriptase (hTERT) and G-quadruplex targeting ligands.

Telomerase enzymes preserve the length of telomeres, allowing cancer cells to become "immortal". Within promoter regions and 5'-untranslated regions, the formation of G-quadruplexes adjusts the translation of many oncogenes. In addition, the formation of G-quadruplexes encourages genomic instability (a distinctive characteristic enabling tumour development) during the cellular replication stage. Due to the effect G-quadruplexes being persistent in cancer cells, their structures are seen as important drug targets in anti-tumour therapeutics as seen in Figure 3 (16).

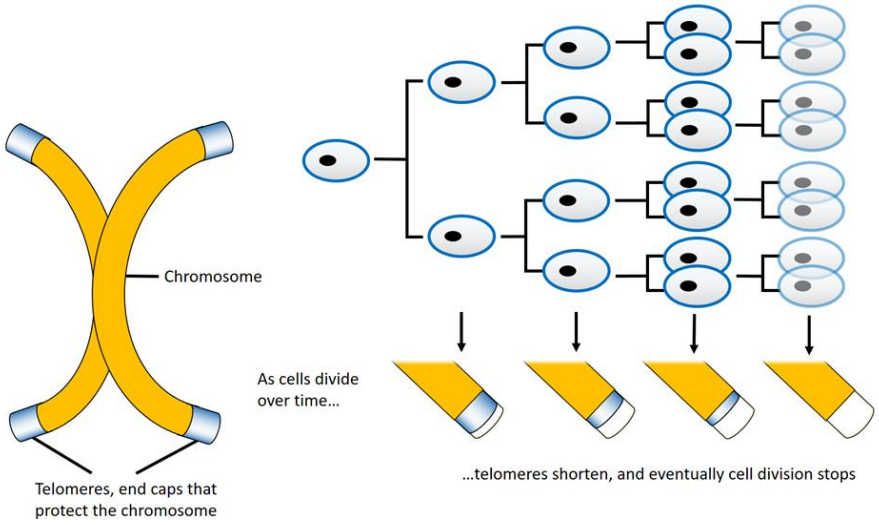

Figure 2 Telomeres shortening mechanism when cells go through normal mitosis.

1.1.2 G-Quadruplex Formation in the Human Telomere

G-quadruplex arrangements can be found at different positions along the chromosome, however, initially G-quadruplex forming nucleotide sequences (as part of the telomere) were thought to protect chromosomes from deterioration. Telomeres are repetitive regions located at the end of chromosomes; these are found in all organisms that exhibit linear chromosomes. During mitosis, DNA sequences lose 50-200 bases per replication and telomeres are thought to be sacrificial sequences, preventing the loss of base pairs occurring to the exons of chromosomes (17)(18).

1.1.3 Action of Telomerase

Telomerase enzymes are activated in a large portion of human cancer cells (80-85%) (19); playing an important role in controlling the malignant phenotype (where cells divide out of control and invade nearby tissues) by maintaining integrity and telomere length (8). Telomerase activity in human cancer cells can be inhibited by the G-rich sequences of telomeric human DNA. These sequences have a strong ability to form DNA G-quadruplex secondary structures. It is very likely that the formation of telomere ends involves intramolecular G-quadruplex molecules; however, their formation may also be associated with a process known as a T-loop invasion complex. T-loop configuration includes single

stranded telomere DNA interfering with the double stranded portion of the telomere causing a displacement of the G-quadruplex structures and their base pairs with the complimentary strand (20).

These secondary G-tetrad structures have shown to hinder telomerase enzyme activity, which makes these intramolecular telomeric structures an active target for cancer therapy as well as potential target of medical pathways (Figure 3) (8). Recent investigations

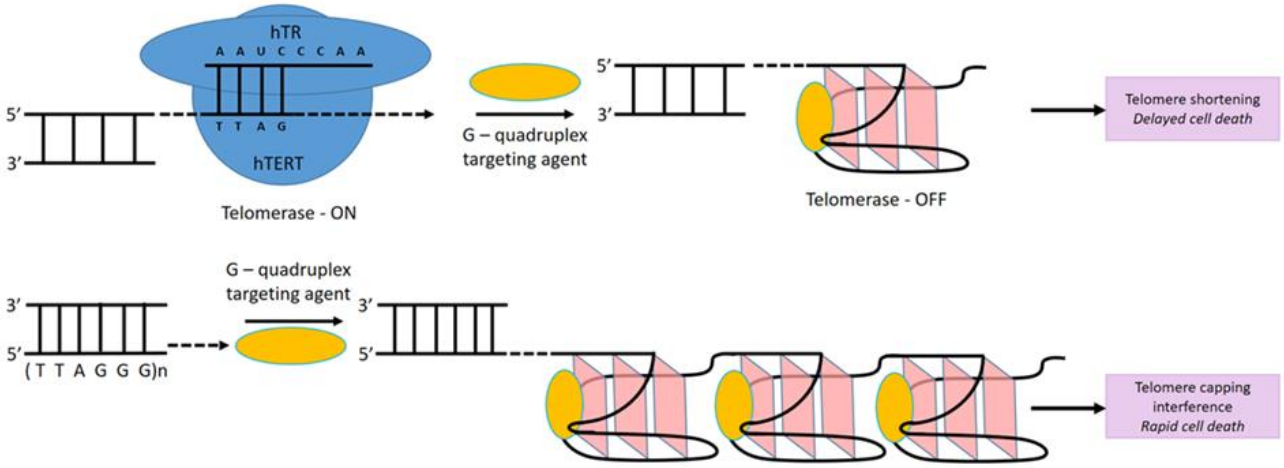

Figure 3 Illustration of the inhibition of telomerase by G-quadruplex ligands followed by drug mediated blocking of telomere capping by ligands. Adapted from Yang, D., & Okamoto, K. (2010). Structural insights into G-quadruplexes: towards new anticancer drugs. Future medicinal chemistry, 2(4), 619-646. (14).

suggested that these secondary DNA G4 compounds interfere with and distort the telomere capping as well as activating apoptosis (Figure 3) (8). Telomeric DNA is known to be linked with a numerous variety of protein structures which interferes with processes of telomere maintenance and interrupts the telomere capping process, e.g. TRF2 (Telomeric repeat-binding factor 2) and Pot1 (Protection Of Telomeres). This may be identified as DNA damage, which therefore promptly activates apoptotic pathways in the absence of telomere shortening (8). In addition to this, G-quadruplexes have also been known to inhibit the alternative lengthening of telomeres (ALT) pathways. ALT is a maintenance mechanism that is telomerase independent, which maintains the stability of telomeres occurring in ~15% of cancer cells in which telomerase is not activated (8).

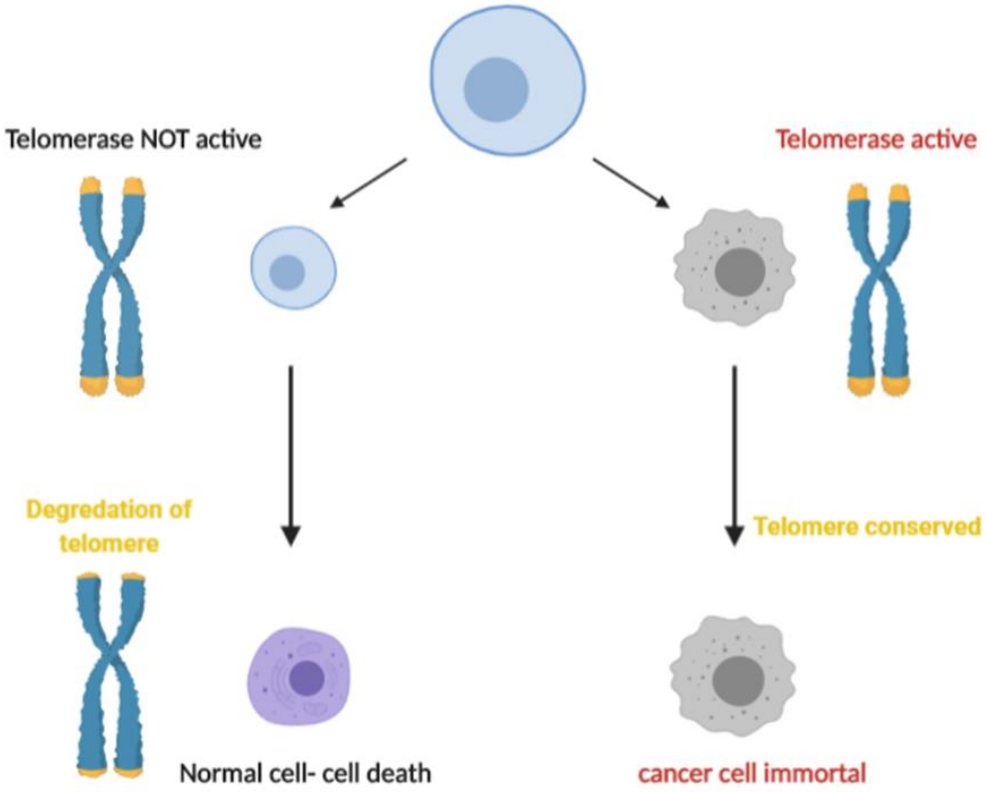

Figure 4 Illustration of telomerase enzyme activity in cancer and normal cells

1.1.4 G-quadruplex DNA as a target for anticancer drugs

G-quadruplex DNA structures led to a new approach to anticancer drug design and development through the targeting of secondary DNA structures (8). In 1997, Sun *et al.* (21), stated that these secondary DNA structures, when stabilised could possibly be clinically curative active compounds within damaged cells. Specifically, small molecules that target G-quadruplex DNA structures alongside hindering telomerase. Small molecule targeting G-quadruplex structures lead compounds were determined from the discovery of the perylene derivative PIPER **1** (seen in Figure 5) which showed intercalation of G-quadruplexes.

1.1.5 G-quadruplex compounds as cancer targeting drugs

Stabilisation of G-quadruplex structures by binding to a ligand molecule predominantly occurs through pi-pi stacking and electronic interactions to the external face of the G-quadruplex DNA structures (22). Investigated and tested G-quadruplex ligands include BRACO-19 **2** (acridine derivative) (23), telomestatin **3** (macrocylic natural product) (24), RHPS4 (pentacyclic acridine) **4** (25), MMQ3(quinacridine) **5**, (26) Mn (III)- porphyrin **6**, (27) BMSG-SH-3,12 (tetra-substituted naphthalene diimide) **7** (Figure 5) (28)and triazoles **8**(29) (30). All these ligands possess a large aromatic planar area alongside a short non-polar alkyl chain with a charged group. These structural motifs have been shown to be effective for a G-quadruplex ligand by improving selectivity by aromatic-aromatic connection and ionic interactions between the ligand and external face of G-quadruplex structure respectively (31)(22). Initial research was mainly focused on improving G-quadruplex ligands selectivity for non-Watson-Crick base paired DNA (22)(32)(33). The first telomere interacting molecular structure was found to be 2,6-diamidoanthraquinone derivatives synthesised by Neidle *et al* (34). Subsequently, TMPyP4 **9** and telomestatin **3** were found to bind to G-quadruplexes (35) (36) leading to the rapid development of selective G4 ligands through improved methods and analytical techniques to investigate the specific binding profile of each drug. There are now G-quadruplex ligands, available commercially, which have almost completely selective binding to G-quadruplex structures. These include BRACO19 **2** (23), pyridostatin **10** (37), Phen-DC3 **11** (38), L2H2-6OTD **12** (39), and L1H1-7OTD **13** (40) as seen in Figure 6.

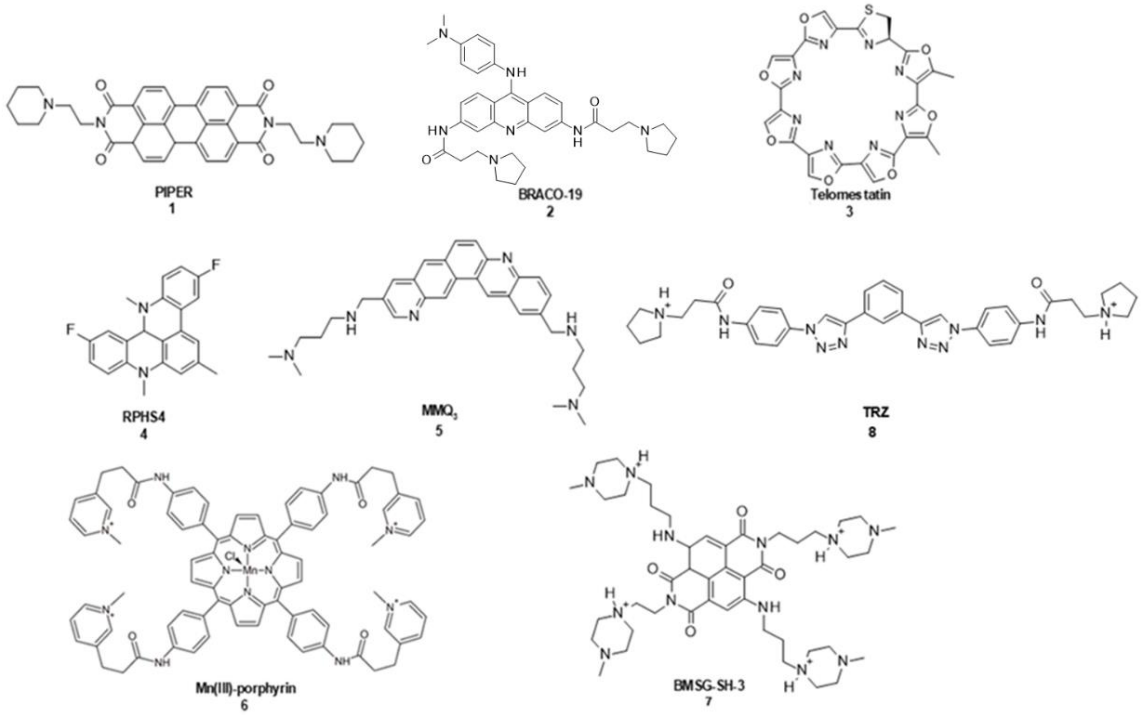

Figure 5 Skeletal structures of G-quadruplex binding ligands **1-8**

It has been demonstrated that G-quadruplexes are present in genes that have been shown to be overexpressed in several different cancers, the stabilisation of which can effectively act as a switch for these genes (41). These studies and investigations of synthetic small molecules for G-quadruplex binding have led to the promise of G-quadruplex ligands as a targeted approach to cancer therapy. An example of a G-quadruplex stabiliser would be that of pyridostatin **10** (2) G-quadruplex ligands are designed to only target the transcription elements of genes that are overexpressed in cancer therefore, it is expected to select for cancer rather than for healthy cells (42). The advantages seen by G-quadruplexes include the time required for inhibition, which has been shown to show anti-tumour activity after one-month (43).There are also several mechanisms of action, from telomere shortening mechanism and stabilisation of gene targets for cancer, these properties make this method selective. Toxicity has also been shown to be lower than other chemotherapeutic treatments for example BRACO-19 **2** compared to Doxorubin (44). We also see a new generation of ligands deriving from acridine derivatives, which allow for further interaction within the

grooves of G-quadruplex structures. This additional interaction activity increases the activity and the selectivity (45). Validation of G-quadruplex ligands in the use of cancer therapy was demonstrated in investigation of the c-myc oncogene (2). The cytotoxicity decrease of these ligands can be explained by the low toxic effects of telomerase inhibitors compared to other drugs when dosed appropriately over a long time.

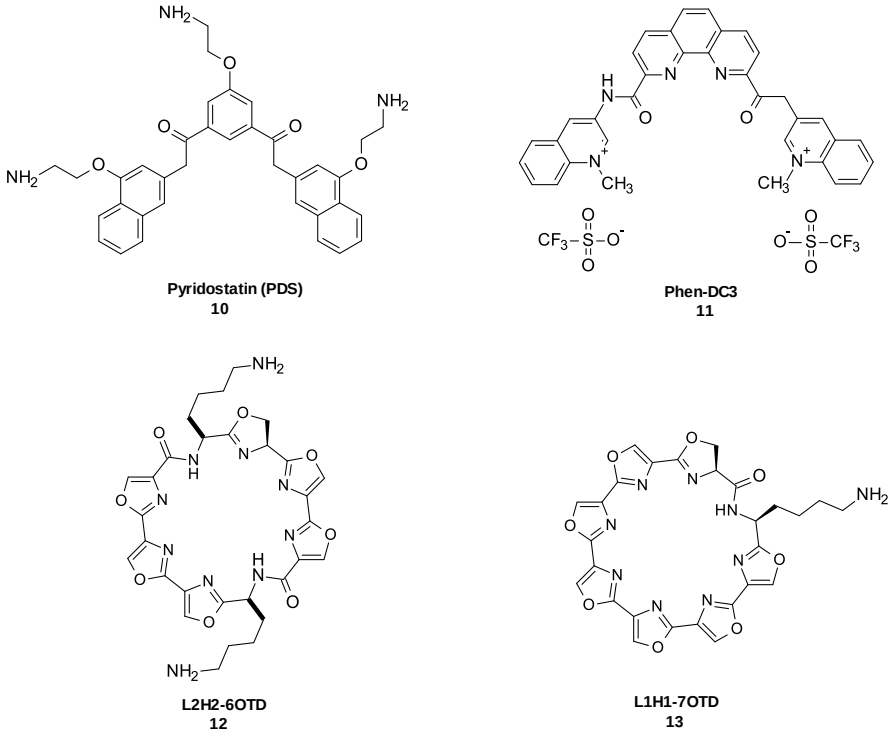

Figure 6 Skeletal structures of G-quadruplex binding ligands **10-13**.

1.2 Gene targets of G-quadruplex ligands

Genes within DNA contain several different regions including a promoter region an encoding region and terminating region. The promoter regions of several proto-oncogenes have shown to form G-quadruplex structures, suggesting possible targets for G-quadruplex ligands. Specific proto-oncogenes include c-MYC, c-KIT, BCL-2, k-RAS, VEGF, HIF1α, and PDGF-A (46)(47)(48)(49)(50)(51).This gives another pathway for cancer drug discovery in that drugs can be synthesised to target promoter regions instead of telomeres (52)(53)(54)(55)(56).

The proto-oncogenes listed above have a wide variety of functions, however it was shown that the G-quadruplex structures in the promoter regions were crucial for transcription

regulation. One of these proto-oncogenes (c-KIT) translates to a tyrosine kinase receptor (c-KIT) that is present within the membrane(56)(57). The c-KIT receptor when activated will phosphorylate downstream targets, which will promote cell growth, proliferation, survival and migration (58). If this receptor is overexpressed it leads to excessive activations of cell growth factors, which is indicated in several cancers such as gastrointestinal stromal tumours (GISTs), pancreatic cancer, melanoma and haematological neoplastic diseases (59)(60).There are several research studies that have demonstrated c-KIT kinase activity inhibition *in vivo* and *in vitro via* G-quadruplex ligands (61)(62). In these studies, there was, a major limitation to clinical use, which was resistance to treatment. Resistance could arise through mutations in the promoter regions, stopping drug binding, which prevents selective inhibition of the kinase when the c-KIT gene is activated within the genome (57). This limitation means that other methods must be implemented which avoid the issues above. One such method is multi-target therapy or the use of G-quadruplex ligands to stabilize G-quadruplexes within the c-Kit promoter regions. Specifically, for the c-KIT, they should target the three guanine (G)-rich regions in the proximal promoter (47)(58)(63). Research done on this has shown that there is a reduction of c-KIT tyrosine kinase receptor expression when G-quadruplex structures are stabilized by small molecules (64)(65)(66)(67)(68)(69)(70). This strategy can be considered as an alternative to overcome mutation-related resistance which prevents traditional gene targeting drugs from functioning.

An example of small molecules working in this way was tested by Mazzini *et al*. 2019 who showed that BMH-21 (RNA polymerase I inhibitor) and its analogue BA-41 did not intercalate DNA but did bind to telomeres and c-MYC promoter G-quadruplexes (71).

This specific example is also complemented by other research showing that stabilization by small molecules of G4 in genes including hTERT (72), KRAS (73)(74), BCL2 (75), and VEGF (76), led to inducing tumour apoptosis.

1.2.1 VEGF

It has been demonstrated that Vascular Endothelial Growth Factor (VEGF) protein overexpression in tumour cells induce the development of new vasculature (neovascularization). Neovascularization in tumour cells is induced by several VEGF proteins, specifically VEGFA, VEGFB, VEGFC, VEGFD, VEGFE, and PIGF. Regulation of these proteins in eukaryotic cells is predominantly done at the point of transcription from DNA to mRNA rather than translation to protein (77)(78).

Evidence of the regulation site of VEGF being at a promoter region in DNA was shown by a reporter assay system on several cancer cell lines. This work showed that regulation was controlled by a sequence at -85 to -50 base pairs (bp) relative to the transcription start site. This sequence was made up of five motifs of >3 consecutive guanine residues (79)(80). This suggests that the guanine tetrad structures formed at these sequences are the regulatory elements of VEGF (76). This makes VEGF a promising target for malignant tumour selective therapies with several antibody drugs previously being approved for the treatment of solid tumours (81)(82).

It has been described previously how the intercalation of TMPyP4 **9** and telemostatin **3** with these G4 structures *in-vitro* has demonstrated the breaking of intra strand interactions to form ssDNA from duplex DNA, which subsequently gives a stable structure for the G4 structures (76). Testing of the regulation of VEGF at this site was done through the use of a universal G4 interacting molecule, Se2SAP, which demonstrated active suppression of several adenocarcinoma cell lines' VEGF expression (83). This study clearly showed the promise that ligands which bind selectively at this promoter region can have for regulation of VEGF expression and therefore mitigate the neovascularisation potential of tumour cells.

This treatment option could thereby give a way of slowing tumour maturation and reduce chances of metastasis and further complications.

1.2.2 c-KIT

The KIT tyrosine kinase is involved in several cancer types in humans. These include gastro-intestinal cancers specifically which demonstrates that the improper regulation of expression is a key factor in the progeny of the disease type (34)(84)(85). It has been detailed that at position -87 to -109 bps and -140 and -160 bps upstream of the initiator site for the c-KIT gene there are G4 structures present (86). Studies on targeting these G4 structures for regulation of the c-KIT genes has been limited to demonstrating correlations between the binding of small molecules to the c-KIT G4 structures and respective inhibition of the KIT tyrosine kinase expression (68)(64)(67)(69)(88)(87).

1.2.3 BCL-2

The apoptosis regulating protein B-cell lymphoma 2 (BCL-2), is a double action protein that either inhibits (anti-apoptotic) or induces (pro-apoptotic) apoptosis. This property is why it is involved in several cancers, ranging from melanomas to carcinomas (88). A region of the promoter at -1490 and -1451 upstream of the P1 promoter has shown that the intramolecular G4's would form at G-rich domains within this region (89). It was identified by Hurley *et al* that there were three G4 motifs at the 5' end, middle and 3' end of the region (90).These three G4 structures were thoroughly characterised by DMS foot printing, Polymerase stop assays and NMR spectroscopy. This characterised the most stable G4 structure as being made up of mixed parallel/anti-parallel G4, containing two lateral and one external loop. (90) (91) (48). Interaction of TMPyP4 **9** with these structures has previously been investigated in *in-vitro* solution (92) however this study was limited by the absence of clarity of the function biologically of BCL-2 G4 structures *in vivo*. Despite this it has been shown that BCL2 dependent pathways contain non defined roles for G4 structures. Evidence for these roles has been shown through reduced transcription to mRNA in the presence of G4 binding small molecule 12459 **14** (seen in Figure 7), a triazine derivative, which correlated to the induction of apoptosis in A549 cells through interaction with mitochondrion-related pathways (93).

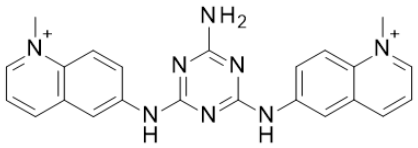

Figure 7 Skeletal structure of 12459 **14**

1.2.4 c-Myb

The DNA binding transcriptional activator MYB, which is encoded by the proto-oncogene c-MYC, is integral in controlling proliferation and differentiation of hematopoietic progenitor cells. Its expression is highest at the early stage of development and gradually decreases as differentiation proceeds (94). The discovery of c-myb in humans was found through the identification of its analogue in avian myeloblastosis virus and E26 (v-myb) through genomic matching (95). Its status as a proto-oncogene is evidenced by the development of haematological cancers and adenocarcinomas, when expression is high through differentiation, and not regulated where it decreases over the time of differentiation (96)(97)(98)(99)(100). Regulation of the levels of mRNA produced from c-myb is reliant on several other transcription activators and inhibitors that are specific to each cell type and cell stage (101)(102)(103)(104)(105)(106). As such, regulatory elements in the promoter region are seen at -17bp to the transcription start site, where a guanine rich region is found which forms parallel G4 structures (105)(107)(108). The regulatory properties of this region for the promoter were demonstrated through targeted deletion of parts of the guanine rich region which inhibited the formation of dimerized G4 structures. This deletion led to enhanced promoter activity and a higher expression of MYB, which suggests that the G4 structures regulated transcription through an inhibitory method of action (negative regulation) on the c-myb promoter (105). It has also been shown that the transcription factor Myc-associated zinc finger protein may bind to this G4-structure and stabilise the G4 which in turn inhibits MYB expression.

1.3 Quarfloxin

Quarfloxin **15** (Figure 8) is one of the G-quadruplex compounds, which progressed to Phase II clinical trials stage as a single-agent treatment for neuroendocrine/carcinoid tumours. Quarfloxin **15** is also referred to as CX-3543 or itarnafloxin (109). This G-quadruplex compound was initially derived from a group of fluoroquinolones, which were presented to have dual topoisomerase II and G-quadruplex interactions (109). Cylene Pharmaceuticals halted research into topoisomerase II activity and increased research into compounds selective for G-quadruplex structures (109). The selectivity of Quarfloxin **15** to G-quadruplex DNA arises from its selective uptake into the nucleolus of cancer cells. No significant toxicities were observed for Quarfloxin **15**, which means apoptosis occurs to cancer cells not to normal cells. Even though Quarfloxin was designed originally for targeting the *c-MYC* promoter G-quadruplex, it has also shown that it has higher selectivity in contrast to TMPyP4 **9** for all-parallel G-quadruplex structures (109). Even though it has been shown to have higher selectivity for G-quadruplex structures it has also been found to concentrate in the nucleolus and has an inhibitory effect on Pol I transcription (109). The inhibition of RNA polymerase I (Pol I) can be explained by the disruption of the G-quadruplex–nucleolin complexes through Quarfloxin **15** binding, which in turn leads to cellular redistribution of nucleolin into the nucleoplasm. Quarfloxin **15** was shown to bind to most G-quadruplexes and disrupt all but one of the nucleolin–DNA complexes (109).

In 2013, Quarfloxin **15** was licenced to TetraGene by Cylene Pharmaceuticals on an exclusive, worldwide basis. Cylene Pharmaceuticals however, ceased operations in 2013 due to the high albumin binding seen which caused disruption to blood transport of active compounds.

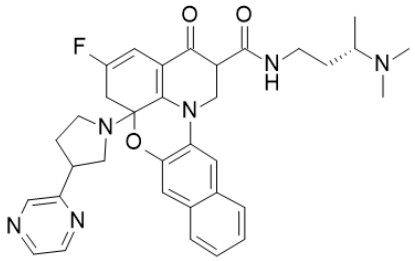

Quarfloxin
15

Figure 8 Skeletal structure of Quarfloxin **15**

1.4 BRACO-19

BRACO-19, 3, 6, 9-*tri*-substituted acridine; 9-[4-(*N, N*-dimethylamino) phenylamino]-3, 6-*bis* (3-pyrrolodinopropionamido) acridine **2** (Figure 9) is derived from trisubstituted acridine, through modification of position 3 and 6 with pyrrolidine and position 9 with a tertiary amine, which showed direct targeting of telomeres. Computer modelling was used to find compounds which interacted with the three grooves of G-quadruplexes, and stacked on the terminal G-quartet, leading to the design of BRACO-19 **2** (110). The cytotoxicity of BRACO 19 **2** is very low (IC_{50} values 1-3 μM in UXF1138L uterus carcinoma cell line(23)) and it has a much higher G-quadruplex-binding specificity and telomerase-inhibitory activity than its parent disubstituted acridine. It was then shown that BRACO19 **2** inhibits the catalytic function of telomerase in human cancer cells and it also destabilizes the telomere capping complex (110). BRACO-19 has been demonstrated as a powerful anti-cancer agent in studies on prostate cancer xenografts (111) and human breast cancer cells (110). Because of its demonstrated anti-cancer properties BRACO-19 **2** is a heavily researched G-quadruplex ligand. The synthesis of BRACO-19 **2** was achieved after a long and arduous research programme that thoroughly tested the medicinal chemistry required of the molecule. This research begun with an acridine moiety as the planar core (chromophore) different to other G4 ligands. This was done as Read *et al*. showed that this chromophore had higher binding activity than other cores specially anthraquinone (112)(34). This higher activity can be explained by the nitrogen atom within the acridine that when protonated

increases the electron deficiency giving greater interaction with G-quadruplexes (113). The use of molecular modelling and structure-activity relationship techniques gave insight into how the acridine moiety could be added to, to give bi- and tri-substituted derivatives that could give higher binding activity selective for G-quadruplexes (114)(115). BRACO-19 **2** and its derivatives are a class of compounds that have a central planar chromophore that selects for the G-tetrads present in G4 through hydrophobic interactions between hydrophobic core and the centre of the G-tetrads. The grooves formed in the G-tetrad are selected for by the addition of a functional tertiary amine which when protonated at physiological pH will form hydrogen bonds with the backbone oxygens (116). As previously mentioned BRACO-19 **2** was selected from evaluated molecules because of its advantageous properties.

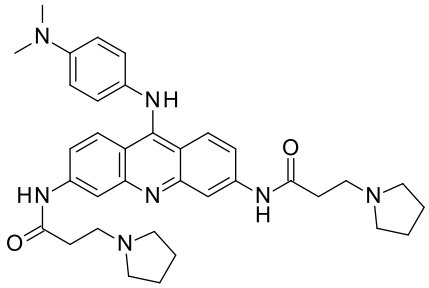

BRACO-19
2

Figure 9 Skeletal structure of BRACO-19 **2**.

1.5 TMPyP4

Porphyrin derived compounds have been selected for study as G-quadruplex ligands as they have preferential properties as a G-quadruplex intercalators. This includes their molecular size which allows for transport into the nucleus, a planar core for interactions with stacked G-tetrads alongside hydrophobicity before any modifications are made. The addition of positive charges to the porphyrin ring can be achieved with several types of tetra modifications but here we focus on the modification through the addition of four N-methyl-4-pyridyl groups to form a 5,10,15,20-tetrakis-(N-methyl-4-pyridyl)porphine (TMPyP4) **9**

(117). Despite initial hopes for TMPyP4 **9** as a cancer targeting drug, where biophysical studies showed stacking and stabilization of antiparallel and parallel structures there was only mild selectivity for quadruplex over duplex DNA (118). Because of this it is primarily used as a research tool as when the pyridyl groups are bound at position 2 rather than 4, it loses any activity. This gives a very useful negative control with an almost identical structure (119)(120). Despite this TMPyP4 **15** has demonstrated human telomerase inhibition, alongside a second target in the proto-oncogene c-myc where expression has been shown to be downregulated (121). There are also several other c-myc-regulated genes, which contain G4 structures, that have shown downregulation with the administration of TMPyP4 **9**. These findings resulted in the reduction in tumour growth and increased survival time within several *in vivo* antitumor models (122).

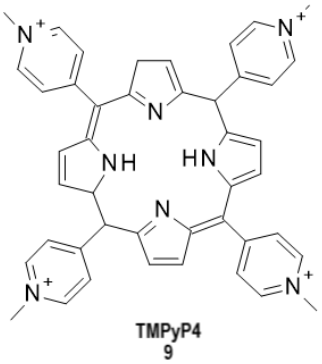

Figure 10 Skeletal structure of TMPyP4 **9**

1.6 Perylenes and naphthalene diimides

This class contains a variety of substitutions to the heptacyclic aromatic planar core. This aromatic planar core is required for selectivity as it interact to the G-tetrads. Substitutions on the aromatic core are used to add protonated side chains which will bind to the external grooves of the G-quadruplex structures. From the substituted derivatives several key properties were identified which gave greater activity. These included the basicity which stops aggregations of the ligands by preventing pi-pi stacking of the chromophore. There is

also a consideration for the distance of the bonding between the aromatic core and the substituted nitrogen which selects for G4 structures and increases water solubility (123).

The perylene structure that has shown the greatest potential through demonstrated stabilization G4 structures in telomeres is PIPER **1** (Figure 5), N,N'-bis[2-(1-piperidino)-ethyl]-3,4,9,10-perylenetetracarboxylic diimide (124). This has led to PIPER being used as a lead compound for further drug discoveries(125). Drugs that can stabilise G-quadruplexes in telomeres like PIPER **1** (Figure 5) can be expected to shorten telomeres, reduce tumorigenicity, cell proliferation and senescence (126). Despite these promising findings it was suggested that modulating the ability to recognise DNA conformations by altering the planar core would lead to more promising compounds. One class of compounds derived from this work was the naphthalene diimide (NDI) **17** derivatives which suggested that a reduced aromatic core of at least four rings was sufficient to select for G-quadruplex structures (127). With NDI **17** there is also the advantage of additional sides for substitution with four available, compared to PIPER'S **1** two. This increase can allow for increased G4 affinity through addition of more G4 structure stabilizing moieties. NDI **17** derivatives have been tested on MCF-7 and A549 cell lines which are cancerous, the results showed that these compounds can, in low micromolar concentrations, interact with telomere G-quadruplex structures and inhibits telomerase activity (128). The introduction of quinone methides precursors to the planar core gave increased alkylating properties towards G4 structures (129)(130). These modified NDI **17** structures increased selectivity for G-quadruplex structures through reversible and irreversible binding to telomeres (131). This greater selectivity led to inhibition of telomerase activity of different cancer cell lines (132)(133)(134). X-ray crystallography work done by Neidle *et al*. showed how NDI **17** ligands form complexes with telomeric structures. They showed that the complex was stoichiometric between ligand and G-quadruplex which suggests that direct interactions between grooves and side chains were achieved and binding affinity was high (135)(136). With the use of molecular modelling and further crystallographic techniques NDI structures

17 (seen in Figure 11) can be further optimized through medicinal chemistry investigations which will improve the specific pharmacological profile (137)(42).

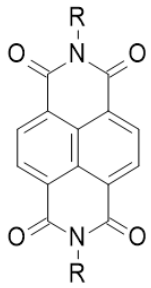

Naphthalene diimide (NID)
17

Figure 11 Skeletal structure of naphthalene diimide (NID) **17**, modifications have been seen on the R groups and one of the phenyl rings to give G4 alkylating properties.

1.7 Anthracene derivatives

Anthracene derivatives with nitrogen rich groups added are required for interaction with quadruplex DNA which requires planar nitrogen rich species which allow for intercalation within the G-quadruplexes and binding to the anionic phosphate back bone of DNA. Anthracene **18** (seen in Figure 12) possesses the correct geometry to sit between the G-tetrads through its hydrophobic core, but lacks the hydrophilic elements, which allows for greater water solubility. Selectivity for G-quadruplexes by anthracene derivatives has been demonstrated through longer linking between the hydrophobic core and hydrophilic elements, addition of terpyridine metal complexes and through screening of different hydrophilic arms for hydrogen bonding (138).

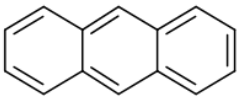

Anthracene
18

Figure 12 Skeletal structure of anthracene **18**.

1.8 Other potential G-quadruplex targeting drugs

Various levels of selectivity and potency in binding to G-quadruplexes has been seen in quindoline derivatives, the diamidoanthraquinones (110).

Moreover, aptamers, short single-stranded DNA structures which selectively bind to targets (protein, peptide, DNA), were found to be good target molecules for G-quadruplexes, due to their size, high selectivity and stability making aptamers an ideal drug candidate for cancer therapy. A cancer selective treatment with antiproliferative activity against a wide range of malignant cell types entered Phase I trials in September 2003, AS1411 (Antisoma plc, London, UK) inhibits the growth of malignant cells by inducing apoptosis. AS1411, It also has went through a Phase 2 study in August 2008. However, Antisoma has since halted their research and they have become an investment company named Sarossa.

For G-quadruplex ligands selectivity and low toxicity is required for drugs to progress to Stage II Clinical Trials. For selectivity we need to have an extended planar structure to aid intercalation of stacked Hoogsteen bonded G-tetrads.

1.9 Ligands that disrupts G-quadruplex folding

Disruption of G4 structures by small molecules can be achieved in several different ways through intercalation at different parts of the structure or formation of different structures through molecular interactions. An example is in the previously detailed porphyrin derivative TMPyP4 **9** that, specifically in the Fragile X FMR1 gene, disrupts the bimolecular G4 structure and decreases the thermic stability of the structure as shown by melting temperature investigations (139). TMPyP4 **9** has also been shown to unfold G4 structures in the mRNA of MT3 endopeptidases, which leads to an increase in expression of this gene in cancer cells (140). Alongside this investigation of TMPyP4 **9**, studies done by Waller *et al*, which used a triarylpyridine **19** (Figure 13) as a scaffold for designing G4 targeting small molecules, identified a derivative that disrupting G4 structures within c-kit 1 and c-kit-2

genes at 50μM concentrations (141). Interestingly it was also demonstrated that other small molecules using this scaffolding were shown to stabilise G4 structures (142).

CD spectroscopy of G4/ligand complexes containing an anthrathiophenedione derivative **20** (Figure 13) by Kaluzhy *et al.* showed unfolding of telomeric DNA structures in the same way as spectra of thermal denaturing of telomeric DNA structures showed it (143). However, the mechanism of how G4's unfolding occurs after interaction of these derivatives in the binding site has not been elucidated as of yet but understanding this would allow for more intuitive design of G4 ligands.

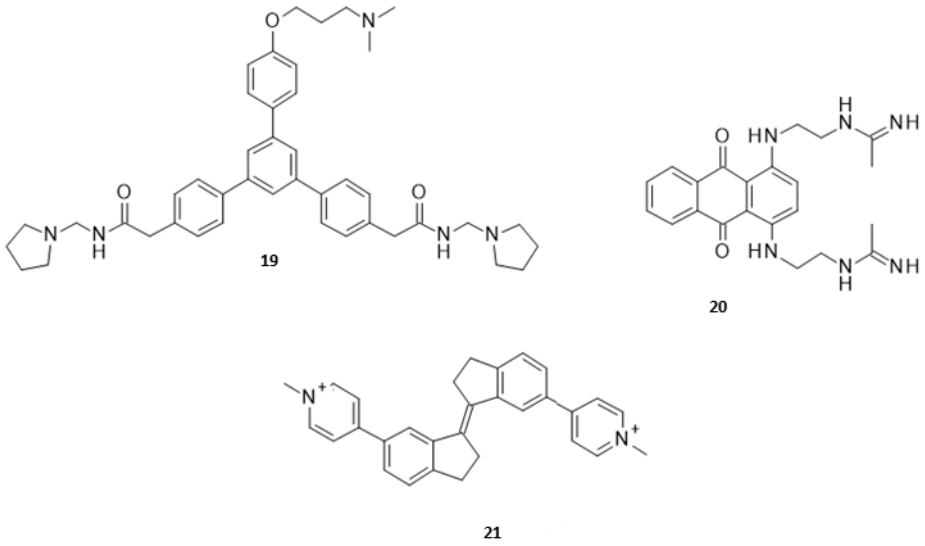

Figure 13 G-quadruplex ligands that previously demonstrated ability to induce unfolding of G4 structures.

Recent addition to research on these structures was done by O'Hagan *et al.* who discovered stiff-stilbene derivative **21** (Figure 13) that, when introduced to Tel23 (d[TAG3(T2AG3)3]) induces unfolding of its hybrid sodium form (144). Contrary to this action the stilbene derivative also stabilizes the hybrid potassium form of Tel23(d[TAG3(T2AG3)3]). Molecular modelling has been used to illustrate what the lowest energy form of the ligand is which allows for characterisation of the most feasible binding site within the structure and how the unfolding commences. These investigations led to the suggestion that the ligand binds initially to the G4 grooves and then intercalates with the G4 structure, thus leading to distortion of hydrogen bonds with the tetrad structure. The central stilbene scaffold also has

an additional useful property; in that its photochemical potential allows for the use of light as an activating agent when introduced into tumours therefore giving greater potential for selectivity. The use of different wavelengths of light for example 365/385 nm allows for switch from *E* to *Z* conformations, allowing for changes in potential activity.

1.10 G-quadruplexes in viruses

Sequences that form G-quadruplex structures are present not only in humans but also other eukaryotic cells, and they are seen in prokaryotic cells. The G-quadruplex structures will be expected to be found in the promoter regions of exon genes as transcription regulators. These regulatory systems have even been found to be developed in viruses. Specifically, G4 structures have been observed in the genomes of Human immunodeficiency Virus (HIV) (145) and Herpes Simplex Virus-1 (HSV-1) (146) which implies the G4 are important in transcription regulation of replication genes, recombination and regulation of gene expressions (145). Small molecules designed through medicinal chemistry investigations for hydrophobic intercalation with G-tetrads and anionic grooves could be used for inhibition of the mechanisms in place for viral replication. This means that infectivity and pathogenesis of viruses could be reduced. To test this hypothesis, several investigations into G4 ligands, which target the HIV genome have been undertaken (145)(147). The drug discovery strategy for this purpose has, in the last two decades, moved more to the development of aptamers that form G4 structures that can be recognized by HIV proteins which has been suggested by several research papers. This has led to the synthesis of a magnitude of guanine rich aptamers that are promising lead compounds for anti-HIV drug discovery (145)(148)(149)(150).

Specific proteins that have been shown to interact with these proposed aptamers are envelope proteins, integrase and reverse transcriptase. The design of these have been done by several approaches, classed as rational or randomized fragments design.

G4 structure regions are found in the genome of HPV through the identification of guanine rich sequences (151). These guanine rich sequences are only found in eight HPVs, however

a possible aptamer target that is present in most HPVs is the viral protein E1, that modulates the transcription, replication of the genome in its function as a helicase. The reason it is a possible target is its similarity to SV40 TAg which is a well-known dominant acting oncoprotein helicase (152), this means that E1 could present activity for unfolding G4 structures. G4 structure sequences are in in the long control region of HPV52 and HPV58, alongside the promoter region for the L2 protein in HPV57 and E1 and 4 in HPV32/42 and HPV3/9/25 respectively suggesting roles in transcription and the production of viral proteins from alternative splicing. Targeting of these genes could be one of the reasons why BRACO-19 **2** and TMPy4P **9** have shown HIV-1 replication inhibition (153)(154) where BRACO-19 **2** acts as inhibitor of reverse transcription and post integration by the viral promoters. Both of these functions can be explained by the intercalation with G4 structures present in genes, promoter regions and proteins specific for transcription regulation.

This inhibition of HIV-1 by BRACO-19 **2**, which is targeted in the promoter region of specifically LTR, works by intercalation of G-quadruplex structures in LTR-II and LTR-III. This intercalation, rather than blocking function or unwrapping, actually forms an additional G-quadruplex structure called LTR-IV as more LTR-IV is formed through increasing concentration of BRACO-19 **2**, we see a reduced LTR promoter activity. This action was illustrated by the demonstration of no activity in mutants, which were unable to form G-quadruplex structures. Short term and long-term *in vivo* testing showed the potential of BRACO-19 **2** where the acridine derivative was able through G-quadruplex intercalation and transcription regulation to reduce the viral load to negligible levels (155).

We have seen the use of BRACO-19 **2** in the modulation of the regulation of HIV infection however BRACO-19s **2** activity in viruses was first shown in the Epstein-Barr virus (EBV). In this study, the function, and biochemical properties of Epstein-Barr virus nuclear antigen (EBNA1) which is conversed in all EBV-related malignancies, was investigated. The investigation showed that the G-quadruplex structures in the viral RNA was stabilised by BRACO-19, this suggests that during infection the number of genome copies were reduced in Raji cells. Norseen *et al.* saw the inhibition of dependent DNA replication and transcription

regulation in EBNA2 and EBNA3A. These findings give an indication that G-quadruplex ligands can inhibit specific functions of EBNA1 related to viral DNA replication (156).

The stabilization of G-quadruplex structures in telomeric DNA by BRACO-19 **2** was assessed in cells infected by human herpes virus (HHV-6A). The treatment gave 50% reduction of integration into the chromosome. Investigation of the effects on replication and expression of genes are future work in HHV-6 research (157).

Another virus that has been analysed for G-quadruplex structure and their position is Hepatitis-B virus (HBV). This analysis showed that G-quadruplexes may have a regulatory function. The use of BRACO-19 **2** is currently limited to being a reference compound in G4 structure research because of its poor permeability across biological membranes (158), however it has shown by use in a luciferase reporter assay that G-quadruplex have a transcription regulation role in HBV (159).

Another small molecule besides BRACO-19 **2** that has been shown to have a similar mode of action is TMPyP4 **9**, which induces G4 structures formation within standard Watson crick base pairing and stabilization within the NEF coding region in HIV-1. TMPyP4 has also been shown to inhibit the viral activity of the TZM-bl (HeLa cell derivative) reporter cell line (specific to nef-dependent HIV-1 replication), with dose dependent correlations seen (154). It has also been demonstrated to block viral replication in lurkat-derived T-cell lines which have latent HIV-1 infection. Work done by Bambara *et al*. showed the rate of cell death/apoptosis was positively correlated with antiviral activity, with enhancement of this effect achieved through links to DNA damage repair inhibitors (155). TMPyP4 **9** was also found to be a promising anti-viral agent for the Hepatitis C virus as RNA G-quadruplexes were demonstrated to be stabilized and fluorescent reporter genes were used to show the inhibition of HCV C gene expression. To corroborate these findings, introduction of TMPyP4 **15** into a HCV infected cell culture led to a decrease of viral RNA levels dependent on the concentration of TMPyP4 **9** used (160). Besides the regulatory mechanisms inhibited by TMPyP4 **9** it has also been used to determine the roles of G-quadruplexes in the L gene of EBOV.

1.11 G-quadruplexes in bacteria

The genome of prokaryotes (bacteria) exists in a very different state to that of eukaryotes, such that the genomic data does not reside in a separate organelle (nucleus) but is stored in uncondensed circular chromosomes and plasmids that can transfer between cells through transduction (161). Since the genomic material is not protected in a nucleus and condensed to form protective chromosomes *via* protein interactions, the stability of bacterial genomes comes from secondary structures that form in the bacterial genomes (162). This stability is epitomised by G4 structures that are present throughout, which have shown slower unfolding kinetics to even duplex DNA in Eukaryotic cells (163).

Despite these findings not many studies have been done investigating the role of genomic stabilising G4 structures for bacterial survival and virulence of specific bacteria strains (164). A function of G4 structures that has been demonstrated by Pooja *et al* was that amino acid biosynthesis and signal transduction are negatively regulated by the presence of G4 structures within the encoding gene (165). We see a distinct difference in the number of studies relating to G4 structures with prokaryotes (166), when compared to eukaryotic studies (167) which means that there is a lack of clarity on several aspects of the G4 structures within prokaryotic DNA. Despite the obvious need for G4 structures within prokaryotic DNA for stability, we see a great variability in the GC (Guanine-Cysteine) content, which is a determining factor in whether G4 structures will form (168), between different bacterial genomes 17-75% (169). There has also been shown in the order *Deinococcales* a bias of G4 forming motifs around the transcription start sites of genes suggesting a role in regulation of expression (170). Looking at variability of GC (Guanine-Cysteine) content more closely we can elucidate another role for G4 structures. Specifically, in *Thermus aquaticus* we see one of the highest GC contents at 68%, which would allow for maintenance of duplex DNA even at higher temperatures (171). We also see a large number of G4 forming sequences upstream of the NasT gene in *Paracoccus denitrificans* which is exposed to toxicity from digestion of NO_3- (172). The genes that participate in the

host-pathogen interactions of *Stretoccocus pneumoniae* have also been shown to contain G4 structure motifs within their genomic sequence (164). These findings clearly demonstrate the importance of G4 structures within bacteria that experience unique DNA damaging environment, alongside the role played within circular DNA in chloroplasts and mitochondria which were evolutionarily taken from prokaryotic organisms. Mitochondrial DNA's reliance on G4 structures has been illustrated in several papers using several different assays and analytical techniques (173)(174)(175). Chloroplasts have also shown G4 like structures within their regulatory domains of chloroplast DNA (176).

1.12 Synthesis of G-quadruplex ligands

1.12.1 Anthraquinones, Porphyrins and Acridines derivatives

Derivatives in the class of anthraquinones (177) porphyrins and acridines were the first small molecules synthesised to intercalate G-quadruplex structures within telomeres to indirectly inhibit telomerase. Specifically, disubstituted acridines were synthesised followed by the addition of another substitution to give trisubstituted acridines(178). Porphyrins (179) were also synthesised alongside anthraquinones and trisubstituted acridines to give greater efficacy to intercalation of telomeres leading to regulation of telomerase.

In this class of G-quadruplex ligands BRACO-19 **2**, a 3,6,9-trisubstiuted derivative of acridine showed the greatest potential for therapeutic use. Neidle *et al*. showed that BRACO-19 **2** (180) could inhibit cancerous cell division *in vivo* and *in vitro* at sub micromolar concentrations (23).

3,6,9-trisubstiuted acridine derivatives **29** as shown in Scheme 1 (23), are synthesised *via* an acridone precursor which has a chloro group added at the 9 position to form compound **28** of the acridine structure through treatment with $POCl_3$. Substitution of this chloro then takes place to form a final acridine derivative **29**. Interest in these derivatives has increased through the demonstration of a 10X selectivity between G-quadruplex structures (181).

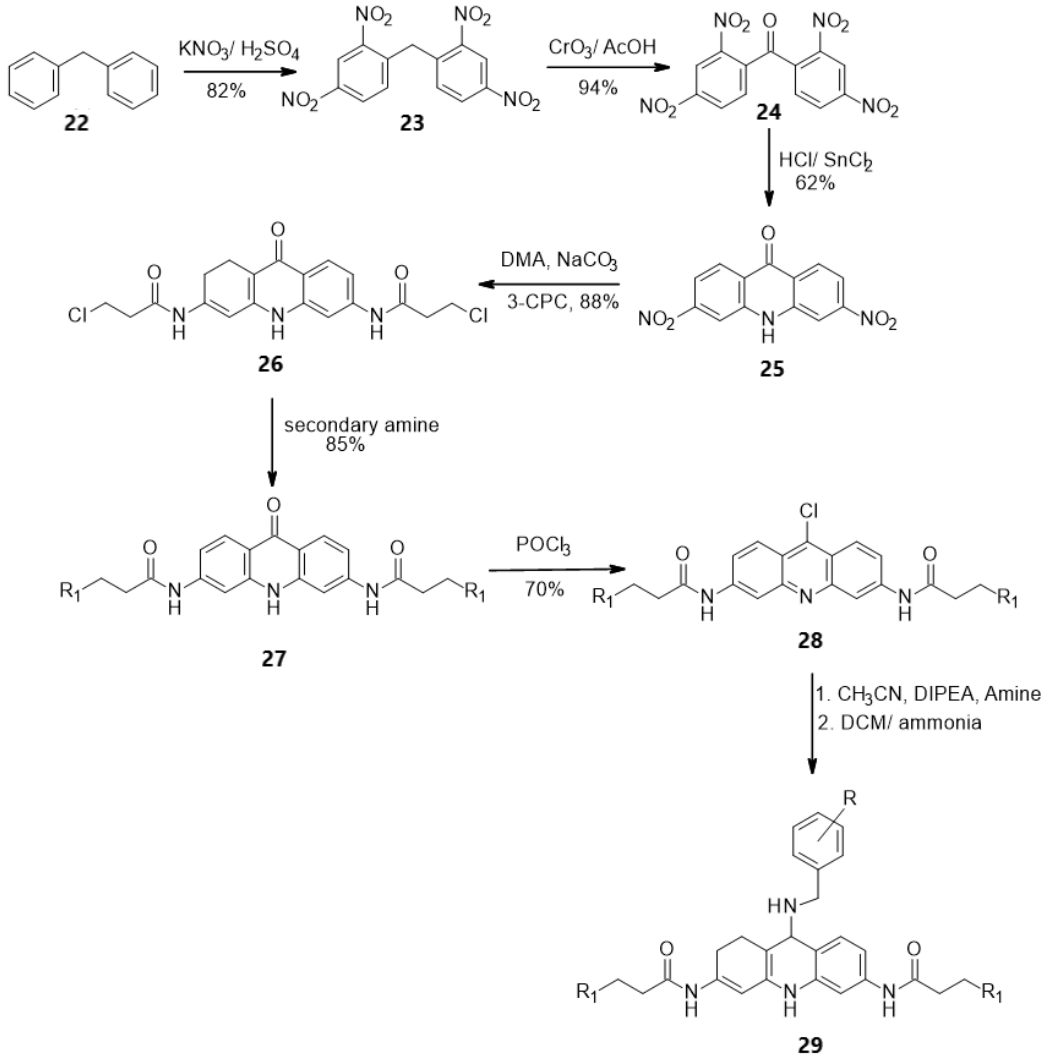

Scheme 1. General synthetic scheme for 3,6,9-trisubstituted acridine **29** derivatives. (DCM = dichloromethane, DIPEA = N,N-diisopropylethylamine) (182).

1.12.2 Natural products showing telomerase inhibition

It has been shown that berberine **29** (183) and telomestatin **3** (184) have human telomerase inhibiting properties. Telomestatin **3** is the focus of most research as it has a greater inhibition of telomerase. *Streptomyces anulatus* produces telomestatin **3** and it was isolated after wide spanning screening process for inhibitors of telomerase (185). Telomestatin **3** has demonstrated at sub nanomolar concentrations to have inhibitory activity. Its structure which contains two methyloxazoles which are linked to five oxazoles separated by a thiazoline ring was characterised allowing for biosynthesis and total synthesis to be

understood. This understanding allowed the absolute configuration to be shown as *R* (186). Multiple human tumours including in the brain (187) blood (188) and bone marrow (189) have been shown to be inhibited by the action of telomestatin **3** in *in vivo* and *in vitro* studies.

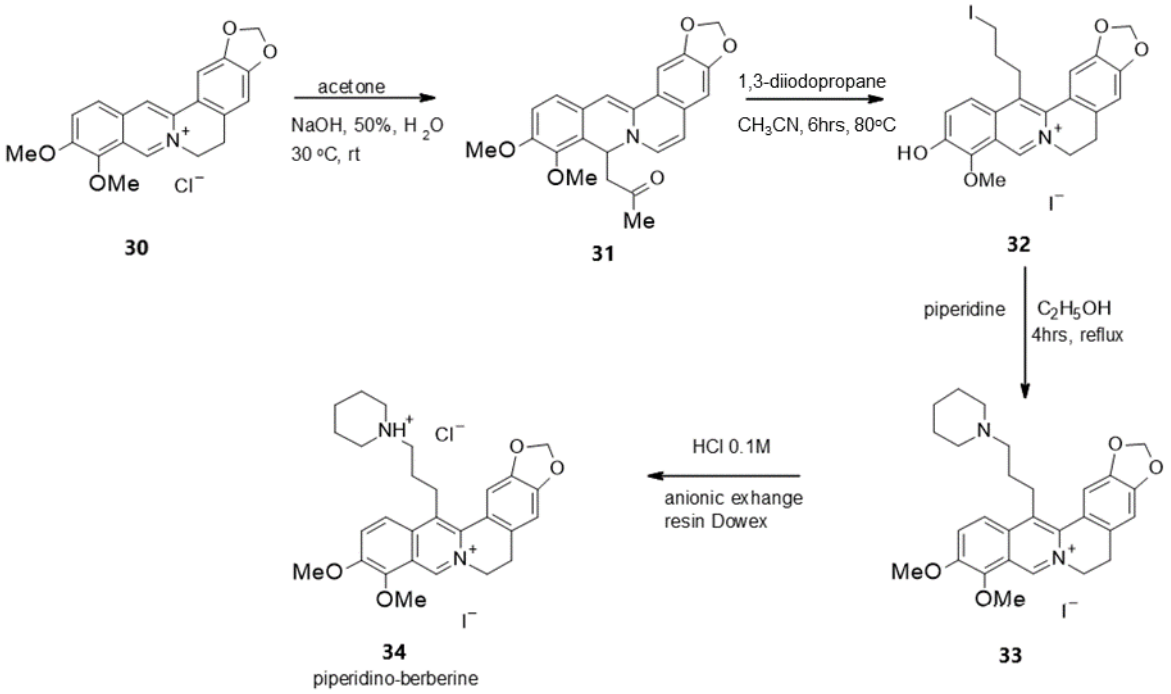

Scheme 2 Synthetic scheme example which was previously reported by Marco Franceschin 13-[3-(1-piperidino)propyl]berberine (piperidino-berberine) (190).

A key intermediate of this synthetic strategy was obtained through the use of acetonyl-berberine. Afterwards, the acetonyl group was displaced with 1,3diiodopropane **32**, following this the iodine atom was substituted with piperidine to give the desired side chain (Scheme 2). According to the research by Marco Franceshin *et al* (190), compared to berberine **30**, piperidino-berberine **34** showed a greater stabilization of G-quadruplex structures and a greater telomerase inhibition as shown through the use of TRAP assay (190).

1.12.3 Perylene derivatives

PIPER **1** structure was first discovered to show telomerase inhibition in 1998 by Hurley *et al* through a NMR study. In the report, PIPER **1** was shown to bind to G-quadruplex and

inhibit telomerase, however the structure was found to stacks on the G-tetrad closest to the 3' end rather than intercalating between the Guanine residue in the G-quadruplex (125).

However, the initial synthesis, by Fedoroff *et al* (125), of PIPER **1** was achieved through 3,4,9,10-perylenetetracarboxylic dianhyride mixing with 1-(2-aminoethyl) piperidine in DMA and 1,4-dioxane seen in Scheme 3. This procedure was adapted from the DAPER synthesis which was done by Zhi-Ren LiuR and L. Ril in 1996 (191).

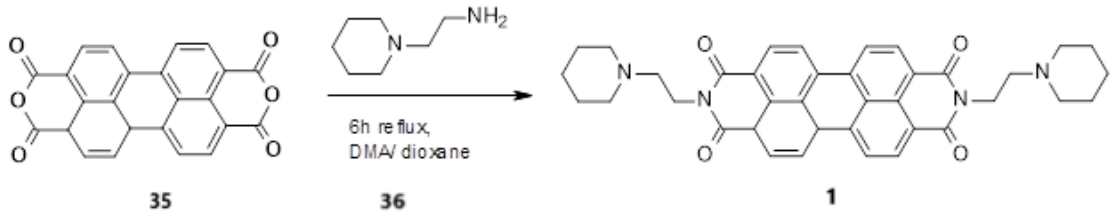

Scheme 3 Mechanism for PIPER synthesis (125).

1.12.4 Methods to synthesise Quarfloxin

Quarfloxin is one of the fluoroquinolone derivatives which consists of different conjugated aromatic systems alongside many other side chains designed and synthesised by Cylene Pharmaceuticals (109). Quarfloxin was the most promising fluoroquinolone derivative which was found to be extremely selective for c-myc G-quadruplex structures.

Looking at the compound synthesis, which was done by Whitten *et al* (192) and patented, they started preparing the substituted benzoaxanize analog using 2,3,4,5-tetrafluorobenzoic acid **37** in methylene chloride with addition of oxalyl chloride seen in Scheme 4. The afforded acid chloride oil was then converted to keto ester **39**.

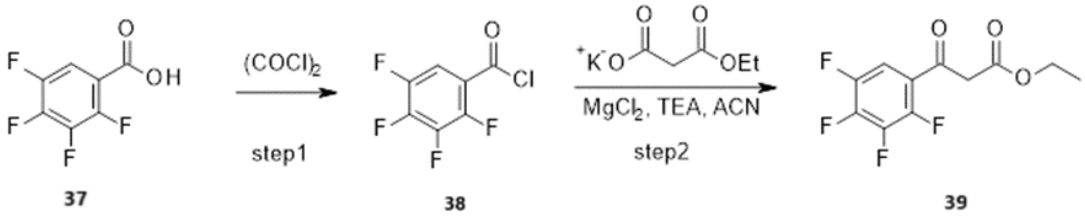

Scheme 4 Generating tetrafluoroketoester **39** from 2,3,4,5-tetrafluorobenzoic acid **37** using oxaxlyl chloride first, then triethylorthoformate.

Tetrafluoroketoester **39** was then converted to enamine using triethylorthoformate and acetic anhydride. This reaction was followed by adding potassium carbonate to the solution of enamine to make difluoroester seen in Scheme 5. The resulted ester group after addition of *N*-Boc-3-(2-pyrazino) pyrrolidine was successfully converted to pyrazine ester **43**.

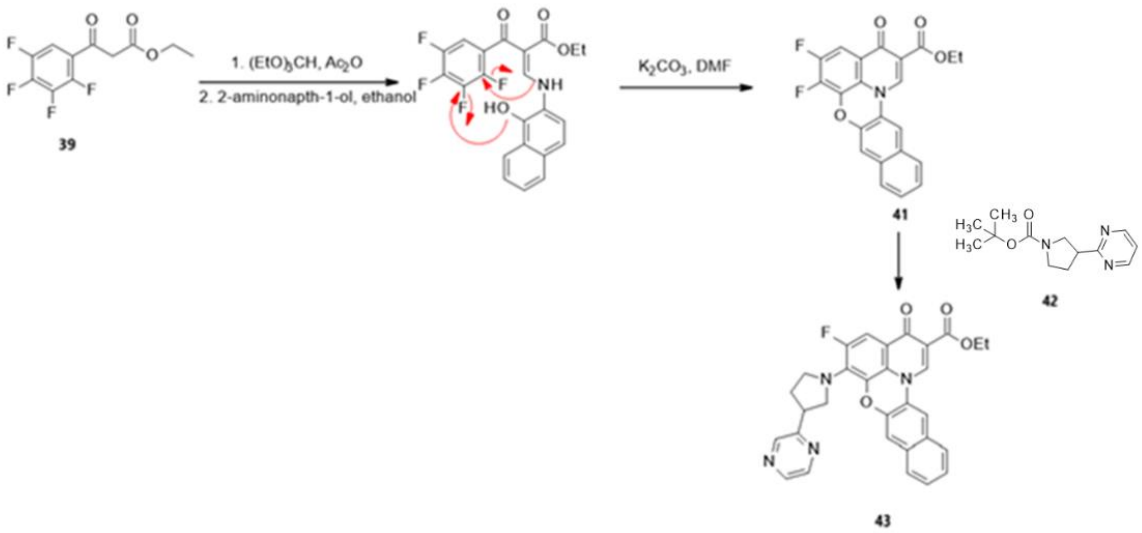

Scheme 5 Illustrated reaction schemes representing the conversion of tetrafluoroketoester **39** to pyrazine ester **43**.

This reaction step then was followed by coupling the 2-(2-aminoethyl)-l-methylpyrrolidine with pyrazine ester **43**, with addition of aluminium chloride to make the amide product which was named as Quarfloxin **15**.

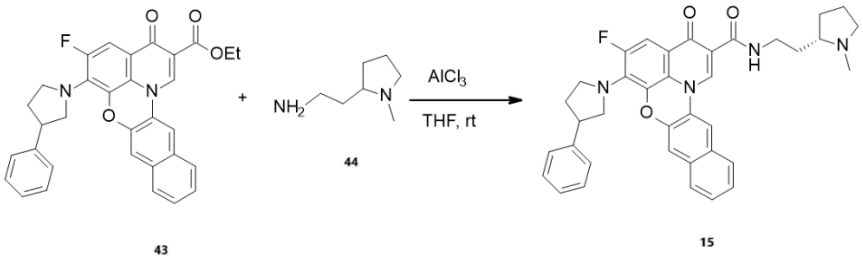

Scheme 6 Amide formation **15** using aluminium chloride to catalyse reaction between 2-(2-aminoethyl)-l-methylpyrrolidine **44** and pyrazine ester **43**.

1.12.5 Heck reaction

Based on the work done by Le Gresley *et al* (193), it was anticipated that a relatively straightforward synthesis of a range of novel acrylamides and their coupling *via* Heck reaction to brominated derivatives of the aforementioned classes of structure would afford a diverse range of potential G-quadruplex ligands, suitable for *in vitro* screening. The Heck reaction was discovered by T. Mizoroki and R.F Heck in the 1970's. Since its discovery, the Heck reaction has come to be one of the most commonly used palladium-catalysed carbon-carbon bond forming reactions for organic synthesis. The Heck reactions versatility comes from its ability to tolerate functional groups e.g. alcohols, carboxylic acids, esters and dienes (194). Because of this, several intermediates in drug discovery involve the Heck Reaction. An example is the active anti-cancer drug, taxol, which has an intramolecular Heck Reaction within its synthesis.

The Heck reaction consists of a soluble Pd catalyst, phosphine ligand and a base making up a homegenous medium. Precipitation of the Pd catalyst is prevented through stabilsation by the phosphine ligand, in aryl bromide reactions the tri-o-tolylphosphine, $P(o\text{-}Tol)_3$ was

found to be more effective than the first ligand used PPh_3. Catalytic regeneration is achieved *via* elimination of HX in the catalytic site by the bases within the medium (195). The Heck reactions C-C bond forming is *via* migratory insertion rather than reductive elimination like other palladium-catalysed cross-coupling reaction's. The traditional mechanism for the Heck reaction is presented in Figure 14.

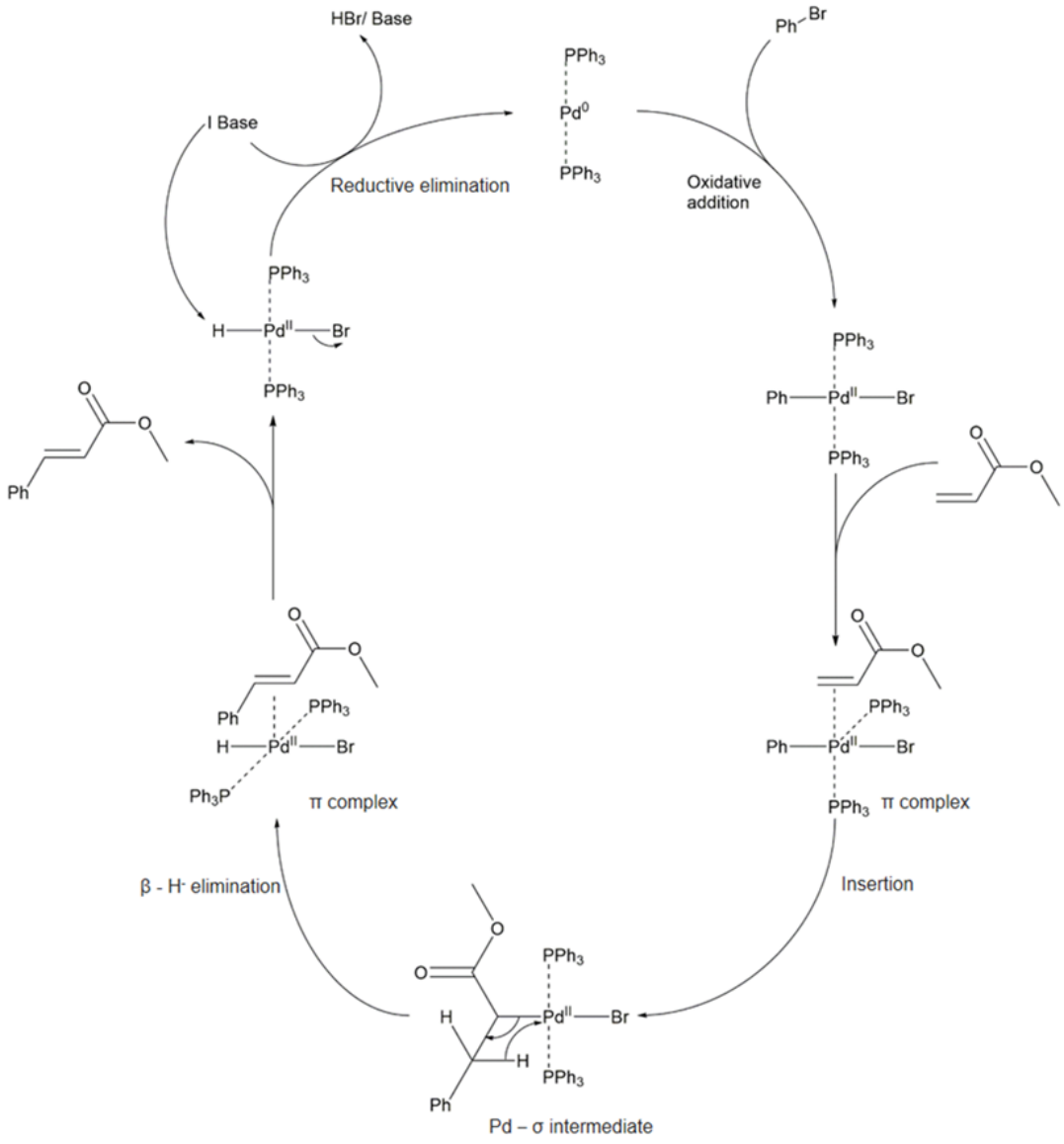

Figure 14 Heck Reaction

1.13 Characterisation techniques for G-quadruplexes

1.13.1 CD (Circular dichroism) spectroscopy

Several analytical techniques have been used to characterise G-quadruplex structures, differentiating between parallel/anti-parallel and different hybrid structures of G-quadruplex DNA. The most commonly used technique is Circular dichroism (CD) spectroscopy, as it allows for analysis of active chiral centres and specific spectra for each type of structural feature. This allows for identification of loop regions,parallel/antiparallel strands and is heavily used in protein research as the peptide bonds are optically active. Despite correlations between the G4 folding and final structure and CD spectra not being validated as of yet, we can still use the technique as a tool to empirically say whether one structure is different to another or comparable to a reference structure. Since CD spectra have been assigned for complete characterisation of many G4 structures in solution and validated *via* NMR and X-Ray crystallography, there is a precedence in place for this characterisation approach. An investigation of the G-rich DNA oligomer, MYC Pu27-Mer which is in the NHEIII1 region of MYC for example demonstrated a CD spectrum which had a broad peak at 240nm, with a large sharp peak at 260nm and a smaller peak at 212nm (196). This spectrum represents an intramolecular parallel G4 structure indicative of the MYC Pu27-Mer DNA oligomer as validated by NMR spectroscopy (197). We can also elucidate from CD spectra with similar features the presence of a hybrid parallel/anti-parallel G4 structure when a broad positive shoulder peak is seen between 280nm and 300nm. These spectral features are seen when the G-quadruplex of the oligomer Pu39WT in BCL-2 suggesting its structure, then further validated by NMR (90)(91). Thrombin binding aptamer (TBA) displayed a chair-type anti-parallel G-quadruplex structure as validated by X-ray crystallography and NMR (198). In the CD spectra a large positive peak was seen at 290nm, a smaller peak was seen at 246nm and a negative peak at 265nm, which is indicative from previous spectral analysis of the validated structure of TBA (108)(199). From these studies with several different analytical techniques alongside the use of other techniques, such as

the CD melting and UV absorbance at 295nm, other properties of G4 structures can be elucidated. These properties include the Tm, ΔH, and ΔG_0, which are crucial to determine the stability of the G4 structures, specifically in human telemetric G4s (200)(201)(202)(203).

1.13.2 NMR (Nuclear Magnetic Resonance) Techniques

The use of Nuclear Magnetic Resonance Spectroscopy (NMR) in the study of small molecules, peptide, proteins and nucleic acid structures has been widely used by many different types of researchers, from molecular biologists to organic chemists. The characterisation of G-quadruplex structures is therefore not surprisingly achieved in a lot of studies by a suite of NMR experiments. There are limitations however when we look at repeating motifs, which are required for the formation of G-quadruplex structures, as the chemical shift differences between the different motif units are not great which raises an issue of resolution within the NMR spectra. Ways of reducing the complexity of the spectra with either compound-based solutions, e.g. using two-fold or four-fold symmetric structures, or NMR techniques that are designed to increase resolution between respective peaks have been used. The limitation was highlighted in the first studies of telomeric DNA using NMR, which did not give sufficient structural information to fully characterise G4 structures however, it did show an abnormality in the structure of telomeric DNA. When the sequence d(TTGGGG)4 was used, NMR spectroscopy demonstrated that that the guanine residues took part in nonstandard base pairing (G-G) and that several guanines were in the *syn* conformation (204). The *syn* conformation was identified by Nuclear Overhauser NMR spectroscopy (NOESY), which showed a strong NOE effect between the protons of guanine at the 8 position (H8) and the HI' deoxyribose proton describing a short distance between the respective protons. Detailed characterisation of a G4 structure *via* NMR was achieved by studies on the oligomer d(GGTTTTTGG), which was previously elucidated to have a tetramolecular complex by calorimetric analysis (205)(206). The torsion angles of sequential glycosidic bonds were shown by NMR to alternate *syn-anti* wise for each adjacent guanine residue along the strand. This structure was also seen in sequences similar to the studied d(GGTTTTTGG), such as d(GGTTTTCGG) (206). Despite the prediction of alternating

glycosidic conformations *via* molecular modelling of the respective guanines that are involved in individual G-tetrads, the prediction of Glycosidic torsion angles along the strand is lacking. This gap in the knowledge was based upon an assumption that glycosidic conformation does not vary along the strand, as models of telomeric DNA structures using fibre diffraction analysis showed models structures with this property (207)(208). From the initial study using d(GGTTTTTGG) it was demonstrated that multiple conformers were seen in the NMR spectra, and that slow exchange was seen relative to the NMR timescale. It was also demonstrated that variation in the counter ion present within the tetrad, e.g. Na+ or K+ varied the structures formed by telomeric DNA, which also determined the relative stability of the structures formed (209). These studies were carried out using the oligomer d(TTGGGG)4 and d(TTAGGG)4 with either sodium phosphate or potassium phosphate buffers being used to determine the respective counter ion within the G-tetrad. Using the imino proton peaks within the spectra it was shown that multiple species of imino protons were present between residues at a high concentration, which was required for sensitivity of the imino protons. Chemical shift differences in the imino proton peaks for Na + and K+ were shown to be significantly different for both oligomers studied, while also demonstrating that K+ as a counter ion gave greater stability when compared to Na+. It was impressive also to see how thermally stable the K+ forms were with imino protons still being observable for the d(TTGGGG)4' oligomer specifically at 90 degrees.

1.13.3 X-Ray Crystallography

Studies on the oligomer d(GGGGTTTTGGGG) using both NMR analyses (210)(211) and X-ray crystallography (212) illustrated the presence of a G-tetrad core structure along the strand. Torsion angles calculated for glycosidic bonds showed alternating *syn/anti-syn* conformation along the residues and specifically in regions related to G-tetrad structures. The presence of thymine within the strands create loops at the opposite ends of the G-tetrad core in a head to tail shape with X-ray crystallography showing the joining of adjacent strands which could not be interpreted with only NMR spectroscopy. Resolution limitations in NMR which prevent the characterisation of several structural features are revealed by the

interpretation of X-Ray crystallographic date. Specifically, it showed that the base geometry in G-tetrads is often distorted from the regular square planar arrangement of guanine bonding. It also highlights that the guanines are pushed out of the plane of the G-tetrad, with the core of the tetrad having an electron density correlating to a bound potassium ion. It was shown that the ion is located between the second and third G-tetrad in the core of the structure.

Looking at the different aspects, G-quadruplex ligands are widespread and can be found in every part of biology. From cell maintenance in bacteria and virus infected cells to a role in the onset of cancer G-quadruplexes have been shown as a key target for therapeutic remedies. Many research groups have done work to synthesise and validate G-quadruplex ligands. Different classes of G-quadruplex ligands have been developed and been tested for anticancer activity. Through the research, many of these ligands were active, however, most of them did not show selectivity for G-quadruplex DNA. From the research only BRACO-19 and Quarfloxin went through to clinical trials, however due to their toxicity they did not successfully pass the trials. This failure to get passed clinical trials, demonstrate the need for more selective and specific compounds to be designed to allow for a new class of drugs with lower toxicity.

Chapter 2 – Aims

The aim of this research was to synthesise a range of G-quadruplex ligands and to build on previously synthesised G-quadruplex ligands. These ligands would be designed to have lower toxicity compared to current ligands through greater selectivity for G-quadruplex structures over duplex DNA. To address this challenge, a series of planar building blocks were to be functionalized with a range of amine groups. These amine groups were selected based upon the physiological generation of positively charged side chains that would bind to the negatively charged phosphates in the ribose backbone in an orientation specific to G-quadruplexes. These amine groups were selected based upon the properties previously shown to have lower IC_{50} values in telomerase activity (213). These properties include more than two aminoalkyl/amido side chains, length of linker between charged nitrogen atom and amide group needs to be two methylene units. In addition to these properties, the chosen planar skeleton needs to be close to the width of a G-quartet, to allow attached amine groups to improve the binding of the ligand. If the chosen linker includes heterocyclic amines, this has been shown to make it a more effective ligand and the position of heterocyclic groups within the structure has also been shown to be important (213). Careful considerations of these properties allowed the construction of a library of potential G-quadruplex ligands.

Our approach to synthesising these ligands was to create a static combinatorial library using Heck methodology, EDCI.HCl coupling and reversible imine formation. Building these static compounds will generate different types of ligands by the combination of simple building blocks with different coupling methodologies. Through this, the most active and stable compounds would be chosen to work with. Heck methodology (Scheme 7) has been used by Le Gresley *et al*. (193) using 9,10-dibromoanthracene **45** seen in Scheme 11, a planar lipophilic core that acts as a hydrogen bond donor and acceptor *via* the branches in the 9 and 10 positions. This afforded potential ligands for assessment using first ^{1}H DOSY NMR and then cell-based assays. In their work, they chose a variety of amine groups which were converted to acrylamide using acryloyl chloride, This was then coupled using $Pd(OAc)_2$ to make diacrylamide derivatives for evaluation.

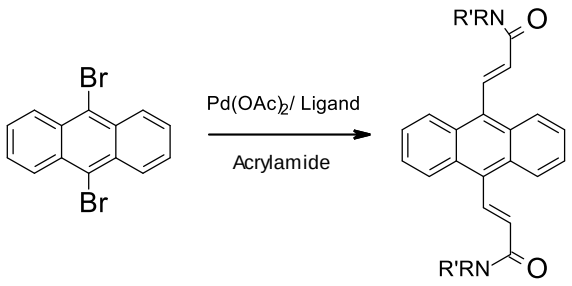

Scheme 7 Heck Coupling of acrylamides to 9,10 – dibromoanthracene.

In addition to this work, Le Gresley *et al.* endeavored to build dynamic combinatorial libraries of G-quadruplex ligands using a conjugate addition (Scheme 8) (214).

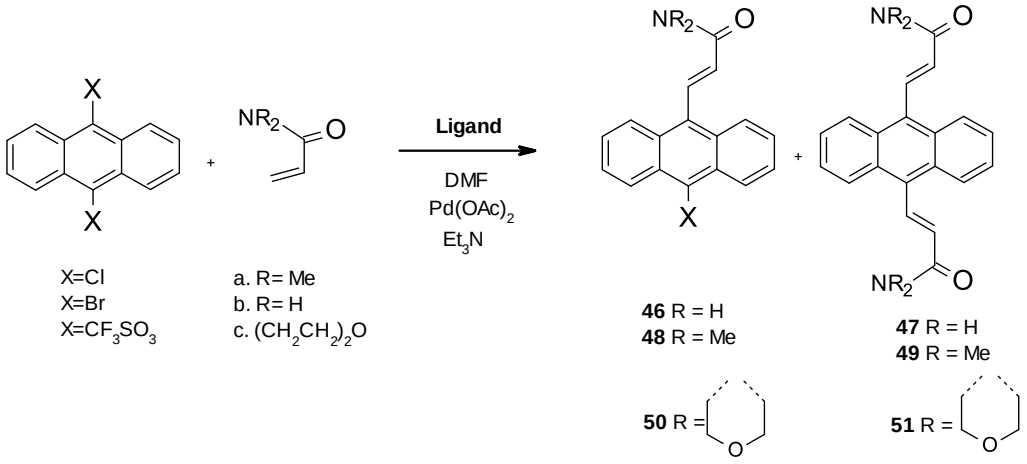

Scheme 8 Bis-acrylamide derivatives of anthracene synthesized by the Le Gresley group.

They synthesized and characterized the compounds **46**, **47** and **48**, then these compounds were tested on MCF-7 cancer cell lines and shown to have acceptable Log P values.

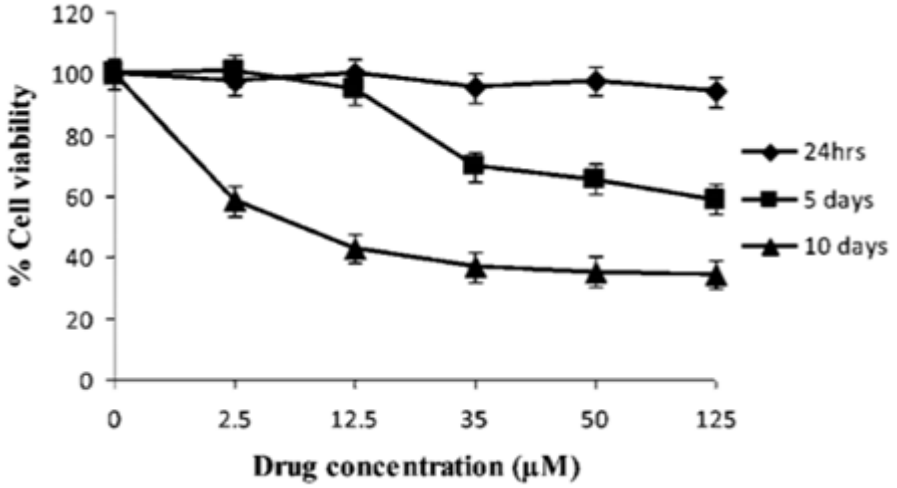

Figure 15 Graph showing MCF-7 cell populations after 48hrs in the presence of a concentration range of **47** (193).

From this work, this anthracene diacrylamide class of G-quadruplex ligand **47** has shown sufficient anticancer activity to make this template worthy of further investigation, in terms of selectivity for both duplex and G-quadruplex DNA. The aim was also to expand the series of G-quadruplex ligands based on the 9,10-dibromoanthracene core and to understand how the structure effects the activity through QSAR analysis.

Where the selected amides were not compatible with Heck coupling conditions, direct EDCI.HCl couplings were considered and, towards the end of the project, investigations into reversible imine formation to generate a static combinatorial library of potential G-quadruplex ligands.

Standard peptide coupling using 1-ethyl-3-(3-dimethylaminopropyl) carbodiimide (EDCI), was undertaken, where limitations were observed for Heck coupling conditions, where the palladium catalyst can be deactivated under certain conditions where unwanted complexation of the palladium catalyst with the acrylamide to be coupled can inhibit the catalyst. An example of this is where EDCI coupling could be used after initial acrylate formation via Heck reaction and hydrolysis (Scheme 9).

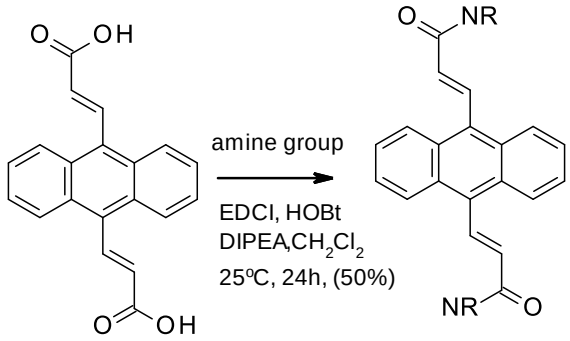

Scheme 9 Synthetic routes for EDCI coupling

Being reversible and thermodynamically driven imine couplings could allow us to exploit selectivity when combining amines with an anthracene aldehyde derivative (Scheme 10). This would allow for a more diverse range of amino groups being coupled to the planar templates.

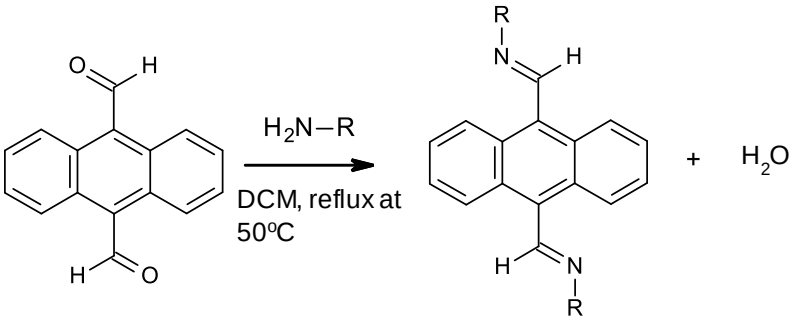

Scheme 10 Synthetic route for imine couplings.

In addition to expanding on the anthracene derivatives to optimise binding to G-quadruplexes, a series of other coupling templates were considered (Figure 16).

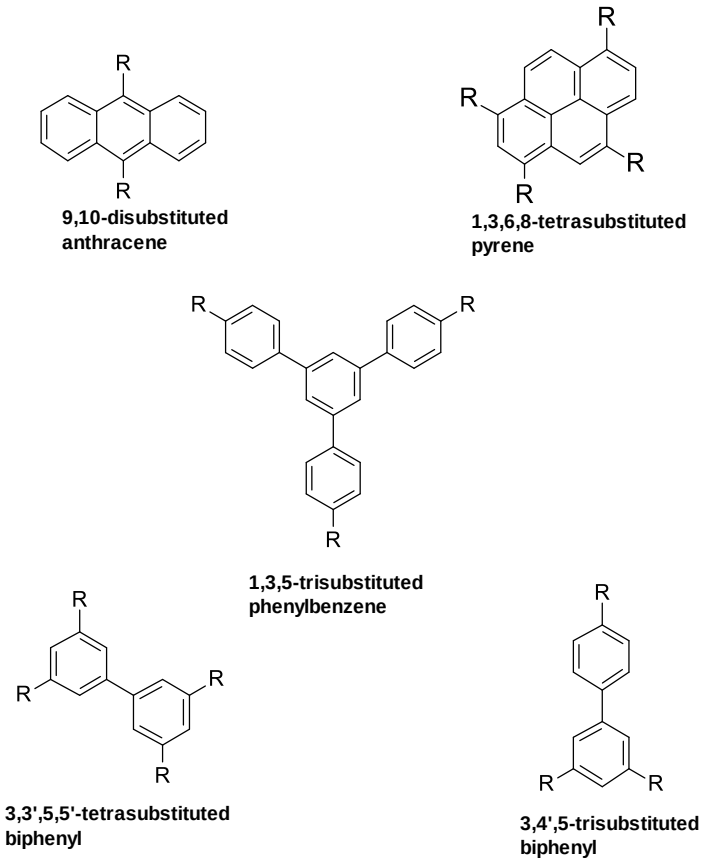

Figure 16 Illustrated structures are the skeleton templates for modification, which were used in this research.

The aim was to optimise the synthesis of a range of amide/imine derivatives of the templates in Figure 16 to ascertain the best binding motif for the G-quadruplex. Finding the best array would then allow us to build a dynamic combinatorial library, an approach to molecular design where building blocks construct libraries of complex structures through reversible chemical reactions which favour thermodynamically stable structures, of these ligands (215).

After the synthesis of a static library of G-quadruplex ligands, these were to be screened for anti-cancer activity through the use of cell culture assays such as, MTT assay, Natural Red Assay and Presto Blue assay. Use of multiple assays gives greater validation of results. These assays were to be done with HeLa cancer cell lines with positive and negative controls to confirm the activity to validate that activity is related to drug (ligand) concentration. Statistical analysis (one sample t-test) was then to be used to rank the activity

of compounds through their IC_{50} values and respective R^2 values. This would allow us to compare the dose response and order of the kinetics. MTT assay assesses the metabolic activity of cells by colorimetric assay which determines cell viability (Figure 17). The colorimetric assay works through the conversion of tetrazolium to formazan by NAD(P)H-dependent cellular oxidoreductase enzymes.

Figure 17 Mitochondrial reduction of MTT to blue formazan product.

This MTT assay allows measurement of cell proliferation and degree of cytotoxicity from added drugs.

The MTT assay is shown to work through a chemically reductive mechanism, however neutral red and presto blue work through a staining and an environmental reductive mechanism. These differences would allow us to determine which technique gives the most reliable results. Neutral red assay determines the number of viable cells and cytotoxicity of drug. The neutral red assay is adapted from histological methodology through staining of lysosomes by eurhodin dye which gives a red colour. If cells are killed or made non-viable, they cannot absorb the stain into lysosomes, therefore a reduction in neutral red intensity correlates to a loss of viable cells with a lower abundance of lysosomes (Figure 18).

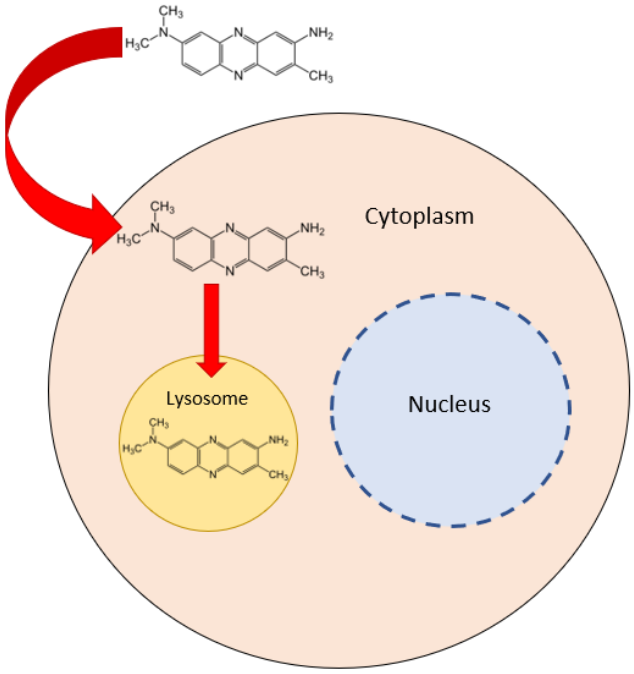

Figure 18 Diagram illustrating mechanism of Neutral red assay**.**

In addition to these two cell assays, Presto blue was used to determine if the cells are alive and healthy. Presto blue reagent consists of resazurin-based solution, which, when in a healthy cells cytosol, will be reduced (Figure 19).

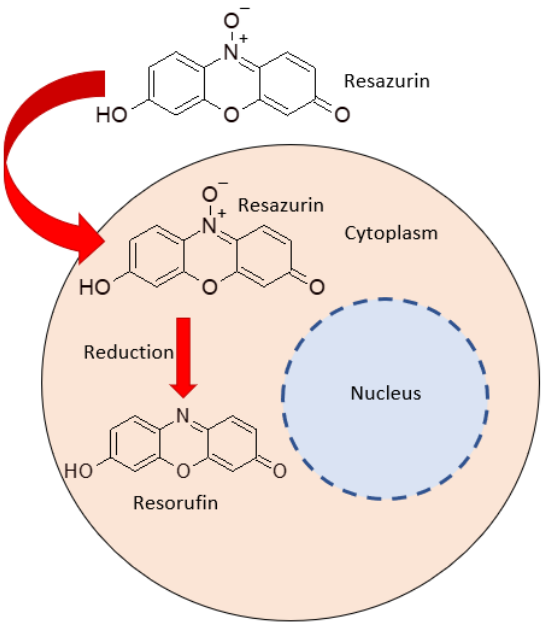

Figure 19 Diagram illustrating mechanism of Presto blue assay.

Following on from this, the compounds that show anti-cancer activity, were further screened for G-quadruplex intercalation to measure whether the ligand structure forms through space bonds with a telomere G-quadruplex model. This screening was also used to demonstrate the likely stoichiometry of ligand to G-quadruplex structure. These insights into structure activity relationship give insight into what parts of the ligand structure are important for intercalation to G-quadruplex structure and therefore would correlate to an inhibitory effect on telomerase.

Combinations of these analytical techniques will give a wide picture of which ligands are best suited for further investigation and modification as drug targets for G-quadruplex targeting drugs in cancer therapies.

Nuclear magnetic resonance (NMR) spectroscopy was selected as the technique to investigate the structures formed by model oligonucleotides under physiological conditions and screen for interactions of compounds that showed activity against HeLa Cells. NMR spectroscopy has been used to assess the synthesised ligands. This was selected owing to the numerous validated protocols already in place (216).

NMR spectroscopy benefits from the ability to study G-quadruplex structures in physiological relevant models. Whereas X-Ray crystallography, which is excellent in distance measurements and structural characterisation, lacks this benefit. NMR also provides detail on kinetics, dynamics, and concentrations, which are powerful tools in the classification of G-quadruplex ligands.

This technique was used to identify structures that bind to the G-tetrad structure and the type of binding. Be it the more common stacking on the terminal G-quartet or less common binding to the groove of the G-tetrad structure. These binding/stacking mechanisms can be determined through the observation of not only the G-tetrad region spectra, but also the 3'- and 5'- adjacent nucleotides, which will have major structural changes, if capping or binding occurs at these locations, to allow for accommodation of ligands. Analysis of the spectra also allows for determination of the exchange kinetics and stoichiometry of each ligand

allowing kinetic and dynamics analysis alongside the structural information. This information was to help explain the IC_{50} values determined through cell culture studies. With this analysis, however we must remember to highlight the limitations of our G-quadruplex oligomer model when comparing to in-vivo telomere G-quadruplex structures and the conclusions we can come to. Despite the limitations of model systems, the aim was to allow future considerations on structure-based drug designs, with decisions made on what parts of the ligand are key and what parts can be optimised for ligand activity and preferential binding mode.

Determination of G-quadruplex structure by NMR from a practical aspect is made simpler through the appearance of the imino peaks of guanine at a chemical shift range of 10.5-12 ppm which is characteristic of G-tetrad formation (Figure 20). These peaks are seen to be distinctly separated from other DNA structure imino peaks with high resolution. This means that monitoring of these peaks allows for determination of G-tetrad formation and any disturbance to these peaks or changes will allow for screening of drug binding interactions. We can also determine the number of guanines associated through Hoogsteen hydrogen bonded G-tetrads through the number of imino H -1 protons in the 10.5 – 12ppm range. These experiments were run in a H_2O-D_2O solution with water suppression to allow for reading of the spectra and interpretation of imino peaks.

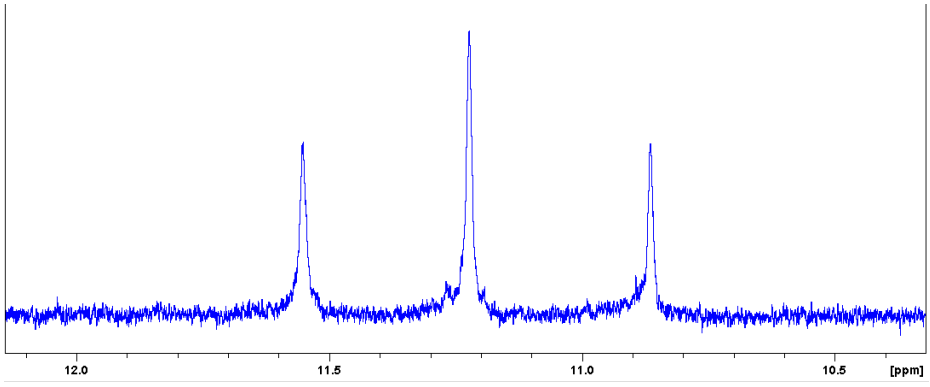

Figure 20 Typical imino protons representative of G-tetrad formation.

The model system used was parallel, tetrameric system to allow for easier identification of peaks. The reason for this is that it has been demonstrated that each monomer in the tetrameric system will present with the same spectra, therefore giving an amplification of

spectra by four rather that giving four overlapped spectra. This simplification of spectra is also required, as assignment of added drug will be done to demonstrate changes in chemical shift and diffusion coefficients properties of ligands as demonstrated in Figure 21.

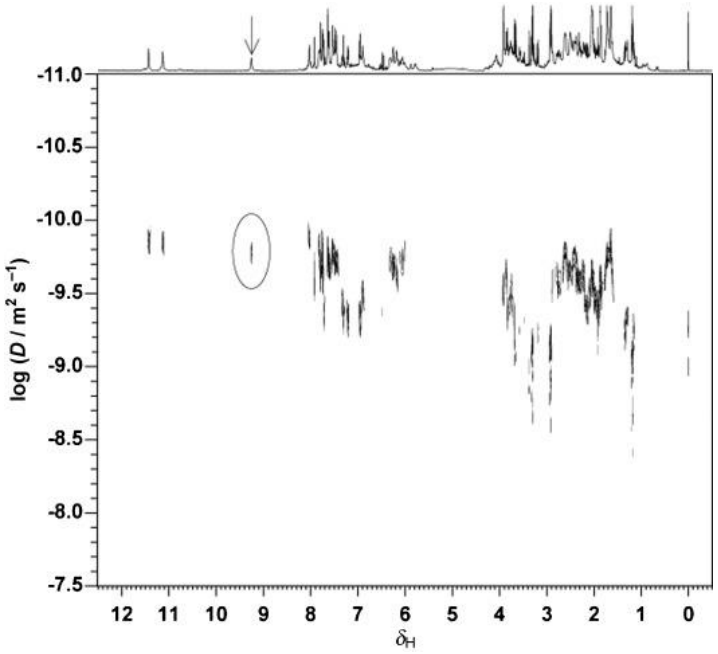

Figure 21 DOSY analysis of a mixture of PE (1.0 mg mL−1) and d(TTGGGTT)4 (0.25 mM). The peak of the d(TTGGGTT)4 ligand(s) is designated by "↓" in the F 2 projection. (Taken from (217)).

Chapter 3 – Results

The aim of this project was to synthesise a library of novel G-quadruplex intercalators based on anthracene and other phenyl-rich arrays. The compounds synthesised were based on the below structure motifs (Figure 22) with cytotoxicity and their ability to intercalate the G-quadruplex being evaluated. This evaluation was done using Presto Blue Assay and NMR titration techniques with a G-quadruplex aptamer.

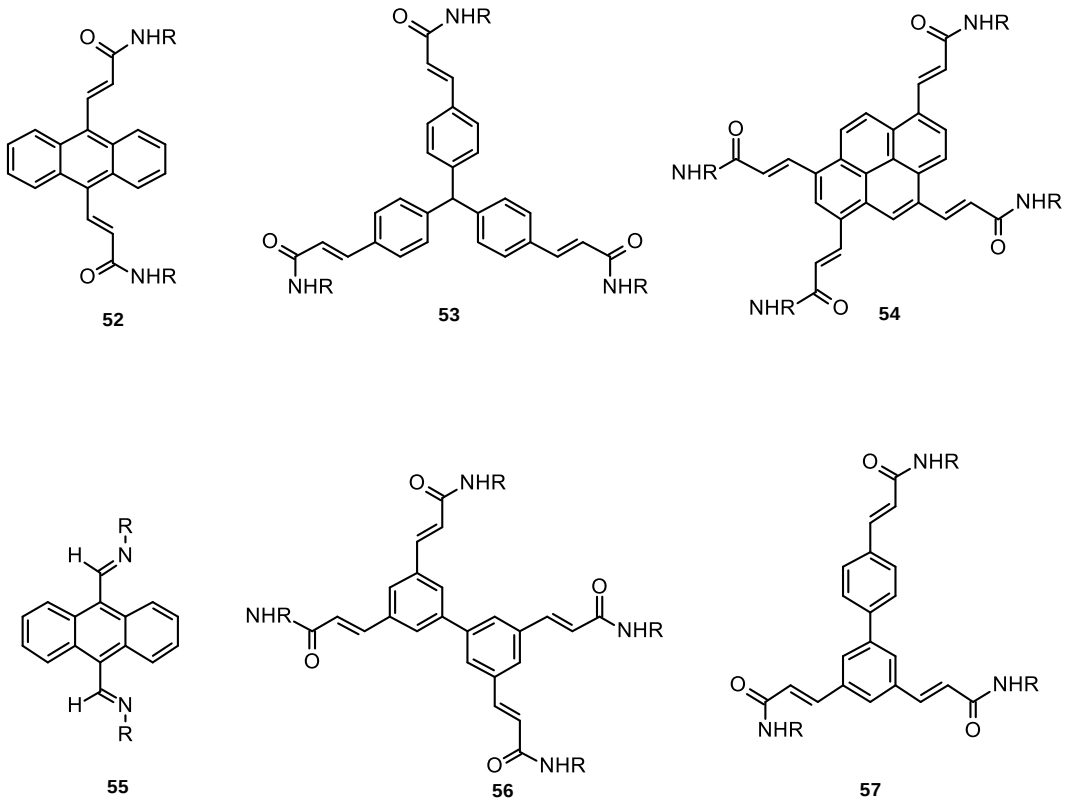

Figure 22 Templates for G-quadruplex ligand development **52-57.**

A number of anthracene-based diacrylamides were synthesised by Le Gresley *et al*. (193) and they generated a small library of G-quadruplex ligands. This was primarily done via coupling of 9,10-dibromoanthracene **45** *via* the Heck reaction. These acrylamides were specifically chosen to provide a greater degree of polar/ hydrogen bond binding to the phosphate backbones of quadruplex DNA. Our research was to develop these previously synthesised acrylamides and built a larger library of G-quadruplex ligands.

3.1 Synthesis of Acrylamides for the Heck reaction

One of the potential methods for synthesising derivatives for the **52-57** classes of compound would be to couple the appropriate acrylamides directly. To enable this, synthesis of a range of acrylamides was undertaken. They were synthesised under dry, standard conditions, i.e. dry DCM was used as a solvent. 2 eq. of triethylamine and 1 eq. of the amine group were then added into DCM. Following this 1.2 eq. of acryloyl chloride was added in a drop wise manner over 5 minutes, while the reaction was in an ice bath. The reaction mixture was warmed to room temperature and stirred for 1 hour. TLC and NMR were used to monitor and characterise the reaction mixture.

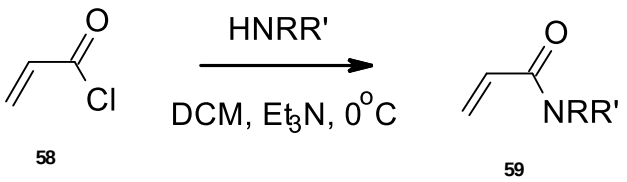

58 59

Figure 23 Synthetic route for acrylamides (based on proposed amines in Figure 24).

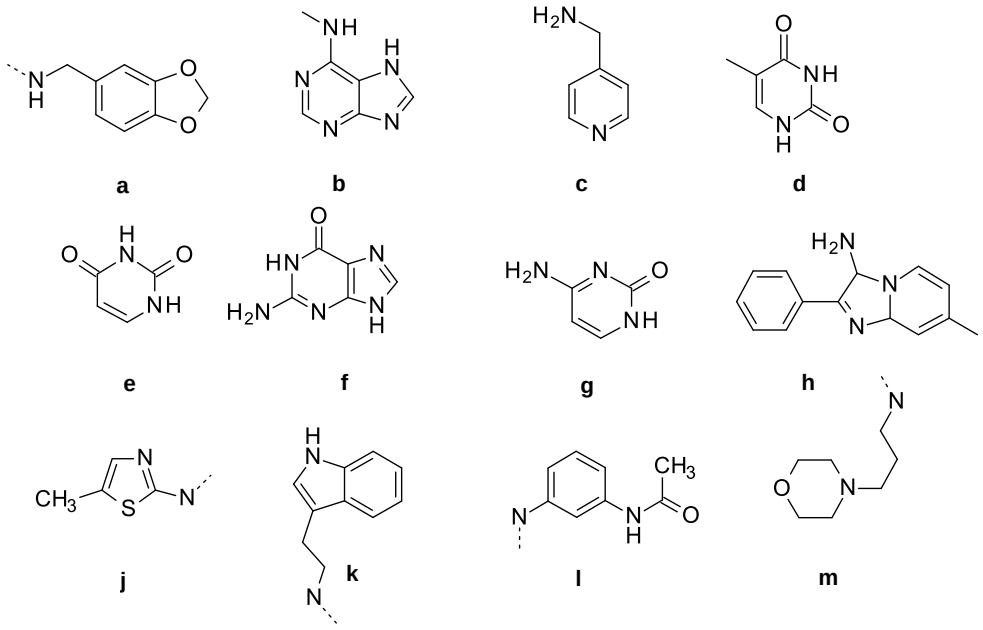

Figure 24 Amine groups (**a-m**) to be used the synthesis of acrylamides.

Table 1 Reaction data for acrylamides **59a-h** (Figure 24) in coupling reactions with 1 in an 8:1 ratio

*very low yield was obtained, as products were unable to be separated from the reaction mixture.

Amine group	Acrylamide	Duration/h	Yield (%)
a	**59a**	72	82.5
b	**59b**	72	5 (crude)*
c	**59c**	150	5 (crude)*
d	-	72	-
e	-	72	-
f	-	72	-
g	-	72	-
h	-	48	5(crude)*

The amines **a**-**h** were chosen based on possessing complimentary binding motifs to the G-quadruplex and there being literature precedent to support potential anticancer activity e.g. piperonylamine contains a benzodioxole ring which is a H-bond acceptor and are found in anticancer drug analogues of capsaicin (218), 4-(aminomethyl) pyridine was used because of previous literature stating its anticancer activity within certain derivatives which targets

G-quadruplex DNA (219). Adenine/Guanine/Thymine and Cytosine were chosen, because they are nucleic acids groups in human body and there exist potential interactions with G-quadruplexes through their H bonding in Hoogsteen base-pairing in DNA (219). The amine groups **j-m** were used to synthesise imine derivatives (in section **3.6**).

A representative piperonylamine acrylamide was synthesised (shown in Figure 25) and confirmed using NMR as seen in the assigned spectra at 5.6ppm(H-6), 6.2ppm(H-4) and 6.3 ppm(H-3); the peaks for the H_a,H_b and H_c of the acrylamide with integrals matching that expected. The integrals are calibrated to that of the piperonylamine peaks at 4.3ppm (H-7), 6.8ppm(H-2),6.9(H-1) ppm and 6ppm(H-5), which have the correct ratio of integrals.

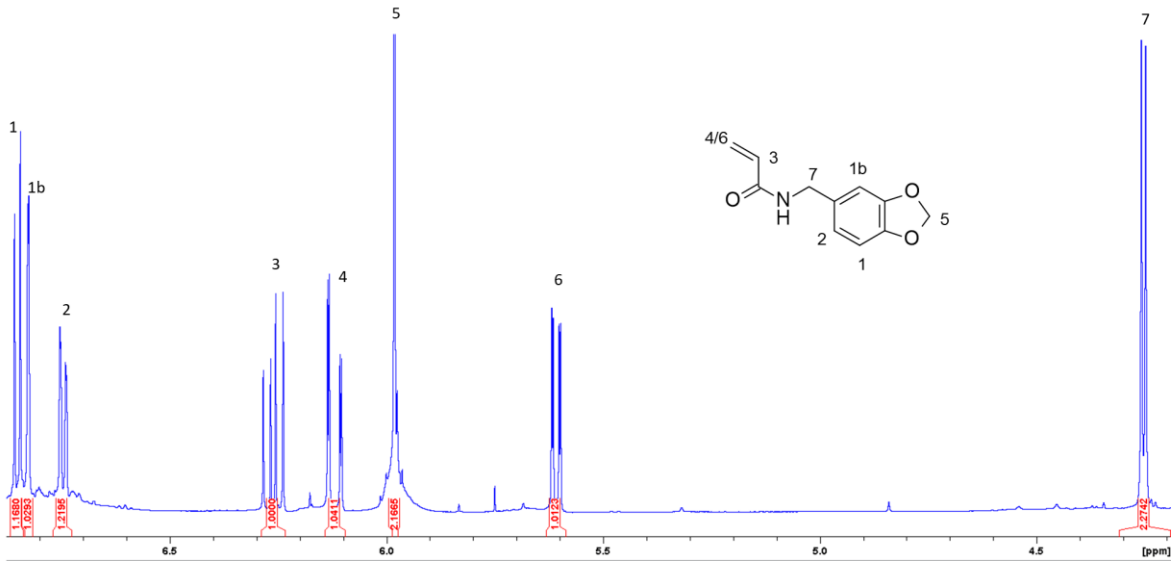

Figure 25 1D-1H assigned spectra of **59a.**

However, as evidenced by Table 1, some of the amines did not prove amenable to conversion into the corresponding acrylamide through coupling to acryloyl chloride.

Therefore, rather than persist in attempting to synthesise the derivatives **59d-h** the decision was made to attach those amines directly via carbodiimide coupling from **52**. (Figure 22) With the piperonylamine acrylamide **59a** in hand we proceeded to couple it to **45**. However, repeated attempts to couple it to 9,10-dibromoanthracene *via* Heck reaction were

unsuccessful. This was potentially because of the acidic acetyl group possibly reacting with the palladium catalyst or causing deacetylation and deactivation of the catalyst through cHeLation. The initial reaction conditions were changed such as changing to Schlenk tube from reflux and introducing a new ligand (DPPP (1,3-Bis(diphenylphosphino)propane, Triphenylphosphine and Tri(o-tolyl)phosphine). These changes did not allow the coupling of the piperonylamine; therefore, a different synthetic route was chosen.

After issues with acrylamide coupling to 9,10-dibromoanthracene (shown in Scheme 11). We ordered two acrylamides to test the Heck coupling to anthracene. Firstly *N*-(butoxymethyl) acrylamide, which was successfully coupled to 9,10-dibromoanthracene with the Heck reaction followed by successful coupling of *N*-(isobutoxymethyl) acrylamide to 9,10-dibromoanthracene. For these couplings we used tri-(*o*)tolyphosphine rather than DPPP as the ligand.

It was possible to source brominated precursors for the general templates **52-57** (Figure 22) such as 9,10 dibromoanthracene **45** (Scheme 11)**.** This facilitated the direct synthesis of a range of acrylamide derivatives of the **52** type using 0.2 eq. of palladium acetate and 0.2 eq. of phosphine ligand in a Schlenk tube, followed by stirring in DMF (Dimethylformamide) for 10 minutes at room temperature to generate the catalyst first. After activating the catalyst 8 eq. of trimethylamine and 1 eq. of 9-10-dibromoanthranece **45** were added to the reaction mixture, at room temperature, followed by addition of 8 eq. of selected acrylamide. The mixture was heated to 90°C for 48 hrs under nitrogen to yield compounds of the type **60** (Scheme 11).

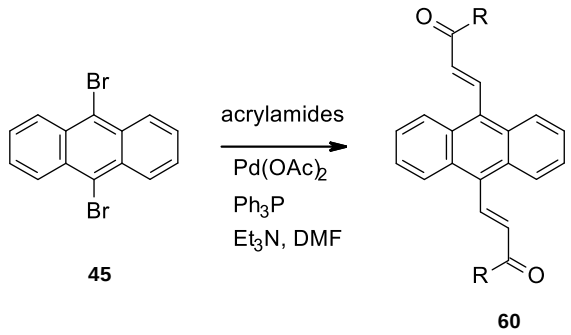

Scheme 11 Synthesis of diacrylamide derivatives via Heck reaction.

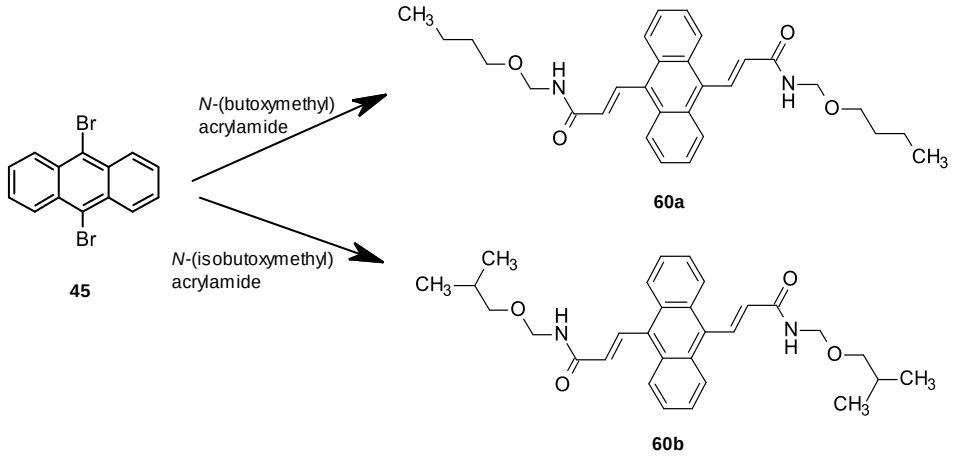

Scheme 12 The synthesis of **60a** & **60b** via Heck coupling; reagents and conditions: $Pd(OAc)_2$/ $(o\text{-}Tol)_3P$/ Et_3N/DMF.

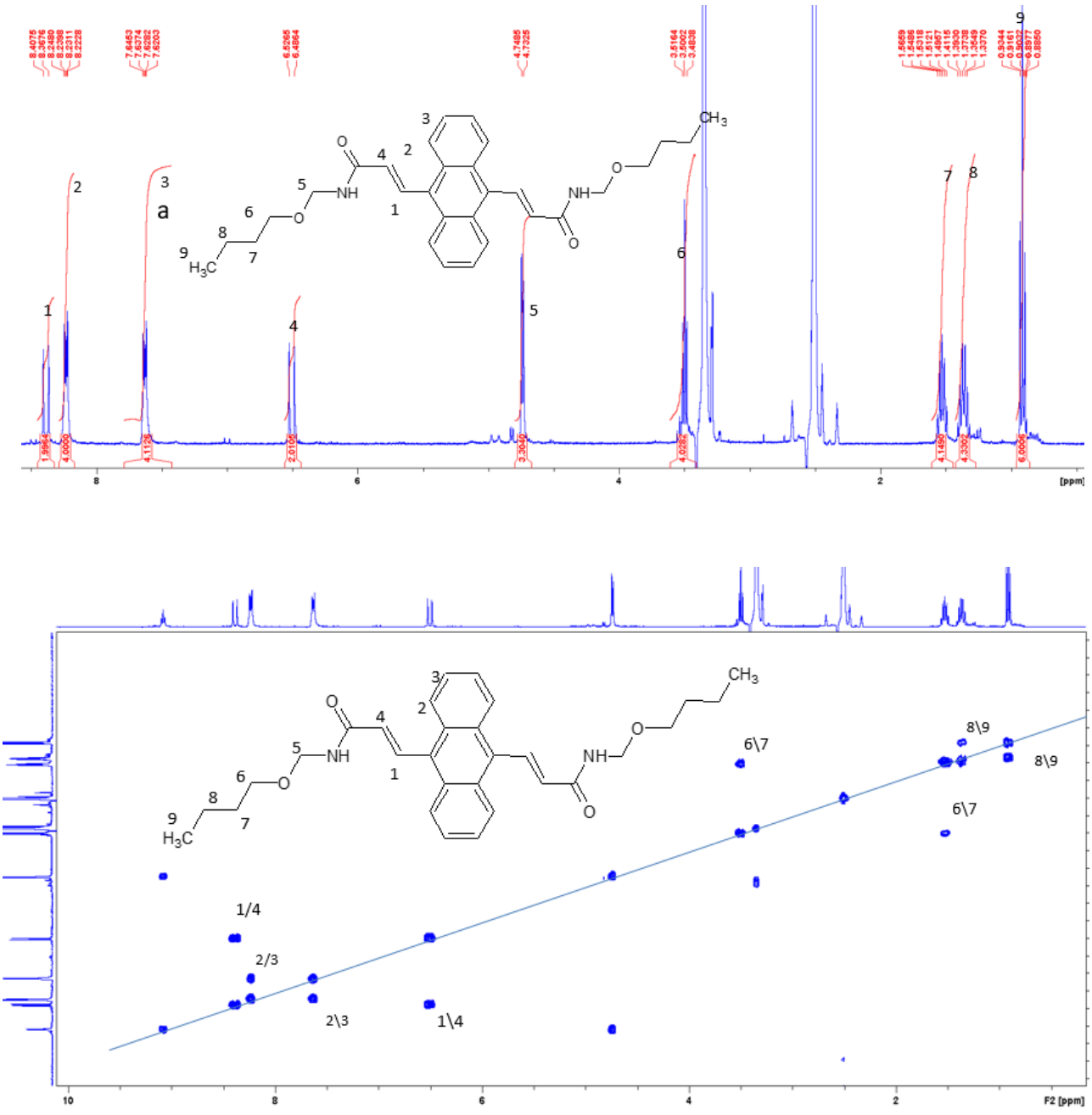

Figure 26 1D-1H and 2D-1H/1H COSY assigned spectra of **60a**.

The synthesis of the *N*-(butoxymethyl) acrylamide (**60a**) (shown in Figure 26) was validated using NMR in (DMSO-d_6) as seen in the assigned spectra at 4.2ppm (H-5) and 8.1ppm (H-2), the peaks for the added alkyne bonds with integrals matching that of the expected integrals when calibrated to anthracene ring. In addition to this spectrum, *N*-(butoxymethyl)

acrylamide had a COSY experiment also run to validate assignments at 0.9ppm (H-9) and 1.4ppm (H-8) for assigned protons 8 and 9. Moreover, the cross peak at 1.6ppm (H-7) and 3.5ppm (H-6) for assigned protons for 6 and 7. These assignments validate the integrals calculated for the 1D spectrum.

Despite having synthesised a number of acrylamides for palladium-catalysed coupling, in our hands we found the Heck coupling to be largely unsuccessful, affording either intractable mixtures, or such poor yields as to make the synthesis of such ligands not viable.

Faced with difficulties in synthesising some of the more interesting acrylamides and poor yields from Heck couplings, it was decided to synthesise the corresponding acrylates and hydrolyse them for amide coupling reactions with EDCI. A Heck coupling of methyl acrylate to 9,10-dibromoanthracene was carried out, to build a more stable scaffold for coupling of amine groups, followed by hydrolysis of the methyl group to carboxylic acid. This would then allow, for example, EDCI.HCl coupling of piperonylamine to the carboxylic acid group to form piperonylamine coupled to 9,10-dibromoanthracene **45**.

Successful coupling of methyl acrylate is shown in Figure 27. The assigned spectra consist of peaks related to *trans* alkynes of the methyl acrylate 6.3ppm (J = 16.81 Hz, H-4) and 8.3ppm (J = 16.25 Hz, H-1). Also, a peak for the methyl group next to the carbonyl group at 3.9ppm (H-5). The corresponding integrals for these peaks match those expected when coupled to 9,10-dibromoanthracene with its peaks seen at 7.3ppm (H-3) and 8.1ppm (H-2). Therefore, the next step is hydrolysis of the methyl acrylate group which is shown in Figure 28. From Figure 28 the carboxylic acid group at 12.2ppm (H-5) alongside the methyl groups disappearing at 3.9ppm. Alongside the rest of the coupled product peaks not changing, hydrolysis is validated by the presence of the methyl group.

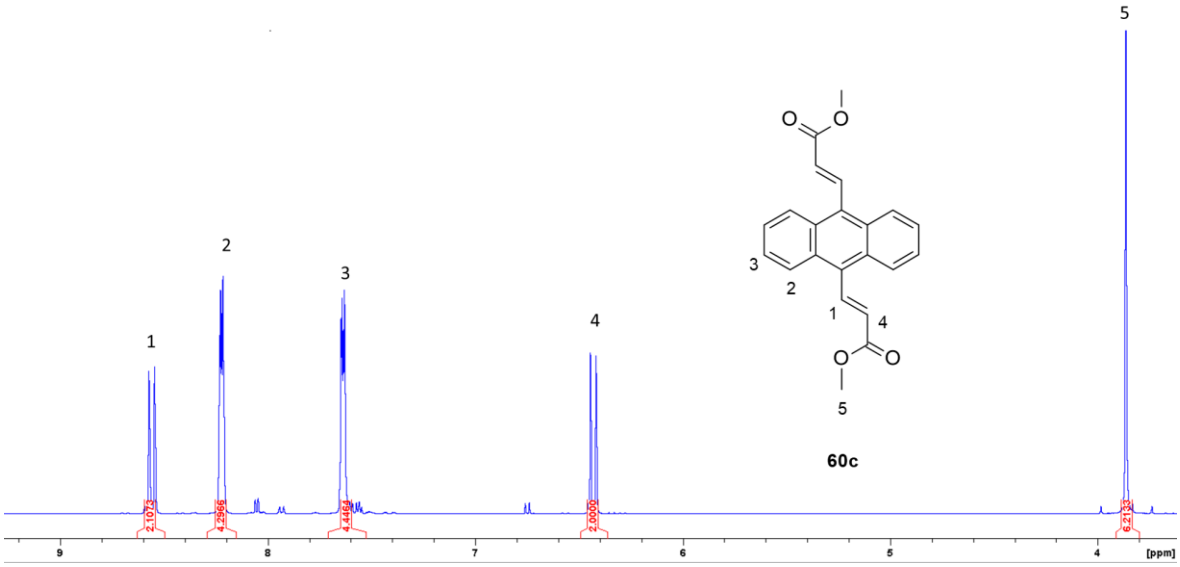

Figure 27 Assigned NMR spectra and structure representing coupled methyl acrylate to **45 (60c)**.

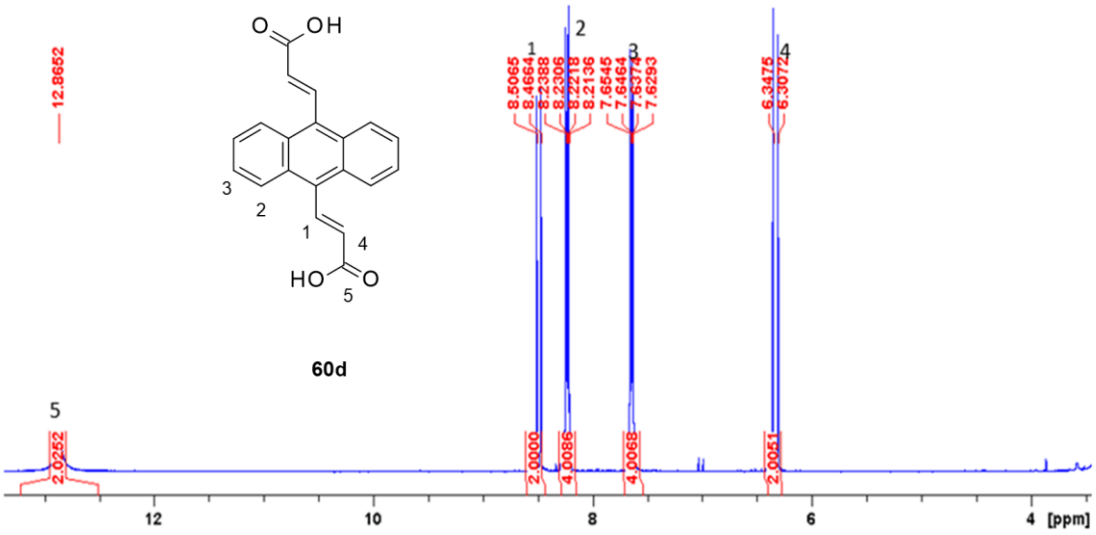

Figure 28 Assigned NMR spectra and structure representing hydrolysed structure of **60c (60d)**.

3.2 Electrophilic substitution reaction of anthracene

Whilst the novel palladium-coupled substitution of synthesised acrylamides in the case of **45** was largely unsuccessful, we wanted to investigate the possibility of coupling more than two acrylamide groups per aromatic core. This idea was conceived because of the properties of the G-quadruplex, specifically the four phosphate ions present in the backbone of each parallel tetrad of the G-quadruplex. Our thinking was that three or four ionisable amine groups binding to phosphate ions would give greater affinity than two.

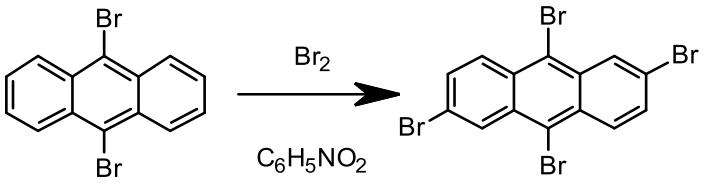

45 **45a**

Scheme 13 Proposed synthetic route for **45a**.

We aimed to synthesise 2,6,9,10-tetrabromoanthracene **45a** following the procedure by Rosso *et al*. (220) using a solution of bromine in nitrobenzene with addition of 9,10-

dibromoanthracene. Steric hindrance favoured the addition of bromine atoms to the para position relative to the ortho position of each individual aromatic ring in anthracene. This favourable addition at the para relative to ortho position of one bromine unit would then preferentially promote addition at the para position relative to the first added bromine. This reaction did not work as the addition of bromine de-activates the ring. The desired product was not synthesised in significant yields, with the predominant products being brominated anthracene with substitution on both sides at the ortho position relative to the bonds between aromatic rings.

The reaction protocol was carried out using a Schlenk tube with a separating funnel attached for addition of reagents. Firstly, 9,10-dibromoanthracene **45** was added and then it was mixed with nitrobenzene (3.5ml). The solution of 9,10-dibromoanthracene in nitrobenzene was then heated to 100^0C. When the temperature was stable at 100^oC, 0.19 ml bromine in 0.5ml nitrobenzene was added dropwise into reaction mixture through a separating funnel. Following the addition of bromine, the reaction mixture was heated up to 160^oC for 5 hrs and then warmed to 200^oC for 30mins. After this, it was left to stir at room temperature. TLC analysis was used during the experiment to monitor the reaction. The whole reaction was filtered and washed with water followed by DCM (3X15ml) and the resulted precipitate was analysed using NMR.

A small quantity of bromine was still present in the reaction; therefore, the reaction could be quenched by the addition of aqueous sodium dithionite $Na_2S_2O_4$ (20%,50ml).

After numerous unsuccessful attempts, varying temperature, duration, and stoichiometry, we decided to find a different type of aryl core with 4 or 3 bromo groups on the ring system.

1,3,6,8-tetrabromopyrene **61** and 3,3',5,5'-tetrabromo-1,1'-biphenyl compounds **62** (Scheme 14) were chosen to work with the Heck reaction because of favourable steric considerations.

The initial reactions attempted featured the coupling of acrylamide to 1,3,6,8-tetrabromopyrene **61**. For this, $Pd(OAc)_2$ (86.2mg) and Tri(o-tolyl)-phosphine (115 mg) were placed in a Schlenk tube and mixed with DMF (20 ml). Following this, acrylamide (1 g), 1,3,6,8-tetrabromopyrene (250mg) and triethylamine (2mL) were added. Same as previous reactions, the mixture was heated up to 90^oC and left for 24 hrs. This reaction did not successfully take place, potentially owing to solubility issues. Several other solvents were tested in order to enhance the solubility. The choice of the solvents was investigated through a small volume solubility testing.

Table 2 Reaction conditions tested in order to couple acrylamide onto 1,3,6,8-tetrabromopyrene via Heck Reaction.

Conditions	Results
DMF, $Pd(OAc)_2$, tri-(o-tolyl)phosphine,Et_3N, 90^oC	No reaction
Toluene, $Pd(OAc)_2$, tri-(o-tolyl)phosphine,Et_3N, 90^oC	No reaction-insoluble
DCM	No reaction-insoluble
Acetonitrile	No reaction-insoluble
MeOH	No reaction-insoluble

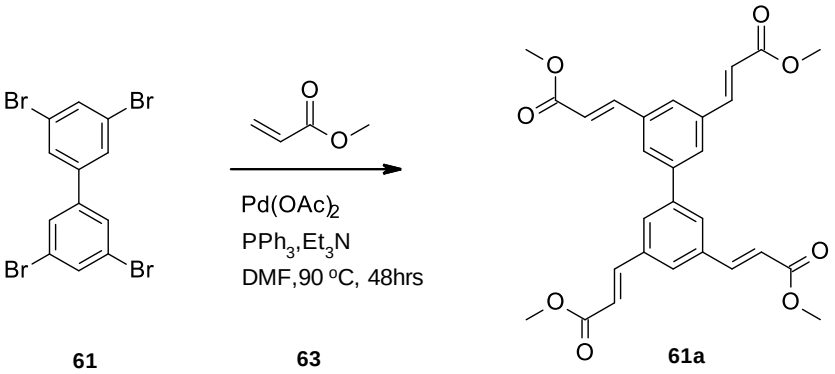

61 **63** **61a**

Scheme 14 Heck Reaction was used to couple methyl acrylate to 3,3',5,5'-tetrabromo-1,1'-biphenyl **61**.

Despite trying numerous solvent systems, we decided to work with 3,3',5,5'-tetrabromo-1,1'-biphenyl **61** and methyl acrylate **63** which was successfully coupled to four positions (Scheme 14). The reaction was completed as shown by TLC monitoring. This structure was confirmed by NMR and Mass Spectroscopy to validate successful coupling of all four positions. Following to this reaction, we decided to couple amine groups onto these four positions using EDCI couplings. However, hydrolysis only occurred at two positions.

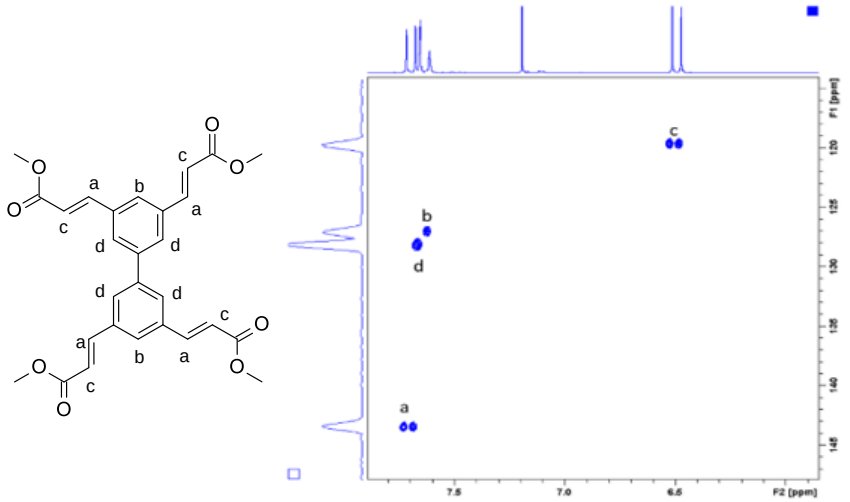

Figure 29 Assigned HSQC (Heteronuclear single quantum coherence spectroscopy) and integrated 1D-1H spectra for 3,3',5,5'-tetrabromo-1,1'-biphenly **61** coupled with methyl acrylate. From the 1D proton, we see the four protons of the alkenes groups at 6.5ppm (H-a) (integrated as 4) and the other one is at 7.7ppm (H-c) integrated as around 4. We also see by this peak there is a peak giving an integral around 6, therefore this matches the phenyl ring (H-b).

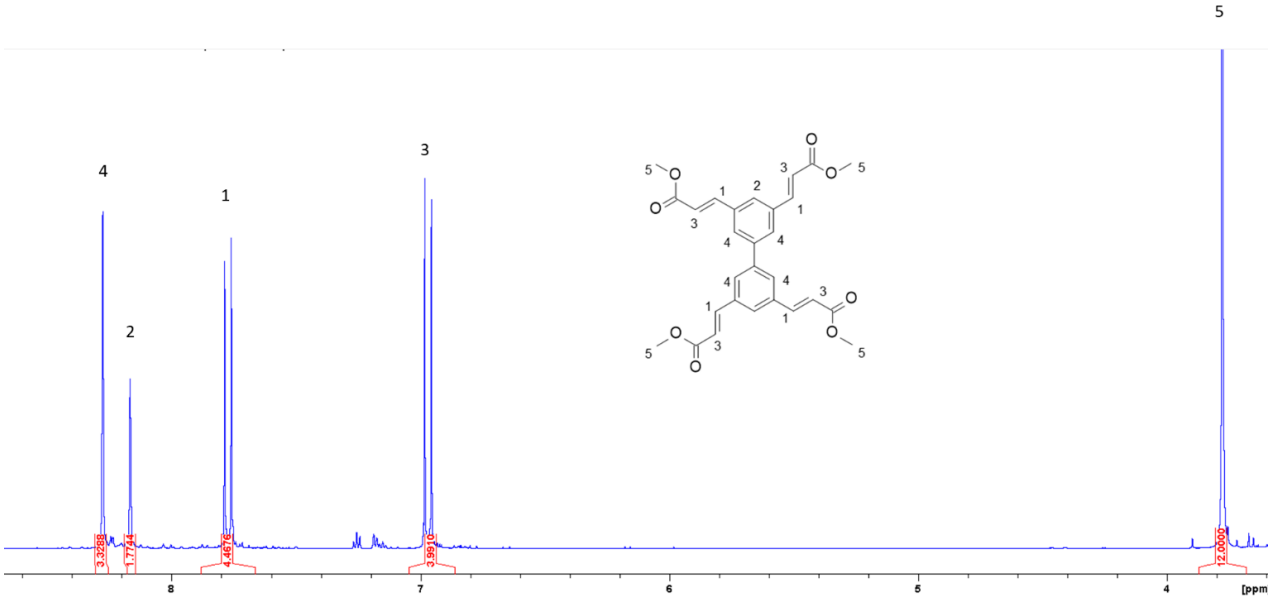

Figure 30 Assigned NMR spectra and structure representing coupled methyl acrylate **63** to 3,3',5,5'-tetrabromo-1,1'-biphenyl **61**.

3.4 EDCI.HCl coupling

Since many of the more complex amines would not be well suited for conversion to acrylamide and/or coupling via the Heck reaction, it was necessary to consider different possible routes to synthesise a library of compounds based on **52** and **53**. Whilst, in our hands, the acrylamide couplings using palladium catalysts afforded poor yields, the corresponding coupling with acrylates, has been shown to proceed to completion with high yields. As a result, we used the synthesis of methyl acrylate derivatives of **60c** with a view to subsequently hydrolysing them for coupling using carbodiimide methods.

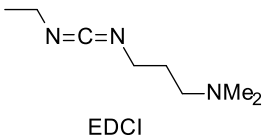

EDCI

64

Figure 31 Coupling agent EDCI **64**.

EDCI is the most common coupling reagent for peptide synthesis and with the addition of HOBt it becomes more efficient. Therefore, it was decided to try the first coupling with this coupling reagent.

In the case of the anthracence bis-(carboxylic acid) **60d**, 1 eq. of diester and methanol (5ml) were stirred and KOH (2 eq.) was added and stirred at 77°C under reflux until the starting product was consumed (checked by TLC). HCl (4M) was used to quench the reaction mixture and pH was taken down to 2. Hydrolysis was verified by NMR.

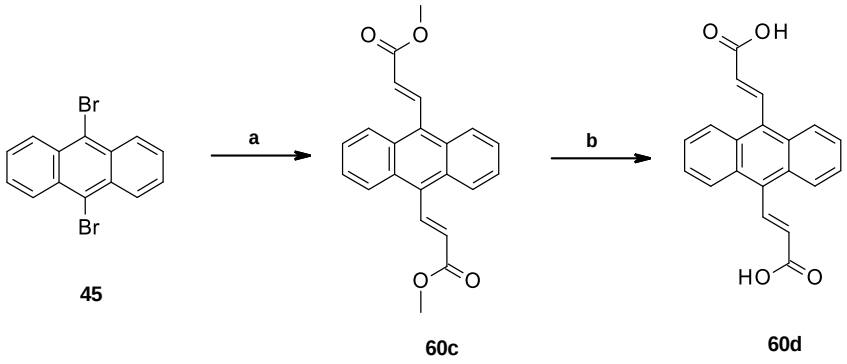

45 **60c** **60d**

Scheme 15 Reagents and Conditions: a) $Pd(OAc)_2/Ph_3P/ CH_2=CHCOOCH_3$/DMF,84-95%; b) MeOH, 4N NaOH, 92%.

With the diacrylic acid derivative **60d** in hand, facile conversion to the corresponding amide could be achieved using diacid (1eq.) and amine group (4eq.) in DCM solution at room temperature under N_2. To this solution, a mixture EDCI.HCl (4eq.) (1-Ethyl-3-(3-dimethylaminopropyl)carbodiimide) and HOBt (Hydroxybenzotriazole) (4eq.) in DCM (dichloromethane) solution was added dropwise at 0°C. Then, DIPEA (N,N-diisopropylethylamine) (8 eq.) was added dropwise to the solution mixture and was left to stir (221). This afforded the amides referred to as type **52** (Figure 22)

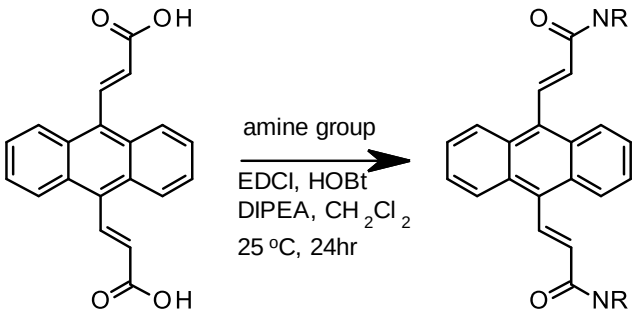

60d **52**

50%

Scheme 16 Synthetic routes for EDCI coupling,50% yield.

EDCI coupling reagent was used to couple chosen amine groups onto **60d**. With the reaction scheme shown in Scheme 16, we successfully coupled two compounds (**52a**-**52c**) (full synthetic routes shown in Scheme 17)). Alongside these two successfully coupled compounds, it was found that two other amine groups were unsuccessful as shown in Table 3. This failure to couple was explained by the amine groups insolubility in the reaction solution of DCM or DMF. Despite numerous reaction conditions being tested to solubilise these amine groups (b and f) (Figure 24), including experiment time, temperature, and solvent choice (THF, MeOH), there was still no successful coupling seen. **52a** and **52c** were successfully coupled at yields of 55% and 41% respectively. This lower than expected yield can be explained by the reaction mechanism where mono amide coupling has to happen first before generating diamide coupled compound. This means that we can lose higher yields through the isolation of mono substituted amide compound.

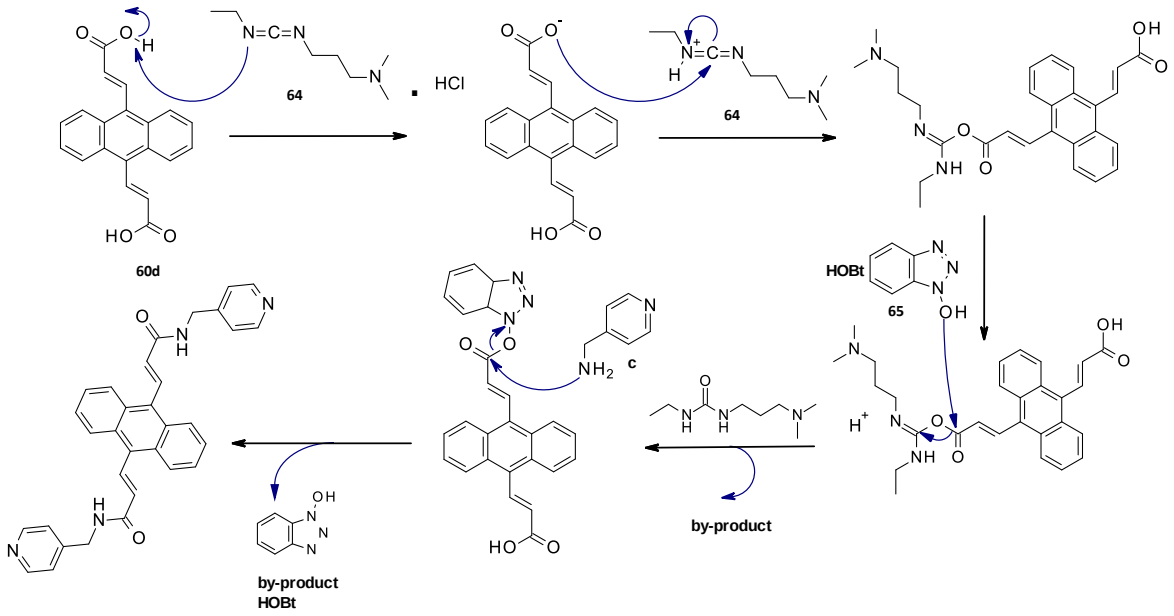

Scheme 17 Synthetic route for 4-(aminomethyl)pyridine *via* EDCI coupling**.**

Table 3 Comparison of yields, experiment times and structures of specific EDCI coupled amine groups to anthracene core.

Amine group (see Table 1)	Target compound	t (h)	Isolated yield
a	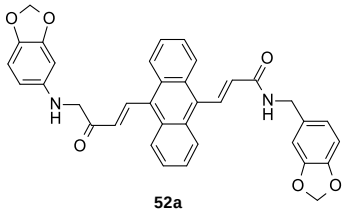 52a	24 h	55%
b	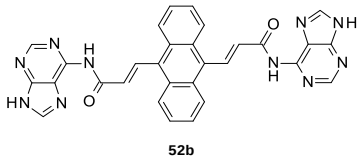 52b	12 h	No reaction - insoluble
c	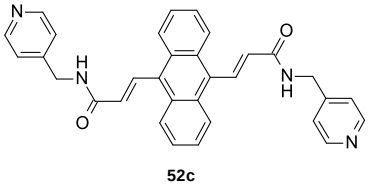 52c	24 h	41%
f	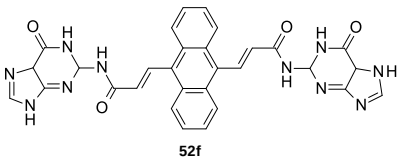 52f	12 h	No reaction - insoluble

3.5 Acrylamides based on 1,3,5-trisubstituted phenylbenzene

Our first example is 1,3,5-tris(4-bromophenyl)benzene **66** which will permit coupling with three amine groups. We prepared 1,3,5-tris(4-bromophenyl)benzene **66** coupled with methyl acrylate via Heck reaction in preparation for 1-ethyl-3-(3-dimethylaminopropyl)carbodiimide (EDCI) coupling with selected amine groups to form a library of derivatives. We optimised the yield of this product to be hydrolysed for EDCI coupling. We found that reducing the quantity of catalyst activating ligand allowed for easier purification of the product. This led to decreased decomposition/loss of product and increased yield. Other steps taken included varying reagent concentration and the relative molar equivalency of reactants.

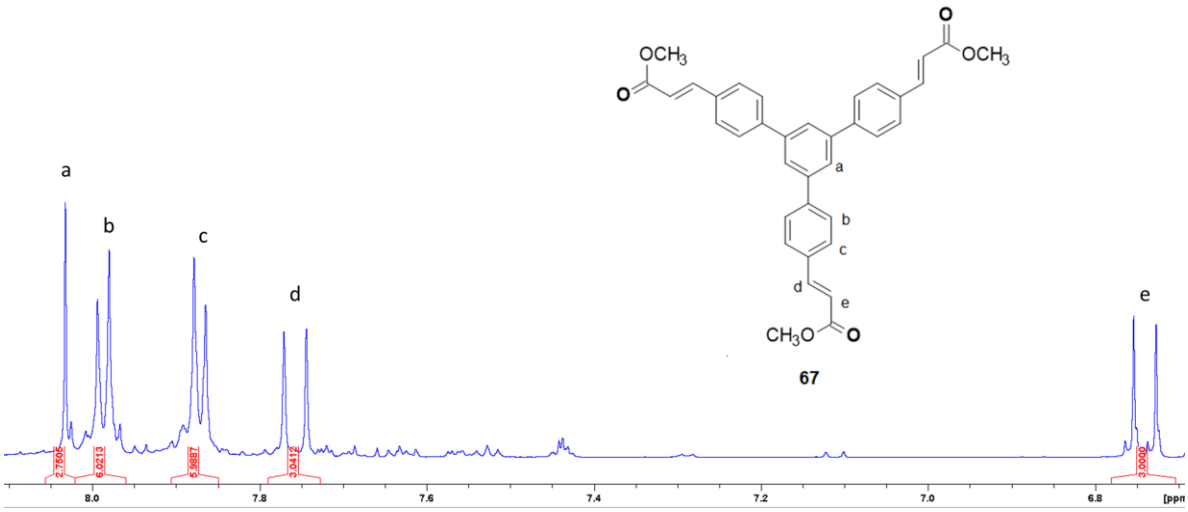

Figure 32 Assigned 1D-1H spectra for 1,3,5-tris(4-bromophenyl)benzene coupled with methyl acrylate. From the 1D proton, it shows that three alkene groups at 6.7ppm (H-e), 7.8ppm (H-d) as integrated 3H. The biphenyl appears at 8.05ppm (H-a), 7.96 ppm (H-b) and 7.85 (H-c). Therefore, the corresponding integrals match those of expected.

Heck Reaction of 1,3,5-tris(4-bromophenyl)benzene **66** and methyl acrylate provided a product of 1,3,5-trisalkyl substituted phenylbenzene derivative. After producing good yields of the ester compound, it was decided to convert it to the trisacid **67a**. We investigated ways to enhance the efficiency of coupling through the use of tandem reactions which judge the

applicability of each reaction to this coupling. The reported effectiveness of couplings allowed us to select agents for this investigation. This procedure was followed by coupling amine groups onto the trisacid compound using EDCI.HCl and HATU couplings.

EDCI.HCl was used to couple benzylamine to the trisacid **67a**. A solution of EDCI and HOBt were pre-prepared in DMF (7.5ml) and then it was added drop wise to a stirred mixture of trisacid and a couple of benzylamine. Then to this mixture 0.2ml of DIPEA was added. These conditions were carried out under N_2. This experiment was done to evaluate whether small amine couplings gave efficient coupling through EDCI coupling at two positions. However, through NMR results we saw that only one position coupled. There were also mixtures of derivatives which were apparent in the spectra. Due to the complexity of the spectra, it was decided that the EDCI coupling produced a number of derivatives and as such that a (1-[Bis(dimethylamino)methylene]1H-1,2,3-triazolo[4,5-b]pyridinium3-oxide hexafluorophosphate (HATU) coupling would be attempted to selectively produce desired product.

HATU **68** has been shown in previous literature to have greater coupling effectiveness when compared to HOBt within solid-phase peptide synthesis. This synthesis was done with sterically hindered amino acids which was relevant to our couplings (222).

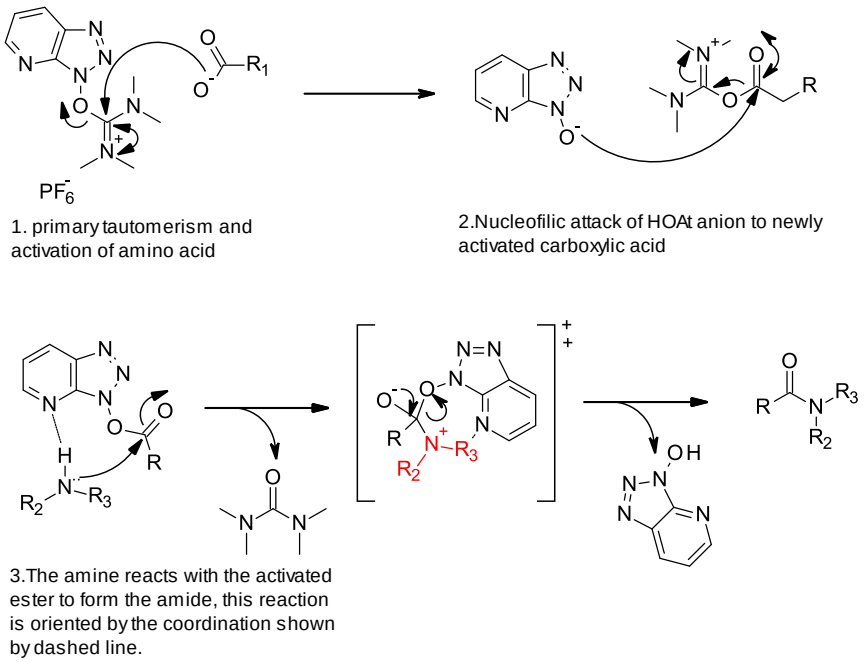

Scheme 18 Mechanism of HATU **68** peptide coupling.

For HATU coupling, the trisacid **67a** compound, benzylamine, HATU and DIPEA were added with DCM as a solvent. This mixture was stirred at room temperature for 20hrs. During the reaction period, TLC was used to monitor the reaction. TLC showed that product was being made at very low concentrations, therefore, temperature was raised to improve the kinetics of the reaction. Subsequent work up of the reaction showed that negligible product was produced. This may have been because of energetically unfavourable conditions leading to only one coupling side in the reaction.

To gain an aldehyde functional group which would make coupling of amine groups more accessible. We decided to attempt reduction of diacid with DIBAL. After several unsuccessful reactions with diethylacetal and DIBAL which resulted in the reduction of the starting material to an alcohol, it was decided to then address this issue with imine couplings to bypass issues common to previous reactions.

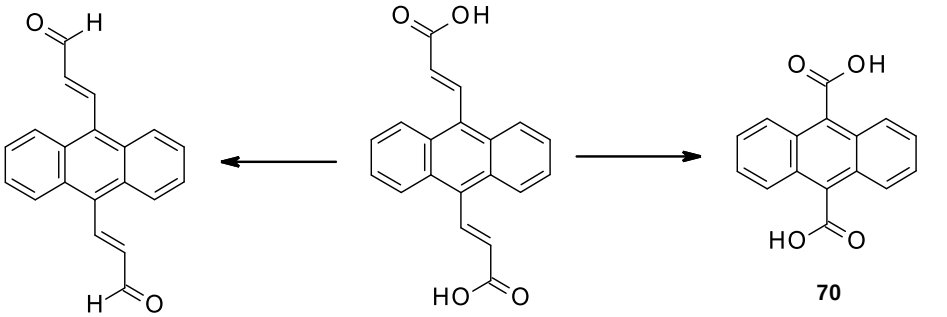

Figure 33 Illustration representing the desired and obtained compound using DIBAL with yield included.

Alongside the DIBAL reduction of diacid **60d** and peptide coupling using HATU of trisacid (**67a**), we attempted to couple acrylamide to 1,3,5-tris(4-bromophenyl) benzene *via* Heck Reaction. To do this, $Pd(OAc)_2$ and DPPP (1,3-Bis(diphenylphosphino)propane) was added to DMF and stirred under nitrogen conditions. To this mixture, triethylamine and acrylamide were added. Reaction was heated at 90^{o}C for 24hrs. TLC was used to monitor the reaction. When one new spot was left the reaction was stopped. NMR analysis confirmed the proposed product had been synthesised. To confirm the molecular weight and atomic structure, mass spectrometry was used to validate the NMR results. From the NMR and mass spectrometry, we saw no impurities, so column chromatography was not needed in this case.

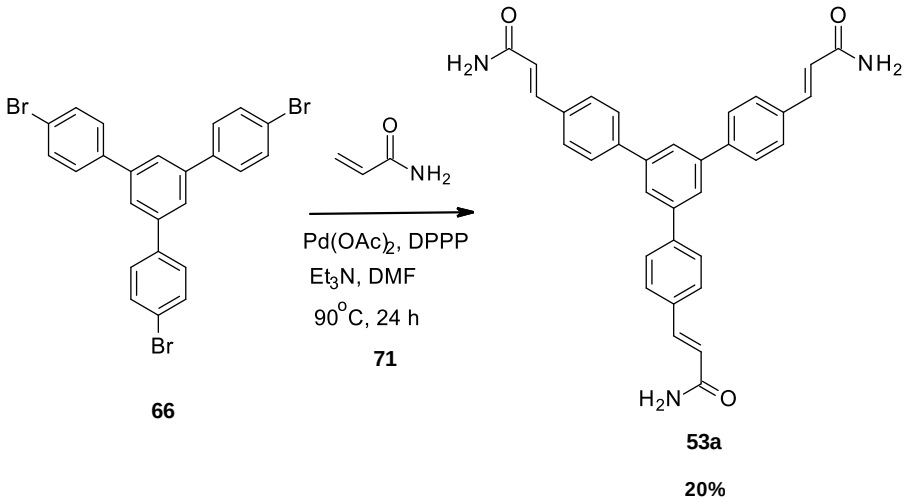

Scheme 19 Heck coupling based on **53** (20%yield).

3.6 Imine couplings

After experiencing difficulties with EDCI, HATU and DIBAL reactions we decided to carry on our research by synthesising imines. Our intention was to couple bulky amine groups to the anthracene-9,10-dicarbaldehdye **72**. The coupling of these bulky amine groups to the anthracene-9,10-dicarbaldehyde follows the reaction mechanism of a Schiff base reaction where an ammonia molecule or primary amine will attack a carbonyl group. We also see a similarity in the formation of an acetal, as when water is eliminated in the acid catalysed reaction, we see a reversible reaction, much like the acetal. Because of this the pH of reactions must be carefully controlled to give the greatest yield of final imine compounds without allowing the equilibrium to return to starting material. It has been shown that for these reactions a pH near 5 gives the greatest rate of equilibrium to the imine product and drops at higher or lower pH for kinetic and electrophilic reasons. This is because at high pH there is less acid to protonate the OH in the Schiff base intermediate and dehydration of H_2O will not occur. Conversely, at low pH the amine reactant will be mainly present as an ammonium conjugate acid and unable to take part in the reaction as it will no longer be nucleophilic.

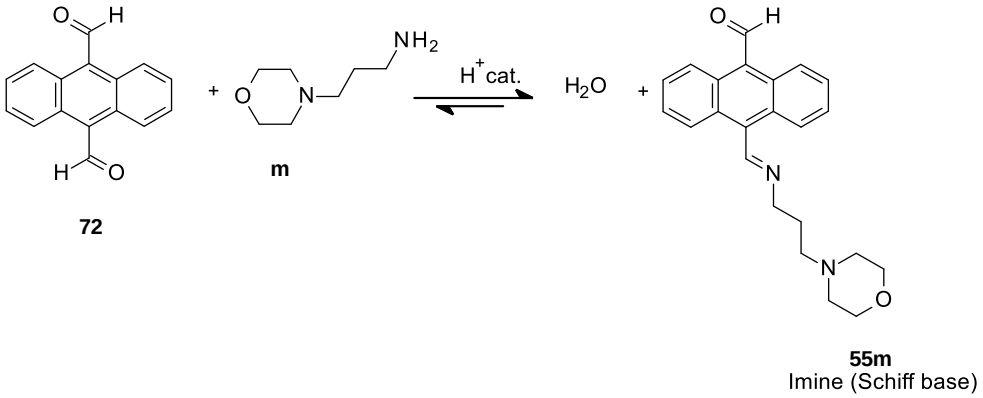

Scheme 20 An example of an imine coupling scheme using 3-morpholinopropan-1-amine **m** to couple onto carbaldehyde derivative **72** to generate **55m**.

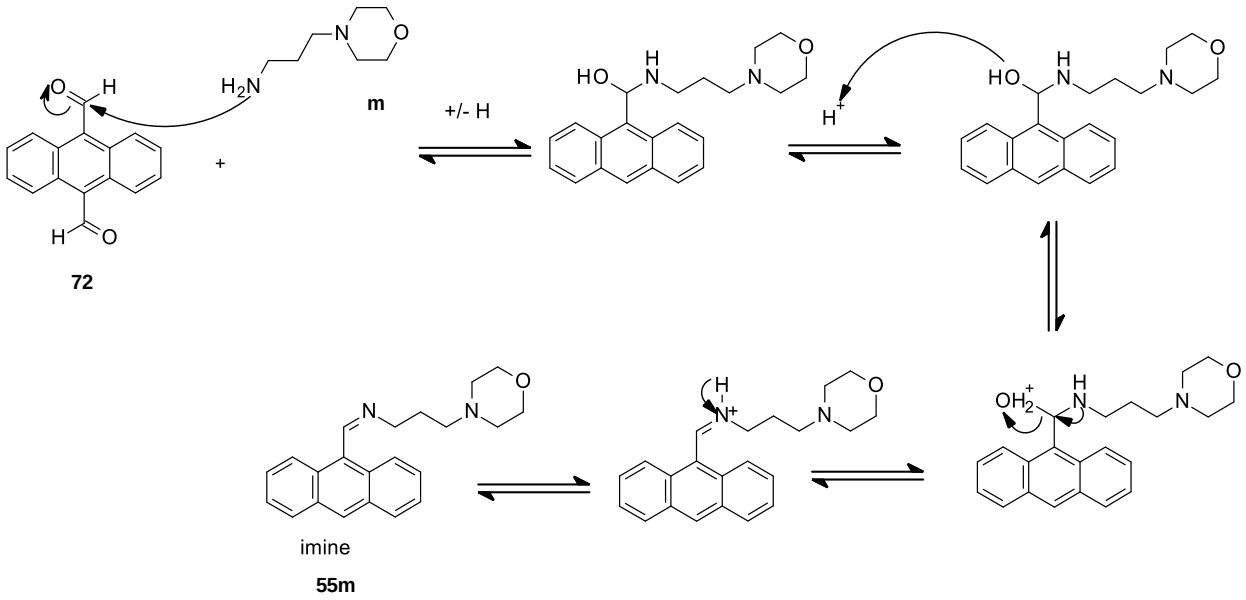

Scheme 21 Synthesis of imine derivative **55m** from **72**.

The reversible nature of the imine reaction facilitates the establishment of a dynamic combinatorial approach to this class. This would enable the in-situ amplification of a specific di-imine from our anthracene derivative depending on the thermodynamics associated with exposure to quadruplex over duplex DNA.

Whilst it was intended that we would combine multiple amines in the presence of a G-quadruplex-forming oligonucleotide, to ascertain amplification of one or more imine

products, we ultimately formed and tested a small static combinatorial library for anti-cancer activity.

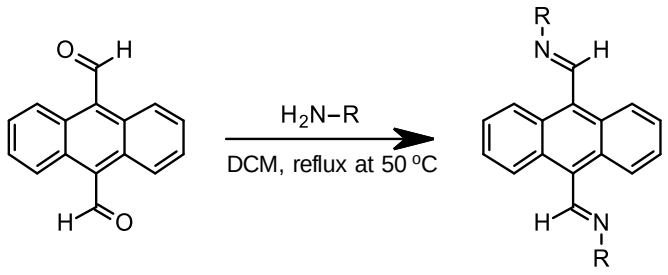

72 **55**

Scheme 22 Synthetic route used to form imine derivatives from **72**.

Reaction of a series of amines **a, c, j-m** to **72** was achieved using 2.3 equivalents of amine in DCM and heated to 60°C. This reaction was performed under N_2 atmosphere for 24hrs. Reaction was monitored by TLC with (1:1) EtOAc+Hexane solvent system until a steady state was achieved after 24 hrs. TLC monitoring showed that no starting material was persisted. Therefore, the resultant product was precipitated and then the solid was recrystallised using MeOH. The yield was 78% which alongside melting point and NMR analysis of impurities being negligible, the reaction was not further optimised.

After the successful coupling of piperolamine (yield 78%), reaction of 3-morpholinoprorylamine and 2-amino-5-methylthiazole with **72** was undertaken. The same reaction procedure was used to achieve the expected compounds. The expected compounds were synthesised smoothly with yields of 60% and 75% respectively. These successful results urged us to couple adenine as we previously had difficulties to couple this compound using EDCI.HCl couplings. Adenine is a nucleotide, the structure itself includes amino protons which present positive charges to bind to O^- in the phosphate backbone of the G-quadruplex structures. However, using the same reaction conditions, due to the solubility issues of the adenine, the coupling reaction with **72** did not occur. Resolution of these issues through changing the solvent system such as dry toluene and dry DMF. In both cases, adenine was still present in the reaction. This was monitored by TLC (1:1) EtoAc+Hexane and 10%Methanol+DCM solvent systems respectively for 48 hrs, but without evidence of any reaction.

Following this success, tryptamine, (1-,2-aminoethyl) piperidine and 3-aminoacetanilide were reacted under the same conditions to the carbaldehyde in 80%,45% and 35% yields respectively. Tryptamine is a known monoamino alkaloid which was selected based upon its amino group position in the ring system. A piperidine compound was also chosen as it's a starting material in the synthesis of anticancer analogues. It was also hoped that 3-aminoacetanilide would afford a well-placed hydrogen bond acceptor/donor configuration to aid backbone binding to the G-quadruplex.

Having successfully coupled several amine groups onto the carbaldehyde, it was decided to introduce 2-aminothiazole-5-carbonitrile a, in cancer research, thiazole derivates have had a huge impact, demonstrated through the reported inhibition of proliferation and growth of cancer cells alongside reducing the ability for neovascularization. These properties are seen through several different modes of action in a diverse range of therapeutic targets.

This reaction of 1 equivalent of carbaldehyde and 2.3 equivalent of 2-aminothiazole-5-carbonitrile were first performed in DCM and stirred at 40^{O}C. The reaction mixture was then left for 24 hrs. TLC was used to monitor the reaction. However, on the TLC comparing resultant to starting material, there were 4 spots appearing for the resultant compared to the one spot for the starting material. The starting compound was still strongly apparent. We wanted to further investigate the resultant using NMR. The NMR showed a mixture of compounds with several aromatic environments. This demonstrated that the reaction did not go to completion and the desired product was not formed. This led us to work with other solvent systems such as dry THF and acetonitrile. However, similar results were obtained.

Table 4 Comparison of yields, experiment times and structures of specific imine coupled amine groups to anthracene core.

Amine group	Target compound	time(hours)	Isolated yield
a	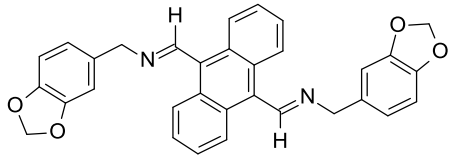 **55a**	24 h	78%
m	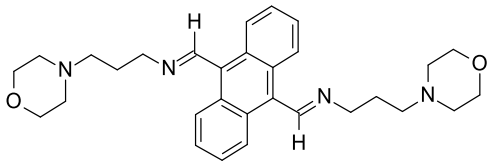 **55m**	24 h	60%
k	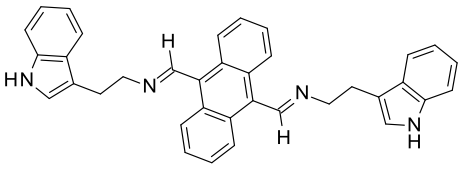 **55k**	12 h	80%
c	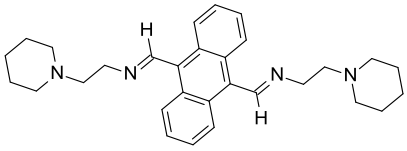 **55c**	24 h	65%
j	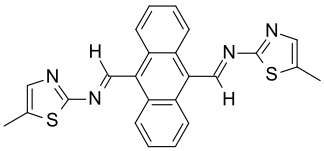 **55j**	24 h	75%
l	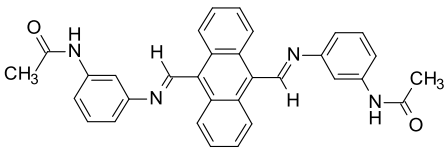 **55l**	24 h	35%

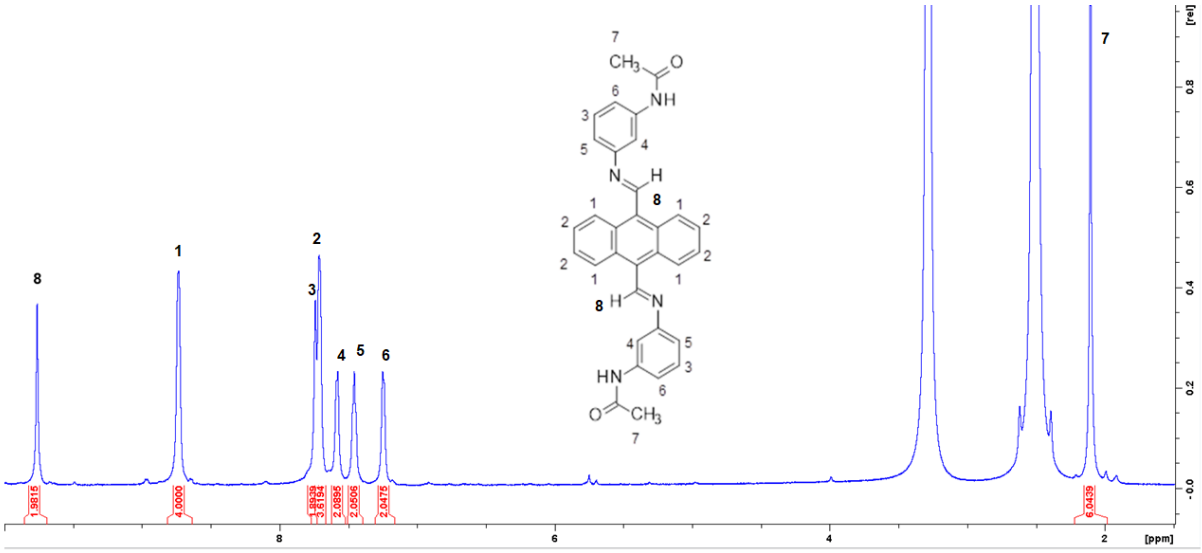

Figure 24 ^{1}H-NMR spectrum and proton assignments of N-[3-[(E)-[10-[(E)-(3-acetamidophenyl)iminomethyl]-9 anthryl]methyleneamino]phenyl]acetamide **55l**.

Before the cell culture work, we decided to test one of the imines synthesised for stability in Dulbecco's Modified Eagle's Medium (DMEM). This work would show if the imine coupled compounds were stabile for the incubation period of treatments and hydrolysis was kept to negligible levels. This was achieved by preparation of the compound concerned in cell culture (DMEM) modal system and monitored *via* NMR. Using an internal standard (TSP), we could quantify compound peaks at time 0 and time 24 to see if hydrolysis of the imine group had occurred.

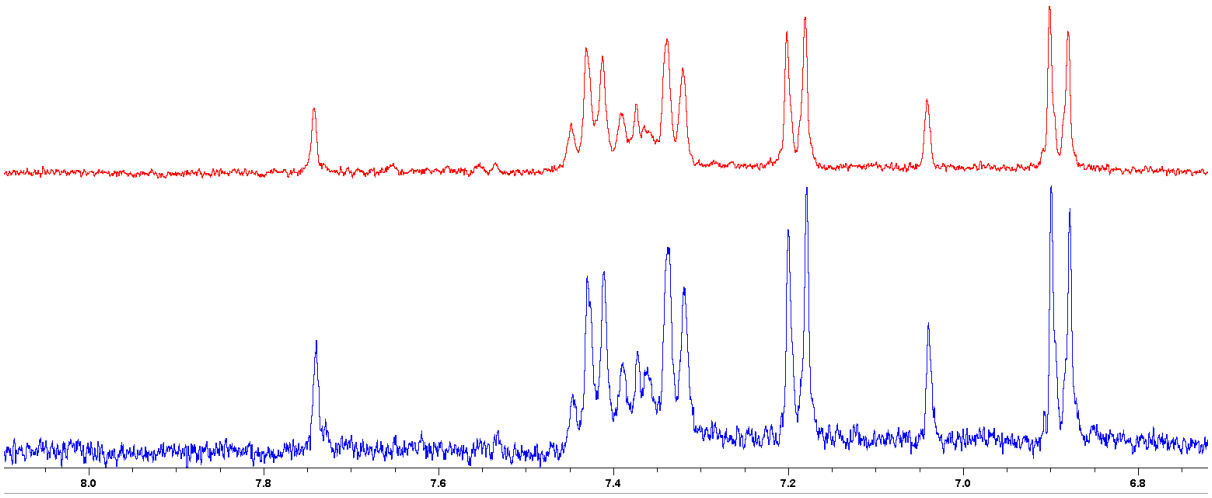

Figure 35 Top NMR spectra represents aromatic and imine peaks for compound **55j** after 24 hours incubation in modal cell culture system (**DMEM**) at 37°C. Bottom NMR spectra represents aromatic and imine peaks for compound **55j** at time 0 in model cell culture system (**DMEM**). Both spectra are matched to internal standard integrals.

We see from Figure 35 that after 24 hours there is a small drop in peak height but no new peaks forming which suggests that minimal to no hydrolysis has occurred. This gives confidence in the stability of our imine coupled compounds when incubated up to 24 hours at 37°C. This was tested to see if the imine bond formed through the coupling is hydrolysed in the water environment. Only one compound was tested as the imine bond for imine coupled structures were seen to be of a relative stability.

3.7 Cell culture results

It was decided to test synthesised compounds on cervical cancer cell lines (HeLa, American Type Culture Collection (ATCC) (ATCC® CCL-2™). For the testing Presto Blue Assay gave the most significant results when compared to MTT and Neutral Red Assay as these two assays were interacting with the compounds when they were treating the cells with the medium. With the neutral red assay, the eurhodin dye during the 24-hour preparation time can precipitate into fine crystals which can become visible and interfere with absorbance readings. This is very difficult to reverse and account for, so induction of precipitation by slightly different conditions can give inconsistent results. Alongside this limitation, the assay is (Neutral red assay) very expensive and is more time consuming than alternatives. With both MTT and Neutral red assay the absorbance levels were inconsistent with many outliers that prevented repeatability measurements. MTT was first shown to interact with the drug, reducing tetrazolium to formazan rather than the cells exclusively carrying out the reduction. Presto Blue was selected because after preliminary testing no anomalous results were seen. Since the presto blue assay functions through the reduction of resazurin to the florescent resorufin, the issue of precipitation is bypassed and alongside this the incubation time is a lot smaller and less time consuming (Presto blue= 30 mins, MTT and Neutral red assay= 1 to 4 hours). This smaller incubation time could be a factor in the reduced effect of drug reduction when compared to the MTT assay despite aspiration of compound there could be drug compound remaining which overtime would give larger discrepancies.

Presto Blue Assay was prepared as per protocol (223). It was added in 200µL per well, all prepared well plates were then incubated for 1 hour. After the incubation time, plates were read at both 570nm absorbance and 600nm reference wavelength with absorbance being proportional to the viability of cells. Linear detection of cells down to 98 cells per well with a Z value of greater than 0.5. This Z factor means that negative and positive controls will have a large separation band. DMSO and Doxorubicin were used as negative and positive controls throughout the Presto Blue assay. 9µL of Doxorubicin stock 1% solution (40mg in 4ml DMSO) was prepared in 9ml of DMEM stock solution to make a 10µg/ml solution and

added in 200µL to wells, and DMSO was prepared in 0.1% solution in DMEM (3µl to 3ml DMEM), then added to cells in 200µL.

All novel compounds were tested against a HeLa cancer cell line (HeLa, American Type Culture Collection (ATCC) (ATCC® CCL-2™) and they were all prepared in 100,30,10 and 1 µM concentrations so that IC_{50} values could be calculated to establish whether drugs were cytotoxic to HeLa cells.

Preliminary experiments were done to screen for activity and synthesised compounds that showed activity were run in triplicate to get an average, SD and SEM values,

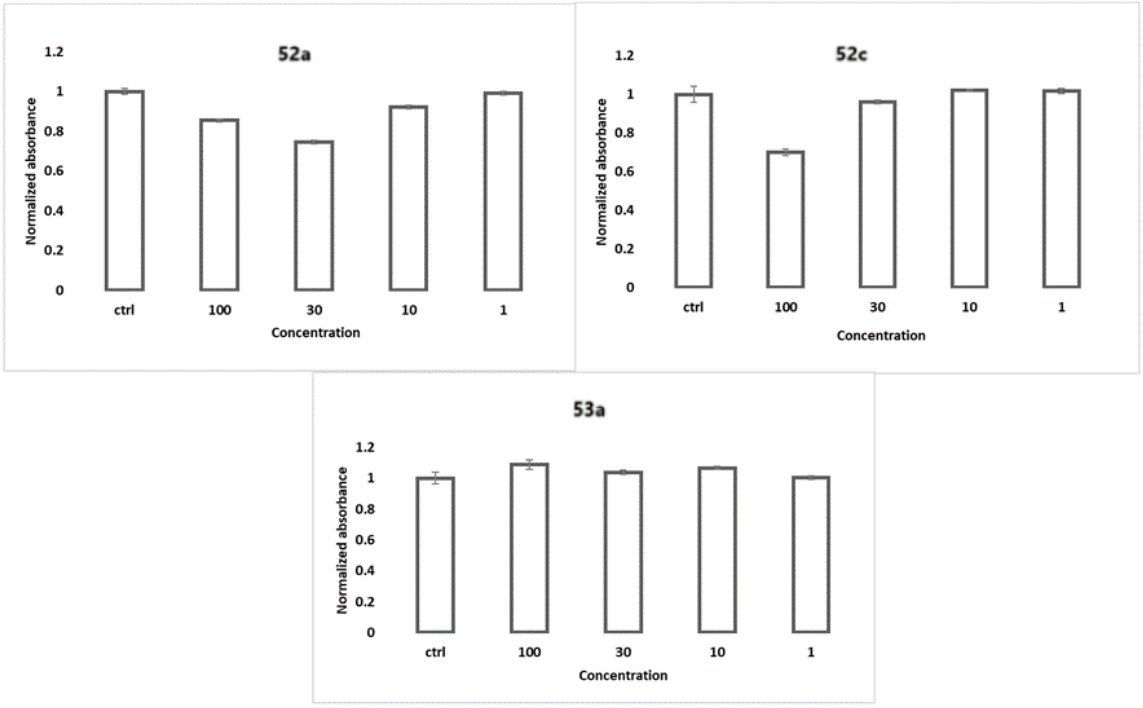

Figure 36 Bar chart showing the normalized cell viability of HeLa cells for concentrations 100...1µM of non-inhibiting compounds; **52a**, **52c**, **53a**. Showing non-significant inhibition of HeLa cells.

Following the preliminary experiments 3 compounds were excluded from further testing; **52a**, **52c** and **53a**. Compounds; **55a**, **55m**, **55j**, **55k** ,**55c**, **60a**, **60b**, **60c** were progressed to triplicate testing and further statistical analysis e.g. IC_{50} determination, repeatability (Mean and standard error of mean).

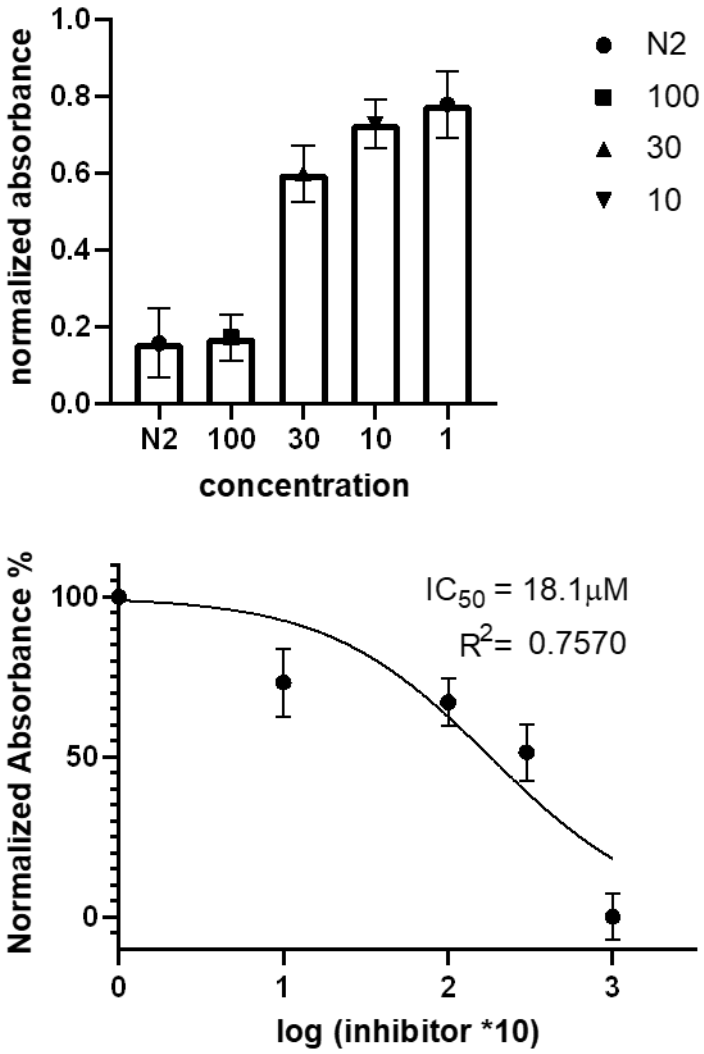

Figure 37 The data shown is after 24-hour incubation of drug (**55a**) treated HeLa cells. Top chart illustrates Mean and SEM of HeLa cell viability at concentrations 100 to 1µM with positive control (N2). In the top chart, values are normalized to negative control at a value of 1 (cell viability). The bottom chart then shows the normalized absorbance percentage to the negative control (percentage cell viability) of log inhibitor concentration (multiplied by 10 to account for 1 µM concentration) IC_{50} value and R squared value included in chart. Error bars indicates standard error of Mean from n=3 experiments.

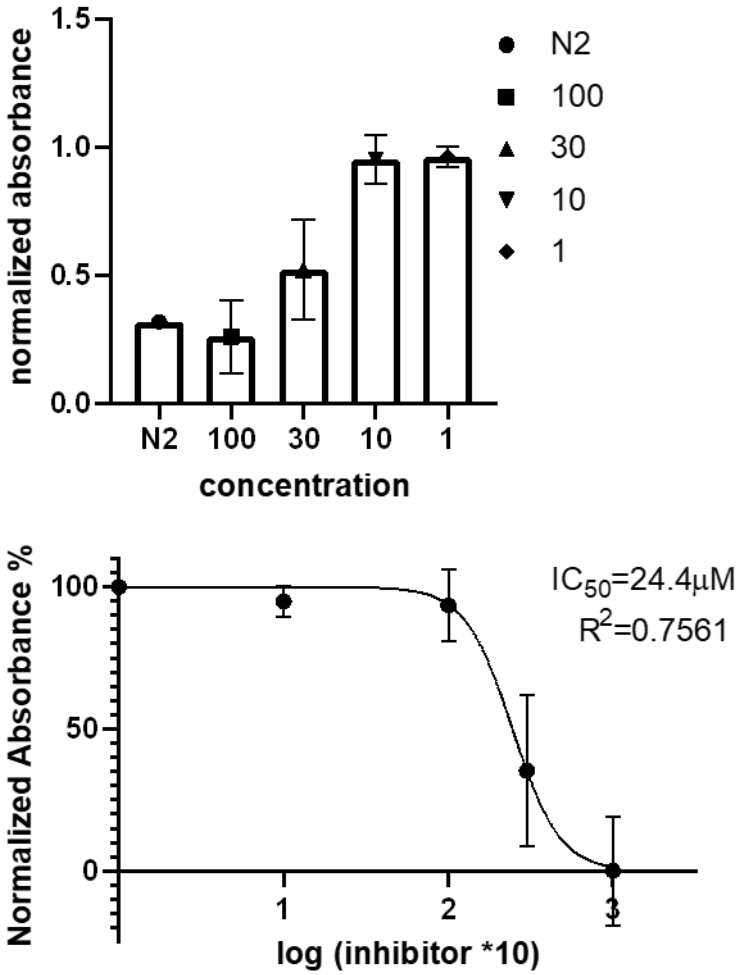

Figure 38 The data shown is after 24-hour incubation of drug (**55m**) treated HeLa cells. Top chart illustrates Mean and SEM of HeLa cell viability at concentrations 100 to 1µM with positive control (N2). In the top chart, values are normalized to negative control at a value of 1 (cell viability). The bottom chart then shows the normalized absorbance percentage to the negative control (percentage cell viability) of log inhibitor concentration (multiplied by 10 to account for 1 µM concentration) IC_{50} value and R squared value included in chart. Error bars indicates standard error of Mean from n=3 experiments.

.

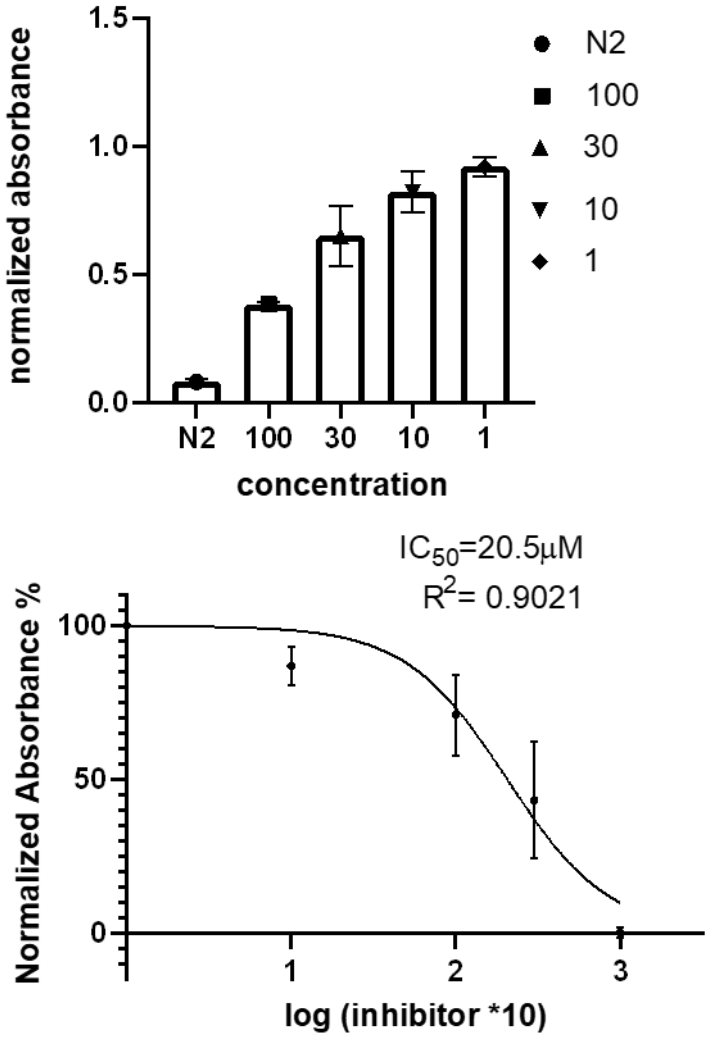

Figure 39 The data shown is after 24-hour incubation of drug (**55j**) treated HeLa cells. Top chart illustrates Mean and SEM of HeLa cell viability at concentrations 100 to 1µM with positive control (N2). In the top chart, values are normalized to negative control at a value of 1 (cell viability). The bottom chart then shows the normalized absorbance percentage to the negative control (percentage cell viability) of log inhibitor concentration (multiplied by 10 to account for 1 µM concentration) IC_{50} value and R squared value included in chart. Error bars indicates standard error of Mean from n=3 experiments.

.

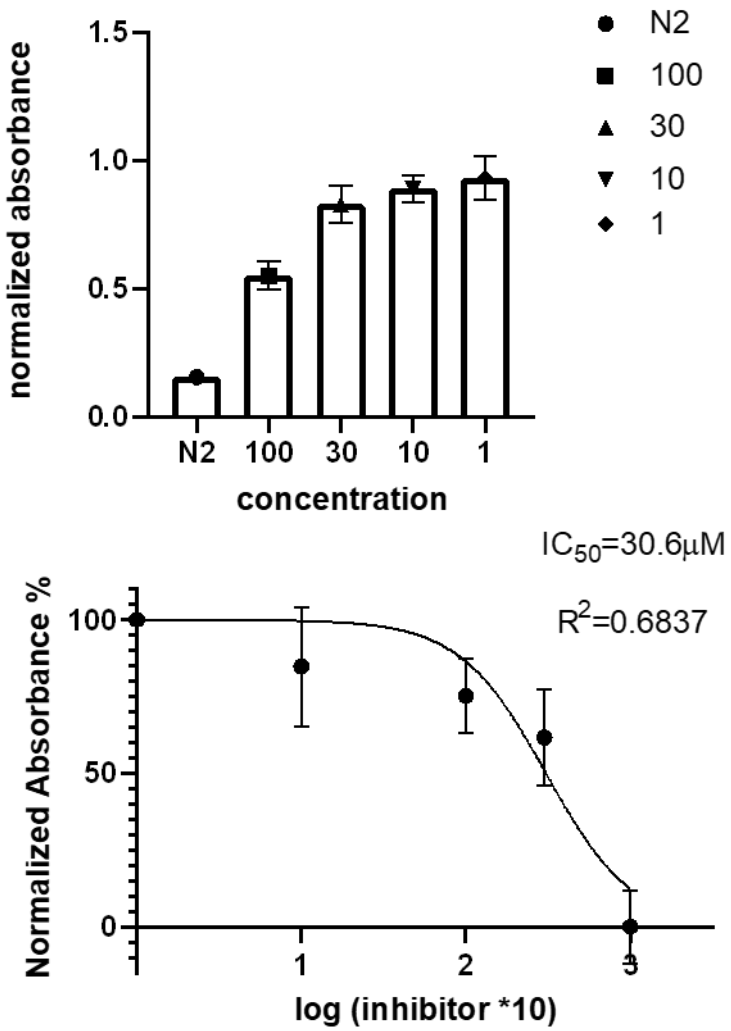

Figure 40 The data shown is after 24-hour incubation of drug (**55k**) treated HeLa cells. Top chart illustrates Mean and SEM of HeLa cell viability at concentrations 100 to 1µM with positive control (N2). In the top chart, values are normalized to negative control at a value of 1 (cell viability). The bottom chart then shows the normalized absorbance percentage to the negative control (percentage cell viability) of log inhibitor concentration (multiplied by 10 to account for 1 µM concentration) IC_{50} value and R squared value included in chart. Error bars indicates standard error of Mean from n=3 experiments.

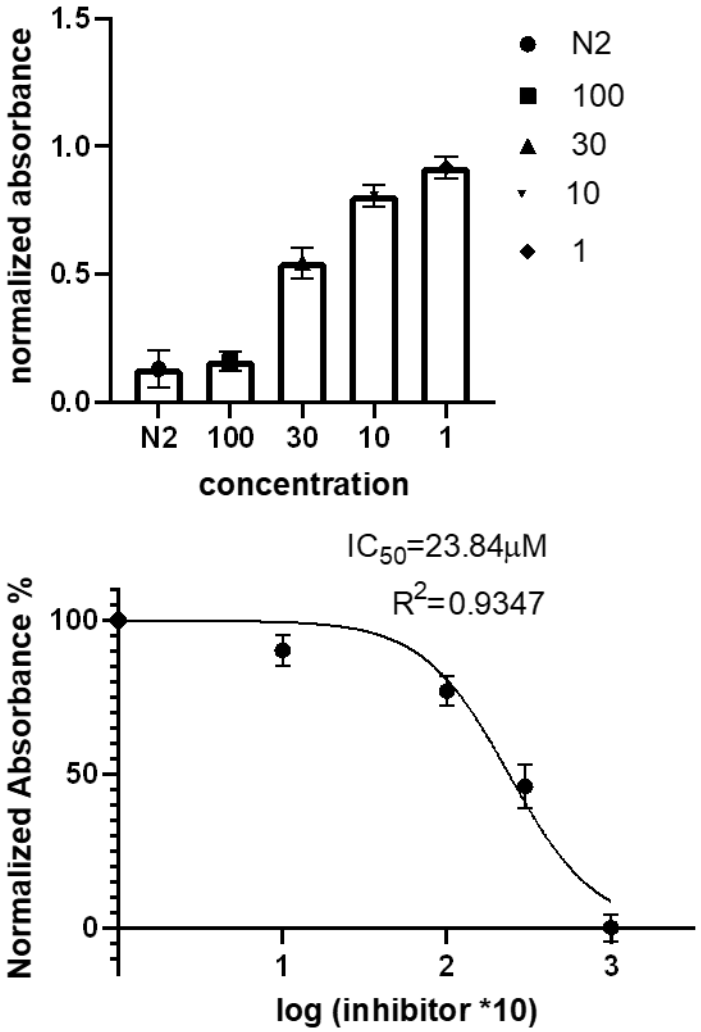

Figure 41 The data shown is after 24-hour incubation of drug (**55c**) treated HeLa cells. Top chart illustrates Mean and SEM of HeLa cell viability at concentrations 100 to 1µM with positive control (N2). In the top chart, values are normalized to negative control at a value of 1 (cell viability). The bottom chart then shows the normalized absorbance percentage to the negative control (percentage cell viability) of log inhibitor concentration (multiplied by 10 to account for 1 µM concentration) IC_{50} value and R squared value included in chart. Error bars indicates standard error of Mean from n=3 experiments.

.

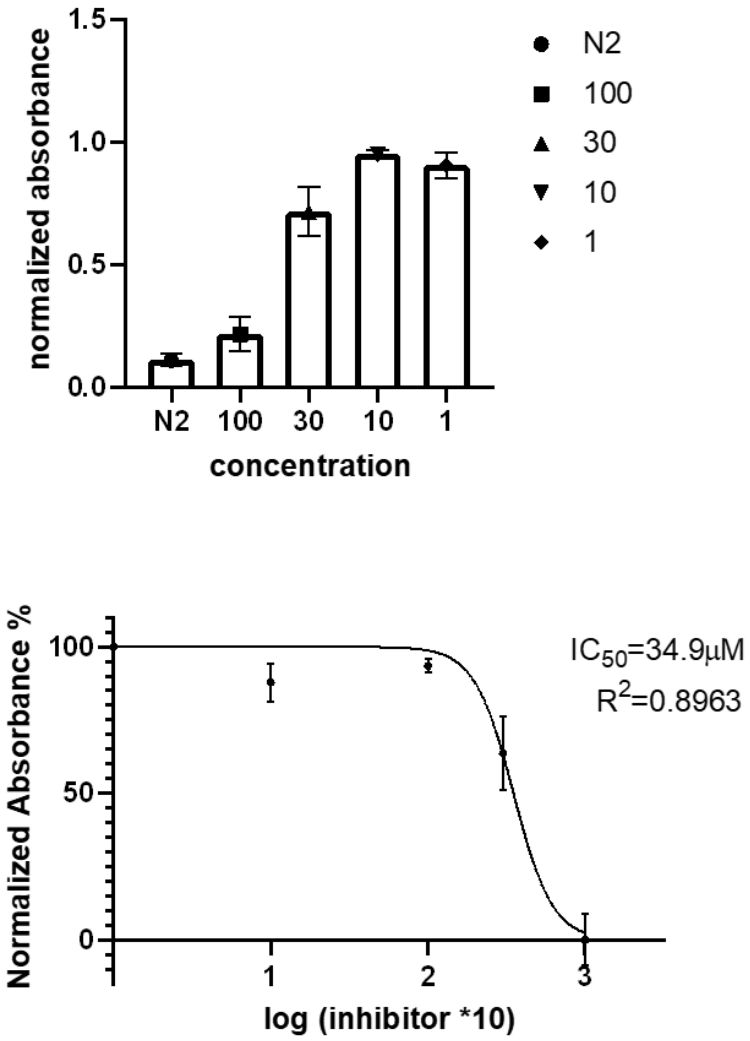

Figure 42 The data shown is after 24-hour incubation of drug (**60c**) treated HeLa cells. Top chart illustrates Mean and SEM of HeLa cell viability at concentrations 100 to 1µM with positive control (N2). In the top chart, values are normalized to negative control at a value of 1 (cell viability). The bottom chart then shows the normalized absorbance percentage to the negative control (percentage cell viability) of log inhibitor concentration (multiplied by 10 to account for 1 µM concentration) IC_{50} value and R squared value included in chart. Error bars indicates standard error of Mean from n=3 experiments

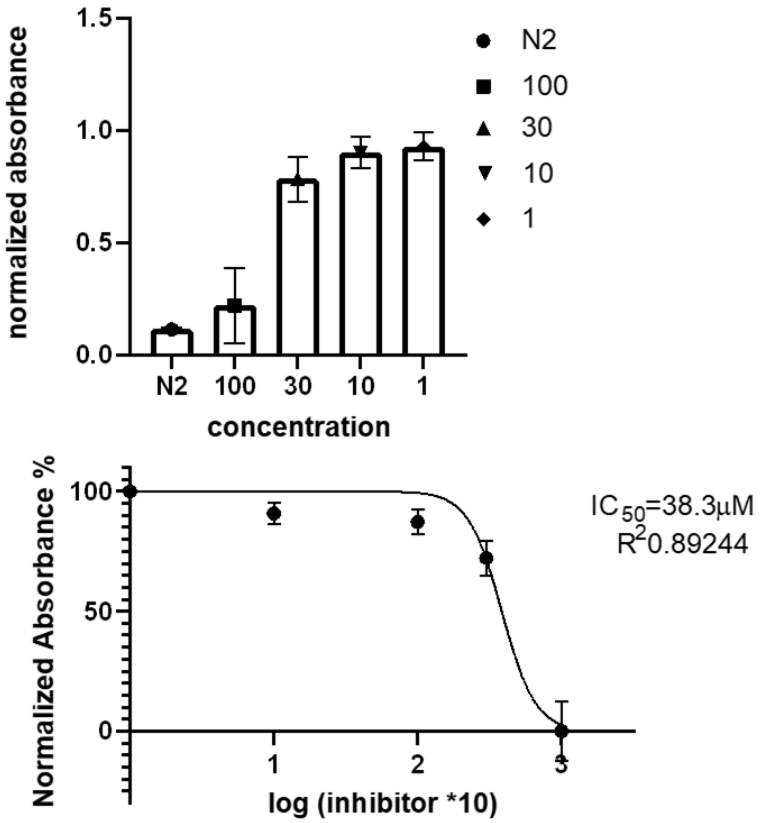

Figure 43 The data shown is after 24-hour incubation of drug (**60a**) treated HeLa cells. Top chart illustrates Mean and SEM of HeLa cell viability at concentrations 100 to 1µM with positive control (N2). In the top chart, values are normalized to negative control at a value of 1 (cell viability). The bottom chart then shows the normalized absorbance percentage to the negative control (percentage cell viability) of log inhibitor concentration (multiplied by 10 to account for 1 µM concentration) IC_{50} value and R squared value included in chart. Error bars indicates standard error of Mean from n=3 experiments.

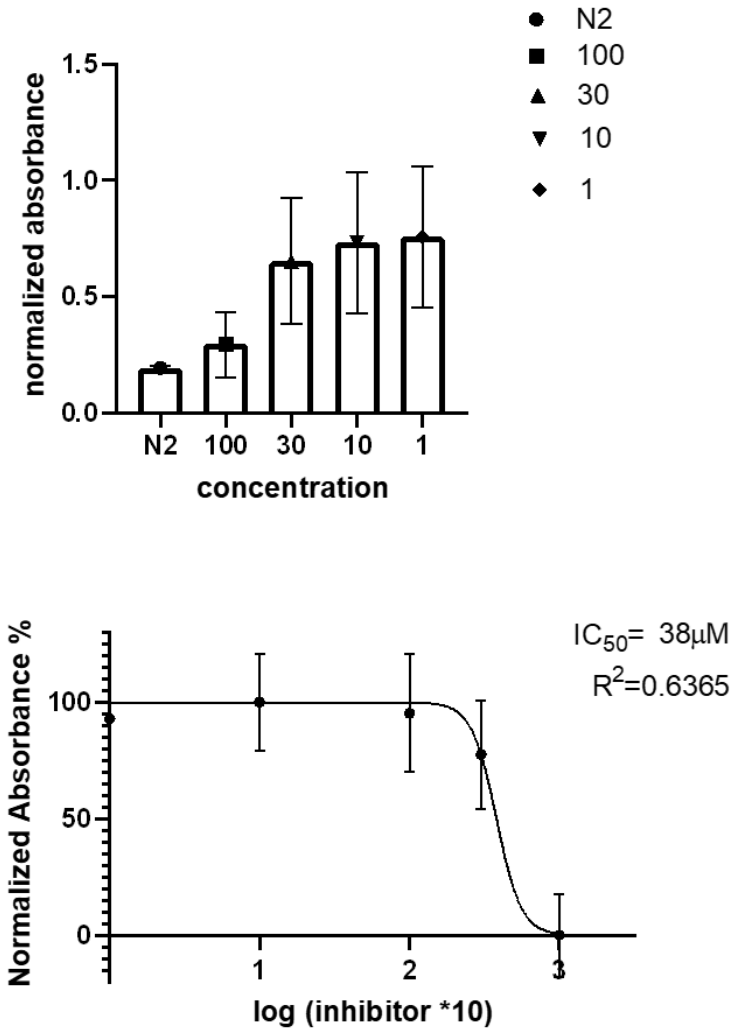

Figure 44 The data shown is after 24-hour incubation of drug (**60b**) treated HeLa cells. Top chart illustrates Mean and SEM of HeLa cell viability at concentrations 100 to 1µM with positive control (N2). In the top chart, values are normalized to negative control at a value of 1 (cell viability). The bottom chart then shows the normalized absorbance percentage to the negative control (percentage cell viability) of log inhibitor concentration (multiplied by 10 to account for 1 µM concentration) IC_{50} value and R squared value included in chart. Error bars indicates standard error of Mean from n=3 experiments.

3.8 Intercalation G4 results

With doxorubicin being used as the positive control in the HeLa cancer cell lines cytoxicity studies, which has been shown to intercalate with G-quadruplex structures, (204) our studies investigated the intercalation of synthesised cytotoxic compounds with the same G-quadruplex model structure used d(TTGGGTT)4. Comparing intercalation of the doxorubicin derivative nemorubicin with d(TTGGGTT)4 and our novel compounds. It has been shown that the motif present in telomeres that forms their G-quadruplex structures is (TTAGGG)n. With this knowledge, it was decided to select an oligomer that had three guanine residues. TTGGGTT was decided upon because of its symmetry, which allows for easier assignment of peaks. It was selected as a 7 base oligomer rather than a larger oligomer with multiple 3xG sites, as it is known that tetramer g-quadruplex's will always be in the parallel configuration. This gives a cleaner NMR spectrum to profile the interaction between G-quadruplex and drug compound. Despite there being an increased stabilisation for oligomers that have an adenine residue at position 2, instead of thymine through the formation of an adenine tetrad, it has been shown to give a 2:1 intercalation stoichiometry for doxorubicin in between A2 - G3 and G5 – T6. This intercalation at A2 – G3 was seen as not necessary for this screening and would make screening more complicated. This idea is supported by previous screening studies that have focussed on the intercalation at position G5-T6, which forms a cap on the complex. Previous literature with **d(T**(1)**T**(2)**G**(3)**G**(4)**G**(5)**T**(6)**T**(7)**)4** (numbers in parenthesis added for reference) has demonstrated that G-quadruplex ligands intercalate specifically at the point between G5-T6 (204) . Large broadening of G5 imino proton peaks, accompanied with an up-field shift, shows this. We also see the peaks for T6 (methyl, aromatic and ribose) shifting to a lower field in accord with the up-field shift of the G5 peaks. This change is explained by the formation of a complex between the ligand and the tetrad formed at G5, which pushes the T6 unit away from the guanine π –system. This intercalation framework was in agreement with ESI/MS carried out which illustrated a 1:1 complex (204).

The comparative intercalation analysis of active compounds was achieved through NMR titration experiments, where differences in peaks were investigated primarily at the guanine imino protons at 10-12ppm and the number 6 thymine (T6) protons, which are at the proposed site of ligand stacking next to the guanine residues which form the G-tetrads. To validate the formation of G-quadplexes, imino peaks at 10-12ppm are first detected. The number of imino peaks at 10-12ppm in an exchanging D_2O environment represents the number of quartets that would make up the G-quadruplex. We see from Figure 45 that there are three guanine tetrads formed with peaks at 11.55, 11.22 and 10.86ppm respectively (224).

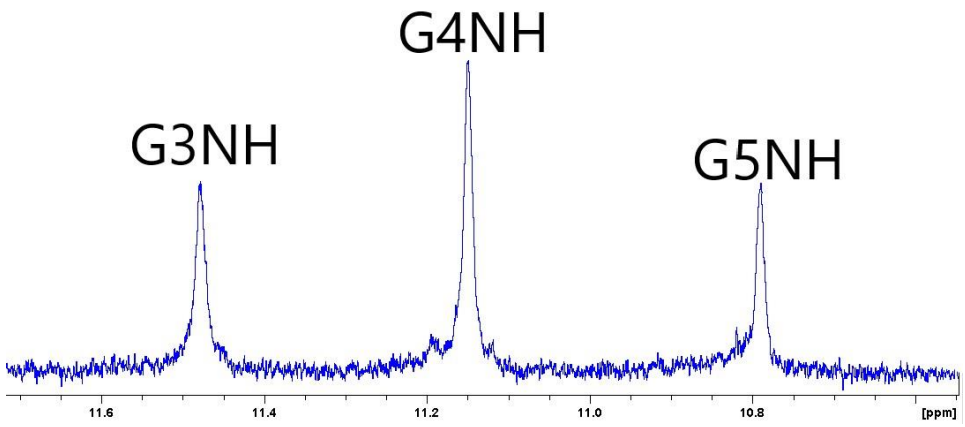

Figure 45 Imino peaks indicative of G-tetrad formation labelled with guanine number in aptamer d(TTGGGTT)4.

We see in Figure 46, much like the work done by (225), that line broadening and up-field shift occurs at peaks representative of proton G6NH (10.79ppm) significantly, alongside the significant peak broadening and down field shifting of T6H6/8 and T6CH3 peaks with the addition of proposed ligands. These significant changes demonstrate distinctly different bound and unbound forms through large broadening effects at a ratio of 0.5:1. There is also subtle line broadening and up-field shifting of G4NH (11.48ppm) and G5NH (11.15ppm) for each ligand that shows chemical exchange between two similar environments of bound and unbound. Maximum line broadening occurs at a ratio of 1:1 drug to G-quadruplex and chemical shift difference changing up to 1:1 with the bound and unbound peaks being

present. This matches the effect seen by nemorubicin intercalation with $d(TTGGGTT)_4$ in previous literature suggesting a 1:1 stoichiometry.

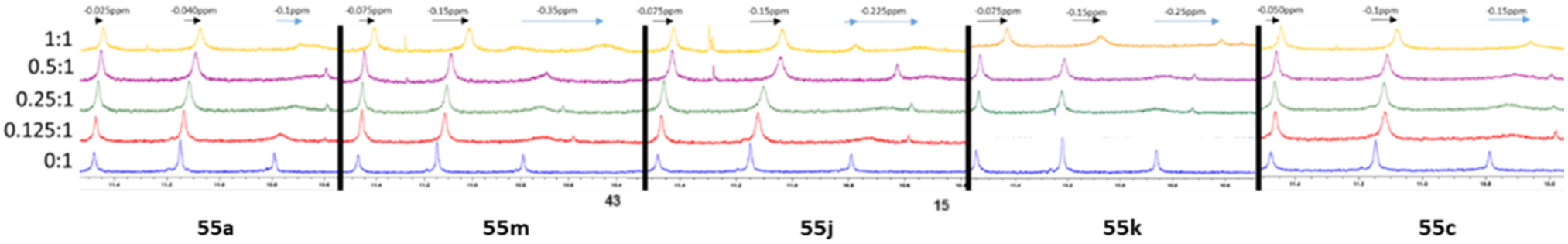

Figure 46 1D 1HNMR Spectra, referenced to TSP, showing titration of drug compounds and d(TTAGGGT)4. A slow exchange interaction, is illustrated with black arrows and fast exchanging interactions by blue arrows

In Figure 46 we see the drug compounds that display Drug-quadruplex interactions that match the effects of nemorubicin on the chemical shifts of d(TTGGGTT)4. In reference to the chemical shift differences values seen for nemorubicin: T6CH3 = +0.24; T6H6/8 = +0.34; G3NH = -0.11; G4NH = -0.15; G5NH = -0.36, which are taken as strongly intercalating values, with 2D NOESY results highlighting strong through space interactions. These values illustrate relative targets for chemical shift difference, which are suggested to elicit greater effectiveness and improvements in IC_{50} values with greater interaction seen between quadruplex structure and ligand. With ppm differences highlighted for the G3, G4 and G5 imino protons and T6 thymine peaks in Table 5 for each drug, we can then group the effects on G-quadruplex environment by different coupled groups and calculated IC_{50} values shown in Figure 47 to determine if the suggested relationship is feasible.

Table 5 Measured at 27°C in ppm (δ) and referenced from internal standard TSP. Solvent H_2O-D_2O (90:10 v/v), 25 mM phosphate buffer, 150 mM KCl, 1 mM EDTA, pH 6.7, R = 1. Δδ = δbound - δfree.

Compound	Difference from 1.58ppm (ppm) T6CH3	Difference from 7.23ppm (ppm) T6H6/8	Difference from 11.55ppm (ppm) G3NH	Difference from 11.22ppm (ppm) G4NH	Difference from 10.86ppm (ppm) G5NH
55a	0.09	0.17	-0.04	-0.08	-0.2
55m	0.093	0.22	-0.066	-0.135	-0.34
55j	0.146	0.19	-0.056	-0.11	-0.24
55k	0.157	0.126	-0.06	-0.115	-0.25
55c	0.094	0.16	-0.03	-0.07	-0.13

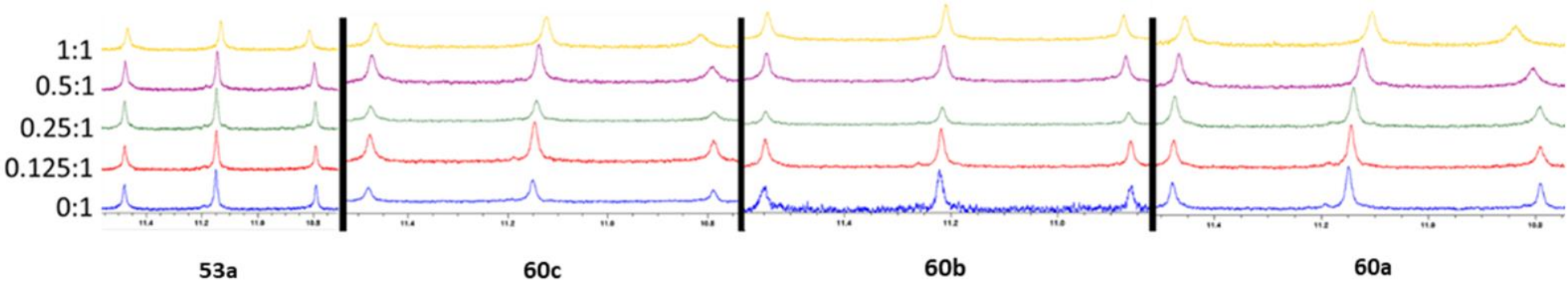

Figure 47 NMR Spectra referenced to TSP, showing titration of compounds that showed no interaction between drug and G4

In Figure 47 we see the compounds that do not show intercalation to the G-quadruplex, with control compound **53a** (no HeLa cell inhibition), HeLa cell inhibitors **60c**, **60b** and **60a** which we propose inhibit cell growth activity through a non-intercalating method of action.

The compounds that show intercalation see significant differences for several of the compounds that we can rank alongside the IC_{50} values of compounds to give a rudimentary correlation between IC_{50} values shown in Figure 48. We see two groups of correlating IC_{50} and chemical shift differences appearing with similar linear correlations of y=44.423x + 9.4167 (r^2 = 0.9864) and y=56.333x + 16.517, with one group of compounds containing mixtures of oxygen, sulphur and nitrogen and another group which contains only nitrogen respectively.

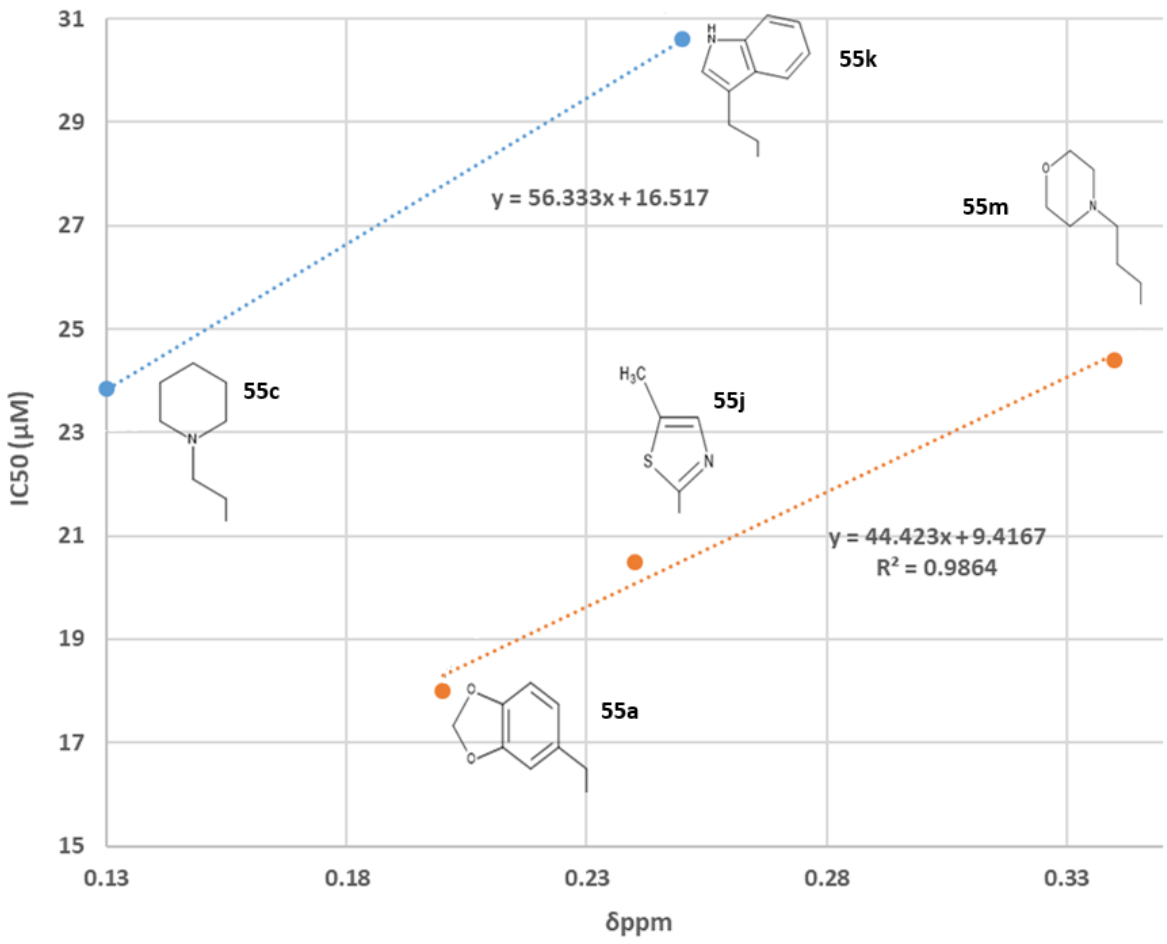

Figure 48 IC_{50} versus chemical shift differences in the G5NH peak of intercalating compounds with proposed groupings of correlations.

Chapter 4 – Discussion

The initial aim was to build a library of acrylamide compounds to couple to 9,10-dibromoanthracene **45,** as demonstrated previously by Le Gresley *et al.* (193) that through the use of Heck methodology, acrylamide couplings could be done after an initial reaction between acryloyl chloride and chosen amine groups. Anthracene was selected as our first structure to be investigated because of its favourable properties as a possible G-quadruplex intercalator alongside its demonstratable ease of use in synthesis. Working with anthracene for synthetic work is made easier by the solubility of anthracene in multiple solvent systems therefore allowing for multiple reaction schemes to be attempted. Another aspect that makes it favourable for this work was its relative inexpensiveness and reactivity, which meant that longer experiments are reduced.

Generation of acrylamides for coupling to 9,10-dibromoanthracene was done in a view to build upon previous libraries and investigate these coupled products for their intercalation potential and also ability for further modification to create novel G-quadruplex ligands with greater affinity.

One of the first amines we worked with was piperonylamine (**59a**) because it has the benzodixol ring, which could promote intercalation with G-quadruplex DNA. We decided to synthesise different types of acrylamides such as 4-(aminomethyl)pyridine and adenine. However, due to difficulties in separating these products from the reaction mixtures, we chose not to pursue synthesis of the acrylamides. The rationale for ceasing synthesis of these acrylamides was that acryloyl chloride substitution was not successful. It is thought the reason for this is that the nitrogen present on the rings of several chosen amine groups interfered with the coupling of acryloyl chloride to the primary amine targeted in this coupling. This hypothesise is supported by the large mixtures of products present after reaction. Despite these difficulties, we carried on using the amine groups in EDCI.HCl coupling and imine couplings.

Working with nucleotides was also problematic, especially with adenine and guanine, as they are difficult to solubilise in organic solvents. Multiple solvents systems were tried, for

example DMF, acetonitrile and chloroform. However, despite many attempts, none of them gave verifiable acrylamides. This suggests that nucleotides, which are interesting amines to investigate as previously stated, aggregate by intermolecular interactions between individual molecules. This interaction, alongside preventing solubility in most solvent systems, could also bring about issues in single nucleotide coupling to acryloyl chloride. Imidazo[1,2-*a*]pyridin-3-amine, 7-methyl-2-phenyl-(**h**) was one of the other amine groups selected due to the presence of two tertiary amines in the structure. Despite being a primary amine, which was thought to readily couple to our acid chloride, the amide was not formed. It was suggested this was because of the large side structure of the primary amine and possible transfer of free electrons away from the primary amine group to the large electron dense side chain of imidazo[1,2-a]pyridine group. In this situation, solubility of amines was also a limiting factor. There is previous evidence showing why nucleotides have poor solubility, which suggests that a similar mechanism may be preventing solubility of other type of amines that contains secondary or tertiary amine groups.

Afterwards, it was decided to couple piperonylamine acrylamide (**59a**) to 9,10-dibromoanthracene using the Heck Reaction. The solvent system used was dry DMF, as previous literature showed that this gave the highest yield when compared to other common solvent systems (226). It is thought this is because DMF demonstrates improved dispersion and reduced aggregation of catalyst during reaction (227). During the reaction, the mixture precipitated a black solid. Analysis of solid by NMR and TLC showed a mixture of the starting material and partial coupling to the anthracene ring. For this reaction, several types of palladium catalyst and ligands were tested, shown in Table 6.

Table 6 List of ligands used in synthesis.

Catalyst	Ligands	Synthesis
$Pd(OAc)_2$	1,3-Bis(diphenylphosphino)propane	**53a**
$Pd(OAc)_2$	Tri-(-o-tolyl)phosphine	**60a,60b**
$Pd(OAc)_2$	Triphenylphonsphane	**61a,60c**

However, in our hands, none of them achieved successful Heck coupling. It is thought that the complexation of the palladium catalyst by nucleophilic groups distal to the acrylamide lead to a deactivation of catalyst. Another intriguing finding was that piperonylamine in its amine form not its acrylamide form was able to couple with modified anthracene ring to form (**60d**). This illustrates that the anthracene ring was either too active when not modified for this reaction and the conditions that might have been required or the piperonylamine acrylamide was not reactive enough. Bond-energy calculations could be interesting to study to decide whether this is the case. A suggested reason for unsuccessful coupling was the low reactivity of acrylamide in the Heck reaction which is illustrated by the long experimental time required for not only the unsuccessful couplings but also the successful ones. The reason for this could be that electrons in the acrylamide are held in more stable positions than acrylates which show higher activity in the Heck Reaction. Complexation of palladium catalyst could also be explained by the amine groups not involved in acrylamide formation having through space interactions with palladium (II) acetate. The formation of a stable complex formation between a simple amine and palladium (II) acetate has previously been detailed where aliphatic amines were shown to coordinate strongly with palladium to form a complex with limited C-H activation (228). This effect is highlighted through the mixing of palladium salts stoichiometrically with 2 aliphatic amines which coordinate to the electrophilic palladium ion and subsequently form a saturated square-planar complex which is unreactive to C-H cleavage this mechanism is shown in Figure 49. This finding supports our proposal that palladium is complexed out of solution and it would be appropriate to protect amine groups with electron withdrawing groups and other directing groups so that C-H activation can be achieved (228).

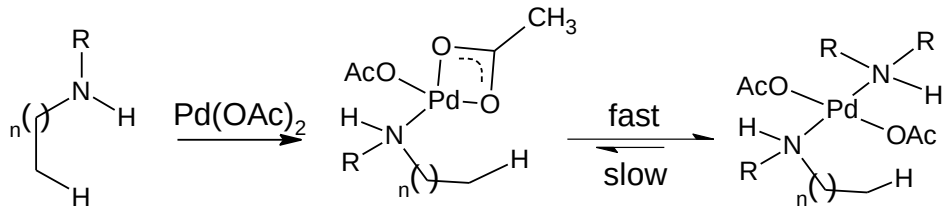

Figure 49 Palladium (II) acetate complexation with aliphatic primary amines to form stable non C-H activating planar complex.

After these unsuccessful coupling attempts, we proceeded with the modification of our anthracene ring with methyl acrylate and subsequent hydrolysis, yielding the carboxylic acid for amide condensation reactions. These reactions met with greater success. With EDCI coupling, we were able to couple two amine groups (**a**,**c**) , however at the same time we had unsuccessful peptide coupling using this coupling agent. Repetition of these couplings with HATU coupling agent, which has previously shown great coupling efficiency and fast reaction rates due to stabilising of the incoming amine through a hydrogen-bonded-7-membered cyclic transition state were also unsuccessful in complete coupling with only partial coupling at one side (229).

Having successfully coupled some amine groups of interest with EDCI on 9,10-dibromoanthracene, we decided to work with other pi-pi staking candidates. To begin with, 1,3,5-tris(4-bromophenyl)benzene was the first trisphenyl structure to be modified. We initially attempted coupling using different types of acrylamide such as N-(Butoxymethyl) acrylamide, N-(Isobutoxymethyl) acrylamide and piperonylamine acrylamide via Heck Reaction. The full coupling of these acrylamides was unsuccessful, due to coupling on one side or two sides rather than three sides and obtaining intractable complex mixtures of different derivatives, which were resistant to our attempts at purification and significant yield. To achieve any yield experiments also had to run for more than 48 hours, with TLC and NMR monitoring showing little product. The synthesis of multiple products with no clear end product could be explained by the 9,10-dibromoanthracene and tris(4-bromophenyl)benzene aromatic structures, where has been previously found that self-

coupling and alkene migration after initial coupling can produce derivatives of desired product (230). Despite these unsuccessful couplings, we attempted to demonstrate that coupling could work through the use of a simple acrylamide to remove any side chain effects in the action of Heck coupling. From previous studies it was shown that potassium carbonate (K_2CO_3) can be used as an effective base to aid the initial reduction from Pd(II) to Pd(0) (230). From the results (Table 4), we see that this coupling was successful and means that modifications to amine group could be done post coupling if this compound showed potential in anticancer activity or intercalation with G-quadruplex structures.

It is thought that if we could couple methyl acrylate to this trisphenyl planar structure and then transform it to tris carboxylic acid it would be the best candidate for subsequent EDCI coupling. The Heck methodology originally used was taken from studies done by Zhao et al. (231) where they synthesised 4,4',4'-benzene-1,3,5-tricinnamic acid at 97% yield. Instead of using a phosphine ligand they used a phase transfer catalyst tetrabutylammonium bromide (TBAB) to improve the yield and make removal of the ligand much easier. Through this method, we also decided to try simple acrylamide (**53a**) coupling to trisphenyl planar structure **53**. The reaction was successfully completed within 24 hours with a yield of 20%. This shows that acrylamide coupling to trisphenyl planar structure is possible, however coupling of larger acrylamides has difficulties from several unknown sources. Possibly steric hindrance, electronic effect, or a combination of functional groups. Further work clarifying reason for this would be beneficial in choosing the best coupling mechanism.

Imine coupling, through condensation of primary amines with a carbonyl (aldehyde/ketone), to form the conjugation between the planar core and selected amine group can be done through conversion of our planar core to an aldehyde. Aldehydes have been shown to be important functional groups for conjugation of compounds e.g the generation of imines (Schiff bases) from aldehydes. The use of aldehydes in this way also benefits from the reaction kinetics versus other functional groups, such as ketones, which show a slower reaction when forming bonds, specifically shown with hydrazones in research done by Leiro

et al. (232) it was also demonstrated that aldehydes higher lability under acidic conditions providing a potential role in pH-responsive drug delivery.

Due to these advantages, we decided to start reducing our methyl acrylate coupled anthracene ester compound to aldehyde using DIBAL reduction. However, due to the reactivity of DIBAL, the ester compound was reduced to alcohol rather than desired compound. Therefore, to minimise this problem and to see if the actual imine coupling would work; we bought the aldehyde version of the anthracene compound. Testing the imine couplings showed relative success in comparison to Heck and EDCI couplings. Getting the actual aldehyde also gave us more time to synthesise imine coupled products. This step proved valuable as several synthesised imines later showed *in vitro* culture anticancer activity and G-quadruplex intercalation. The imine coupling was robust with several different and varied amines coupled to the anthracene aldehyde in good yields (~80% for **55k**, 78% for **55a** and 75% for **55j**). The amines had different atoms present such as piperonylamine with two oxygens in the ring system and nitrogen atoms present in tryptamine, thiazole, 3-aminoacetanilide and 3-morpholinoprorylamine, which shows that the imine coupling seems relatively unperturbed by multiple amine groups.

It was suspected that the stability of the imines in commonly used biological buffer would be too poor when we considered these compounds for cell viability testing. This would be through previously mentioned lability of the imine nitrogen when in aqueous/acidic conditions, such as pH-5.5 to 7 commonly used in biological buffers e.g. phosphate buffer solution. To our surprise the stability of the imine coupled conjugates was shown to be sufficient over the time period and medium conditions measured through incubations of conjugates in model conditions with NMR analysis used to monitor changes (Figure 46). The NMR analysis showed that the imine bond was stable over 24 hours with negligible loss of conjugation in the model system.

After sufficient stability of imine couplings was established, we picked 11 of the potential G-quadruplex ligands to be tested in cell culture and for biochemical testing in a model G-

quadruplex system. These compounds were selected so that imine groups, coupling methodology and planar core type could be compared and conclusions on their effectiveness drawn.

3 out of the 11 compounds showed no anticancer activity as seen in Figure 36, these included 1 Heck coupled and EDCI coupled conjugates, including the trisphenyl planar acrylamide compound **53a**. Cell culture IC_{50} values were subsequently determined. They illustrated that imine coupled conjugates had a much higher anticancer activity than Heck coupled compounds. Alongside a greater variability between different amine groups with IC_{50} values ranging from 18 to 30.6μM with Heck coupled conjugates at 34.9-38.3 μM. This suggests that imine couplings have greater potential in drug design and as seen from intercalation data may have crucial elements required for stabilization of G-quadruplexes that Heck coupled conjugates do not.

In our results we see that 5 of our 9 compounds that demonstrated HeLa cell line cytotoxicity activity demonstrated intercalation with the G-quadruplex model d(TTGGGTT)4. The compounds that showed intercalation were interestingly all imine coupled products with a tertiary amine present one bond away from the planar ring. With compound **53a**, where a primary amine exists at the terminal end of the side chain, we see no intercalation despite their being more opportunity for G-quadruplex hydrogen bonding with a third amine present. We also see that **60c** which has no amine present has no intercalation but has HeLa Cell line cytotoxicity so the method of cell apoptosis must be through a different mechanism than G-quadruplex interaction. We also interestingly see that **60b** and **60a**, which both have the same secondary amine position at 4 bonds away from planar centre of the ligand, have similar IC_{50} values to each other and also **60c** but again show no intercalation. This suggests that these 3 compounds induce HeLa Cell apoptosis/necrosis through the same method. These initial findings from the G-quadruplex intercalation study demonstrates a need for tertiary amines in anthracene derivatives to give G-tetrad intercalation potential.

The anthracene derivatives that contain the tertiary amines, **55a**, **55m**, **55j**, **55k** and **55c** are shown to be have different functional groups present in their side chains; 1,3-benzodioxole, propylmorpholine, 2,5-dimetylthiazole, 3-Methyl indole and piperidine respectively, which we suspect act to stabilise the hydrogen bond between the tertiary amine and oxygens of phosphate. However, all of these groups have been shown in previous studies to demonstrate DNA and G-quadruplex intercalation alongside anti-cancer activity. This suggests that each of these groups may have more of an effect on IC_{50}, than solely effects on hydrogen bond stabilisation. They may also make other intercalations possible through different mechanisms of binding, apart from g-tetrad stacking as described in results.

We see that the two groups which were grouped by their absence of oxygen or sulphur, piperidine and 3-Methyl indole show quite divergent differences in ppm between bound and unbound forms of the G4 model. These two compounds also have 2 of the higher IC_{50} values of the 5 intercalating compounds, 24μM (**55c**) and 30.5 μM (**55k**), which shows that despite the range in changes of ppm these two compounds are relative outliers. Previous studies have demonstrated non-selective binding to DNA and G4 structures where the mode of binding to DNA, like our results, showed a 1:1 stoichometry, with gibbs free energy calculations showing a spontaneous intercalation suggesting a stabilising, energetically favourable reaction (233). It was also shown that using piperidine as a N-propylamino attached to carbazoles gave the highest stabilizing ligands in a study. Interestingly however they did identify that there was an inverse correlation between G-tetrad stabilization and G4 DNA selectivity (234).This is very interesting for our results, as it could begin to explain why we see that the relationship between the change in ppm does not correlate completely with IC_{50} values, even showing an inverse relationship to what was expected from nemorubicin results (204). It could show that G4 ligands intercalate and stabilise very effectively but IC_{50} will be increased as G4 ligand is wasted in duplex DNA intercalation and stabilization. This could explain why we see piperidine having similar chemical difference effects and stabilization effects to other compounds but has a higher IC_{50}. 3-Methyl indole is less

investigated for this purpose because of its role primarily as an odourant, with extensive use in animal studies. There are however genetic studies that show protective mechanisms against damage by 3-methyl indole derivatives that can induce apoptosis at low concentrations. This was shown in a study by Nichols WK, where they look at 3-methyl indole mediated cytotoxicity in human epithelial lung cells, with CYP2F1 over expressed. This is relevant to this study as it shows that 3-methyl indole has a structure activity relationship which relates to cytotoxicity of genetically impaired cells, which could possibly explain anti-cancer activity (235). The anti-cancer activity of indoles has also been shown with indole groups in isoxazolo[5′,4′:5,6]pyrido[2,3-b]indoles, which showed significant anticancer activity comparable to standard drugs however the mechanism of action and structure activity relationship is yet to be investigated (236).

The three groups that contained oxygen, sulphur and nitrogen, and nitrogen and oxygen, 1,3-benzodioxole, 2,5-dimethylthiazole and N-propylmorpholine respectively, showed a close linear correlation between their ability to stabilise G4 structure and IC_{50}. The oxygen, sulphur and nitrogen containing group had also showed the best IC_{50} values with 1,3-benzodioxole and 2,5-dimethyl thiazole as the best candidates for further testing as they have similar differences in ppm and also the best IC_{50} values of tested ligands. Further synthesis and reinforcement of DNA binding potential of 1,3-benzodioxole has been illustrated by a study which showed DNA binding was moderate to mild and suggested that cytotoxic effects were through a different mode of action, which supports the selectivity argument for 1,3-benzodioxole (237) .This assumption is further supported by the demonstration of testing 1,3-benzodioxole as potential telomerase inhibitors. They demonstrated through molecular docking that a benzodioxole derivative had potent telomerase inhibition alongside potent anticancer activity in human gastric and human melanoma cell lines. They illustrated that the docking of their derivative required two intermolecular hydrogen bonds, and two benzene rings which form π-cation interactions (238). This shows that this group may add additional benefit through telomerase inhibition in a different method of action to the one investigated here with G4 stabilisation, leading to

telomerase inhibition. The 2,5-dimethylthiazole has been studied a lot in the form of the fluorescent marker thiazole orange for its intercalation potential. It was shown in early research that thiazole orange binds both as a monomer and dimer to DNA with monomers of thiazole orange stacking between DNA bases. It is also shown as the main way of binding with duplex DNA. Interestingly they also reported binding to poly(dG) which showed binding as a monomer and dimer as well. This supports our results showing intercalation and stabilisation of G4 (239). Selective stabilization of G4 structures by thiazole has further been supported more recently with studies that showed 1:1 stoichometry between dye and G-tetrads in quadruplex DNA. It also illustrated that there was a tight complex formed between the two. Interestingly they showed that in the presence of K^+ ions, this binding seemed to disappear (240).

Compound **55m**, which has a propylmorpholine group has been implemented in the design of compounds for telomeric and oncogenic G-quadruplex affinity with varying degrees of success. It was shown through molecular docking analysis that compounds made with propylmorpholine interact with the groove and or loop of the G-quadruplex, which supports our stacking hypothesis through interaction with these external components. This study also showed inhibition in the growth of A549 cancer cell lines with low cytotoxicity to normal cells. This study concluded that addition of propylmorpholine to naphthalimide supports tumor cell cytoxicity selectivity (234)(241).

With these 5 compounds identified through titration NMR to demonstrate similar binding characteristics to previously tested potential anti-cancer drug compound further validation of the method of action of these compounds, selectivity, and biochemical methodologies etc needs to be done. TRAP assays would potentially be useful and allow for greater modification and potentially provide better IC_{50} values. This would give great insight for medicinal chemists who can use these compounds as scaffolds for further investigation. The use of NMR for through space characterisation experiments, such as NOESY and ROESY alongside molecular docking and interaction studies, STD and tr-NOESY would give a clear understanding of the method of action of each of these compounds.

Table 7 Table comparing IC_{50} and chemical shift difference between intercalated and non-intercalated G-quadruplexes for intercalating compounds and controls from reference (204).

Compound	Δδ (ppm)	IC_{50}
55k	0.25	30.6
55m	0.34	24.4
55c	0.13	23.84
55j	0.24	20.5
55a	0.2	18
Doxorubicin (204)	0.31	0.374
Nemorubicin (204)	0.31	0.08

Looking at Table 7, we see the IC_{50}'s of doxorubicin and nemorubicin are much lower than the IC_{50} values of our synthesised compounds, however we do see that their **Δδ** is comparable to our two lowest IC_{50} compounds. This suggests a similar interaction mechanism where a 1:1 stoichiometry, with planar stacking on the G6 tetrad, demonstrated by the paper where these values were taken from (204). This however does show that G-quadruplex binding may start through this stacking and be an initiating step for cytoxicity, but we see from these results that side chains which give comparable chemical shift differences and intercalation stoichiometry produce very different IC_{50} values. This however could be explained by selectivity measures that further studies could elucidate through incubation of drug solutions with healthy cells alongside the aforementioned TERT assay to measure telomerase inhibition and binding studies with duplex DNA to measure selectivity for G-quadruplexes.

Chapter 5 – Conclusion

5.1 Conclusions

We successfully synthesised and characterised 19 novel compounds, which include potential G-quadruplex ligands, G-quadruplex ligand cores and respective ligand acrylamides.

At the beginning of this research, we attempted to optimise the Heck reaction to facilitate C-C coupling reactions. We varied ligands, temperature, and reaction time. This optimisation afforded three potential novel G-quadruplex ligands. Following this, optimisation of EDCI coupling was done to synthesise two potential novel G-quadruplex ligands. Finally, imine couplings were optimised to produce six potential novel G-quadruplex ligands with reasonable yields (~65.5%).

Eleven of these compounds were selected to be tested on HeLa cancer cell lines. Before testing these novel compounds on cancer cells, stability tests were done. This helped to understand their stability in cell culture media. From cell culture results, it was shown that three of the ligands had no cancer activity and eight of the ligands showed cancer activity with IC_{50} values ranging from (~18-31μM). Compounds that showed anticancer activity were then investigated using NMR titration studies to elucidate whether ligands intercalated and stabilised a model G-quadruplex structure. This investigation showed that the five imine coupled ligands showed G-quadruplex intercalation with 1-1 stoichiometry matching that of current cancer drugs Doxorobucin and Nemorubicin in this model.

The promotion of quadruplex DNA formation, as observed in solution by NMR, and initial biological testing, suggests the class of G-quadruplex ligand based on imine coupled ligands possess an anticancer activity. Further investigation in terms of both duplex/quadruplex selectivity, bioavailability, molecular modelling, and stabilisation power will allow for a greater of understanding of the QSAR that may exist and allow medicinal chemists to build upon these structures.

5.2 Future Work

To validate the proposed correlation between cell culture analysis and intercalation of G-quadruplex structures, a TRAP assay (telomeric repeat amplification protocol) can be used to measure the telomerase inhibition by respective G-quadruplex ligands. Moreover, to be able to use these G-quadruplex ligands for chemotherapy drug targets, we need to quantify selectivity for cancer cells. The incubation and viability analysis of healthy cells with our drug targets will give us this information. Combinations of these techniques will give a wider picture of which ligands are best suited for further investigation and modification as drug targets for G-quadruplex targeting drugs in cancer therapies.

To further modify novel ligands a Dynamic Combinatorial library can be built. This approach uses quadruplex-forming-oligonucleotides to selectively facilitate imine formation, metathesis, and other reversible reactions, which can occur in aqueous media in physiological conditions.

Analytical techniques, which can be used to formulate a robust, high throughput assay include Circular Dichroism Fluorescent assay and Mass spectrometry(242)(243)(244).

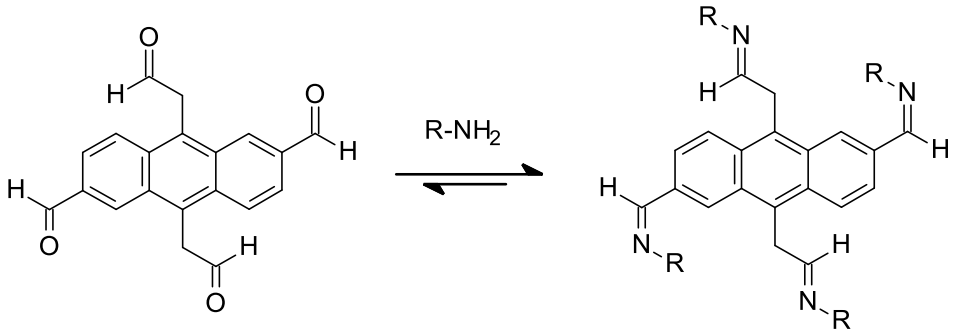

Increased intercalation with G-quadruplex will push equilibrium to the right.

Scheme 23 Idealised reversible reaction of imine couplings with anthracene tetra aldehyde.

For a more selective approach however the use of molecular modelling will allow for site specific alterations to the ligand structures to allow for greater intercalation potential and interaction between ligand and G-quadruplex structures. 2D NOESY experiments can show through space contacts of G-quadruplex structure in solution when in the bound state and

when not in the bound state and this will give insight into how the conformation of the ligand affects its intercalation potential and inhibitory effect. Saturation transfer difference NMR can also qualitatively compare ligand structure proximity to G-quadruplex structure and allow for development of lead compounds with conserved key groups identified. NMR fragment-based drug discovery has been recognised as a widely applicable screening method (245). Lepre has reviewed the construction of a fragment library through development of NMR screening and what to do following a screen to improve drug discovery based upon the findings of the screens (246). Group Epitope Mapping (GEM) allows for quantitative drug-target interaction through providing definitive information regarding ligand binding orientation. This methodology was first applied in 2001 with the 120-kDa protein lectin Ricinus Communis Agglutinin I (RCA/20) and its binding relationship with saccharide ligands.

Further synthesis using amines selected by similarity to coupled amines with high IC_{50} values and intercalation success will allow for more hit compounds to be discovered and elucidate more information on side chain preference. Alongside this selection of new amine groups protection of side chain amines and amine groups can be done to confirm hypothesis that unsuccessful Heck Coupling was due to complexation of amine groups to palladium (II) acetate. Another thing that could be done is coupling of simple primary amines to make acrylamides and investigate Heck couplings between these. This would allow for comparisons between acrylamide side chains and Heck coupling effectiveness, potentially giving access to a larger library of possible G-quadruplex ligands with post coupling modification opportunities.

Chapter 6 – Experimental

6.1 General Experimental Methods

^{1}H-NMR spectra were acquired with a Brüker AV400 FT-NMR spectrometer equipped with a BB-^{1}H/D Z-GRD probe head (broadband multinuclear with autotune) at a probe strength of 400MHz and a Bruker AV600 FT-NMR Spectrometer equipped with a PATXI ^{1}H/D-^{13}C/^{15}N Z-GRD probe at a probe strength of 600MHz. ^{13}C-NMR spectra were acquired with probe routing giving 100 MHz using the Brüker AV400 or 125 MHz when using the Brüker AV600. All NMR spectra were acquired with high throughput 5mm NMR tubes o/d, No Z107374, Brüker BioSpin AG, Switzerland. NMR spectral measurements were acquired with samples completely dissolved in deuterated solvents such as: chloroform-d, dichloromethane-d_2, dimethyl sulfoxide-d_6, or methanol-d_4. All NMR peak chemical shifts are in ppm relative to an internal standard Trimethylsilylpropanoic acid (TSP) at δ = 0.00. All coupling constants use the units of Hertz (Hz). Spectral acquisitions were sweep width optimised in 1D 1H spectra and optimised parameter sets specific to 2D NMR (HSQC and COSY) were used, these included specific setting of relaxation delays, and sensitivity improved pulse sequence for HSQC alongside sweep width optimisation to avoid overlap of peaks which cause data aliasing. Acquired Free induction decays (FIDs) processed with standard Fourier transform NMR with transients averaging to increase S/N. The data was automatically processed with the window function, linear prediction, zero-filling, phasing and baseline optimisation set within TopSpin 3.5 pl7 (c) 2017 Brüker BioSpin.

All solvents were dried using molecular sieves. TLC analysis was performed using Fluka glass backed silica gel plates or Merck aluminium backed aluminium oxide. Identification of spots was achieved at 254 or 365 nm UVR by a UVP UVGL – 58 multiband UV lamp, alongside, iodine, $KMnO_4$, vanillin or ninhydrin stains.

Low resolution mass spectra (LR MS) and High-resolution mass spectra (HR MS) were acquired by MEDAC Ltd. This was done in accordance with BS EN ISO 9001:2008 provision for microanalysis service.

Infra-red analysis was performed using the neat oil or solid powdered sample coated onto ATR disc which is analysed with a ThermoScientific Nicolet iS5 FT-IR spectrophotometer.

Melting points were measured using Gallenkamp melting point apparatus (serial number A090007).

All chemicals were purchased from Sigma-Aldrich or Fisher scientific. Anhydrous reactions were performed using dry glassware which was flame dried under vacuum and carried out under an inert nitrogen environment. For work-up procedure deionised water was used with saturated LiCl and saturated aqueous solutions of NaCl (brine). Evaporation of volatile solvents done on a Büchi RE111 Rotovapor in a Büchi 461 water bath to maintain desired temperature.

_N_-[(2_H_-1,3-Benzodioxol-5-yl)methyl]prop-2-enamide (59a)

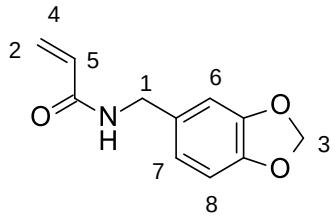

59a

Piperonylamine acrylamide was synthesised under dry conditions, DCM (75ml) was added into a flask and stirred. Trimethylamine (8.23 ml) and piperonylamine (3.40g) were then added into the solution. Acryloyl chloride (2.66 ml) was added in a drop wise manner over 5 minutes, while the reaction was in an ice bath. The reaction mixture was warmed to room temperature and stirred for 1 hour. TLC and NMR were used to monitor and characterise the reaction mixture. The resulted crude product was quenched with iced water (200 ml) and the organic fraction was separated with DCM (3x50 ml). The organic extracts were then washed with acid (3 x 40 ml, 3 M), water (2x 50 ml), NaOH (3x 30 ml, 2 M) and once again with water (2x50 ml). The organic component was dried (Na_2SO_4), filtered and evaporated under a reduced pressure. Recrystallization with hot methanol was used to afford yellow powder **59a** (2.35g, 50.6%).

^{1}H NMR (400 MHz; d_6-DMSO) δ= 4.25 (2H, d, *J* = 5.90 Hz, CH-1), 5.6 (1H, dd, *J* = 10.29, 2.16 Hz, CH-2), 5.98 (2H, s, CH-3), 6.12 (1H, dd, *J* = 17.12, 2.20 Hz, CH-4), 6.26(1H, dd, *J* = 18.19, 10.20 Hz, CH-5), 6.74 (1H, dd, *J* = 8.01, 1.58 Hz, CH-7),6.82(1H, d, *J*= 1.64Hz, CH-6), 6.84 (1H, d, *J* = 7.84 CH-8), 8.48 (1H,s,NH)

^{13}C-NMR (400 MHz; d_6-DMSO) δ= 40.688, 101.299, 107.964, 109.063, 147.72, 125.879, 126.933, 131.613, 132.628, 146.544, 165.6

IR (ATR): v= 2971.79, 2864.31, 1649.93, 1248.41, 1054.43

HR MS (ES) m/z = found 204.0660, requires 204.2029 $[M-H]^+$

MP=111-113^{o}C

(*E*)-3-[4-[3,5-bis[4-[(E)-3-amino-3-oxo-prop-1-enyl]phenyl]phenyl]phenyl]prop-2-enamide (53a)

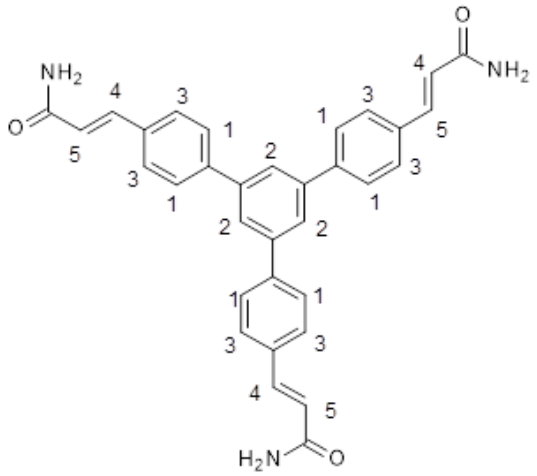

53a

Palladium acetate (14mg, 0.25mmol) and 1,3-bis(diphenylphosphino)propane (80mg, 0.75mmol) were added to a Schlenk tube in DMF (10ml) and stirred at room temperature for 10 minutes to generate the active catalyst. After this, trimethylamine (0.6ml) and 1,3,5-tris(4-bromophenyl) benzene (0.7g) were then added to the reaction mixture, at room temperature, followed by addition of 0.3g acrylamide. The mixture was heated at 90°C for 48hrs under nitrogen. The reaction was allowed to cool and dilute HCl (15 ml, 2M) was added. The resulting precipitate was filtered and washed with water (3x 20 ml) and diethyl ether (3x15 ml) and dried under vacuum to afford **53a** as a white solid yield: (0.49g,74%).

^{1}H NMR (400 MHz; d_6-DMSO) δ= 8.01 (3H, s, CH-2), 7.99-7.94(6H, 7.97 (ddd, *J*=8.28, 4.12 , 2.12 Hz, CH-1), 7.97(d, *J*=16.02 Hz, CH-4), 7.74-7.68 (6H, 7.71 (ddd, *J*=8.51, 8.41, 1.71, CH-3), 6.7(3H ,d, *J*=15.86 Hz, CH-5)

^{13}C-NMR (400 MHz; d_6-DMSO) δ= 122.424, 125.483, 127.624, 128.684, 134.876, 138.626, 141.226, 141.416, 167.165

IR (ATR): v= 3706.08, 3679.45, 2980.20, 2921.54, 1658.28, 1591.5.

HR MS (ES) m/z = found 514.2136, requires 514.5927 $[M+H]^+$

MP=222-224^{o}C

(*E*)-N-(butoxymethyl)-3-[10-[(E)-3-(butoxymethylamino)-3-oxo-prop-1-enyl]-9-anthryl]prop-2-enamide (60a)

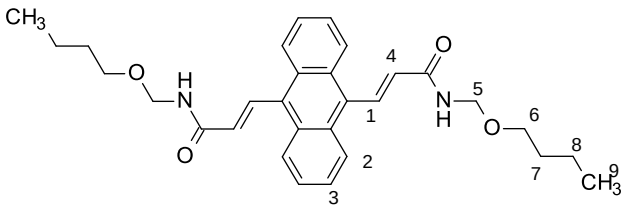

60a

Palladium acetate (119mg, 0.534mmol) and tri-(*o*-tolyl)phosphine (162.5mg, 0.534mmol) were added to a Schlenk tube, followed by stirring in DMF (10ml) for 10 minutes at room temperature to generate the catalyst. After activating the catalyst trimethylamine (2.98 ml) and 9,10-dibromoanthracene **(**0.8g) were added to the reaction mixture, at room temperature, followed by addition of *N*-(butoxymethyl)acrylamide (3.38g). The mixture was heated at 90°C for 48hrs under nitrogen to complete of the reaction. The reaction was allowed to cool and dilute HCl (15 ml, 2M) was added. The resulting precipitate was filtered and washed with water (3x 20 ml) and diethyl ether (3x15 ml) and dried under vacuum afforded **60a** as green solid; yield: (1.02g, 87%).

^{1}H NMR (400 MHz; d_6-DMSO) δ= 0.89 (6H, t, *J* = 6.88 Hz, CH-9), 1.36 (4H,m-5, *J* = 7.71 Hz, CH-8), 1.5 (4H, tt, *J* = 7.42, 6.45 Hz, CH-7), 3.49 (4H, t, *J* = 7.24 Hz, CH-6), 4.7 (4H, s, CH-5), 6.5 (2H, d, *J* = 16.04 Hz, CH-4), 7.6 (4H, ddd, *J* = 7, 3.8, 3.1 Hz, CH-3), 8.2 (4H, ddd, *J* = 6.81, 3.23, 3.46 Hz, CH-2).8.3 (2H,d, *J* = 16.05 Hz, CH-1)

^{13}C-NMR (400 MHz; d_6-DMSO) δ= 13.8, 19.3, 31.8, 68.4, 70.3, 119.7, 126.4, 126.6, 129.7, 130.6, 133.2, 163.7

IR (ATR): v= 3279.77, 1658.76, 1551.60, 1247.83, 1135.69, 1110.44, 979.01.

HR MS (ES) m/z = found 488.2673, requires 488.6178 $[M]^{+}$

MP=333-335^{o}C

(*E*)-N-(isobutoxymethyl)-3-[10-[(E)-3-(isobutoxymethylamino)-3-oxo-prop-1-enyl]-9-anthryl]prop-2-enamide (60b)

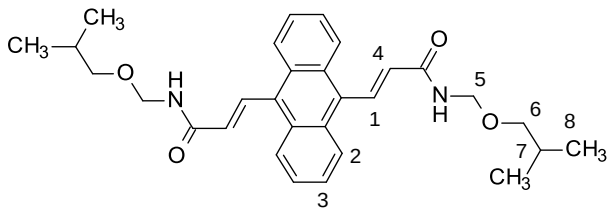

60b

Palladium acetate (119mg, 0.534mmol) and tri-(*o*-tolyl) phosphine (162.5mg, 0.534mmol) were placed in a Schlenk tube, followed by stirring in DMF (10ml) for 10 minutes at room temperature to generate the catalyst. After activating the catalyst, trimethylamine (2.98 ml) and 9,10-dibromoanthracene (0.8g) were added to the reaction mixture, at room temperature, followed by addition of *N*-(isobutoxymethyl)acrylamide (3.38g). The mixture was heated at 90°C for 48hrs under nitrogen to complete the reaction. The reaction was allowed to cool and dilute HCl (15 ml, 2M) was added. The resulting precipitate was filtered and washed with water (3x 20 ml) and diethyl ether (3x15 ml) and dried under vacuum afforded **60b** as green solid; yield: (0.83g, 74%).

^{1}H NMR (400 MHz; d_6-DMSO) δ= 0.8 (12H, d, *J* = 6.7 Hz, CH-8), 1.6 (2H, septt, *J* = 6.62, 6.34 Hz, CH-7), 2.7 (4H,d, *J*=0.55Hz, CH-6), 2.8 (4H, s, CH-5), 6.5 (2H, d, *J* = 16.03 Hz, CH-1), 7.6 (4H,ddd, *J* = 6.8,3.25,3.17 Hz, CH-3), 8.24 (4H, ddd, *J* = 6.8,3.25,3.17 Hz, CH-2),8.3(2H, d, *J* = 16.03 Hz, CH-4), 9.2 (2H, broad singlet, NH),

^{13}C-NMR (400 MHz; d_6-DMSO) δ= 19.1, 28.1, 68.4, 70, 119.7, 126.3, 126.4, 129.7, 130.8, 133.4 163.9

IR (ATR): v= 3296.18, 1650.72, 1547.66, 1248.16, 1141.80, 1120.13, 992.67

MS (ES) m/z = found 488.2678, requires 488.6178 $[M]^{+}$

MP= 339-341^{o}C

(*E*)-3-[4-[3,5-bis[4-[(E)-3-hydroxy-3-oxo-prop-1-enyl]phenyl]phenyl]phenyl]prop-2-enoic acid(67)

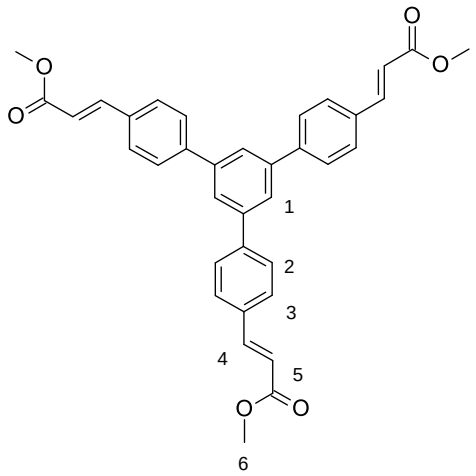

67

Palladium acetate (20.6mg, 0.092mmol) and triphenylphosphine (48.2mg, 0.184mmol) were placed in a Schlenk tube, followed by stirring in DMF (10ml) for 10 minutes at room temperature to generate the catalyst. After activating the catalyst, trimethylamine (0.225ml) and 1,3,5-tris(4-bromophenyl) benzene (1g) were added to the reaction mixture, at room temperature, followed by addition of 0.145ml of methyl acrylate. The mixture was heated at 90°C for 72hrs under nitrogen to complete of the reaction. The reaction was allowed to cool and dilute HCl (15 ml, 2M) was added. The resulting precipitate was filtered and washed with water (3x 20 ml) and diethyl ether (3x15 ml) and dried under vacuum afforded **67** as white crystals; yield: (0.5g, 52%).

^{1}H NMR (400 MHz; d_6-DMSO) δ= 3.7 (9H, s, CH-6), 6.7 (3H, d, J = 16.8 Hz, CH-5), 7.7 (3H, d, J = 16.3 Hz, CH-4), 7.8 (6H, d, J = 8.61 Hz, CH-3), 7.9 (6H, d, J = 8.2 Hz, CH-2), 8.0 (3H, s, CH-1).

^{13}C-NMR (400 MHz; d_6-DMSO) δ= 51.485, 117.8, 124.723, 128.688, 128.918, 133.962, 141.298, 142.146, 144.014, 145.071, 167.218

IR (ATR): v= 2948.21, 1716.89, 1312.94, 1266.90.

HR MS (ES) m/z = found 559.2119, requires 559.6268$[M]^{+}$

MP=152-154^{o}C

Methyl (E)-3-[3-[3,5-bis[(E)-3-methoxy-3-oxo-prop-1-enyl]phenyl]-5-[(E)-3-methoxy-3-oxo-prop-1-enyl]phenyl]prop-2-enoate (61a)

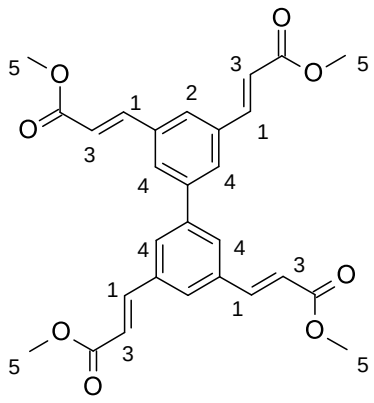

61a

Palladium acetate (23.79mg, 0.106mmol) and triphenylphosphine (55.6mg, 0.212mmol) were placed in a Schlenk tube, followed by stirring in DMF (10ml) for 10 minutes at room temperature to generate the catalyst. After activating the catalyst, *N,N*-diisopropylethylamine (1.48ml) and 3,3′,5,5′-tetrabromo-1,1′-biphenyl (0.25g) were added to the reaction mixture, at room temperature, followed by addition of methyl acrylate (0.76ml). The mixture was heated at 90°C for 72hrs under nitrogen to complete the reaction. To the reaction mixture, EtOAc 20ml was added and the organic solution was washed with brine (20ml x 3) and LiCl (20ml x 3), then it was dried using Na_2SO_4. The organic residue was recrystallized from toluene to give **61a** yield; (0.039g, 15%).

^{1}H NMR (400 MHz; d_6-DMSO) δ= 3.7 (12H, s, CH-5), 6.9 (4H, d, *J* = 16.25 Hz, CH-3), 7.76 (4H, d, *J* = 16.24, CH-1). 8.17 (2H, s, CH-2), 8.27 (4H, d, *J* = 1.26 Hz, CH-4)

^{13}C-NMR (400 MHz; d_6-DMSO) δ= 51.6, 116.5, 121, 127.7, 132.3, 138, 144.4, 167.7

IR (ATR): v= 2950.92, 1699.03, 1434.56, 1165.54, 846.59.

HR MS (ES) m/z = found 490.1628, requires 490.50124 $[M]^+$

MP= 266-268^{o}C

(E)-3-[3-[3-[(E)-2-carboxyvinyl]-5-[(E)-3-methoxy-3-oxo-prop-1-enyl]phenyl]-5-[(E)-3-methoxy-3-oxo-prop-1-enyl]phenyl]prop-2-enoic acid (61b)

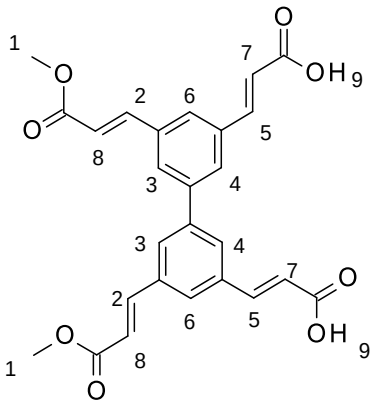

61b

Methyl (E)-3-[3-[3,5-bis[(E)-3-methoxy-3-oxo-prop-1-enyl]phenyl]-5-[(E)-3-methoxy-3-oxo-prop-1-enyl]phenyl]prop-2-enoate **61a** (0.039g,79.5µM) compound was stirred with 4 equivalence of KOH in Methanol and then the mixture was heated to 60 ^{o}C for 24 hours. After the TLC result, reaction was stopped and cooled down to room temperature. To this mixture 4M HCl (5ml) was added and resultant precipitate was filtered. (17mg, 46%).

^{1}H NMR (600 MHz; d_6-DMSO) δ= 3.56 (6H, s, CH-1), 6.84 (4H, d, *J*=16.09 Hz, CH-5,8), 7.07 (4H, d, *J*=16.11, CH-2,7), 7.57 (2H, dd, *J* = 2.0, 1.8 Hz, CH-4), 7.63 (2H, dd, *J*= 2.0, 1.7 Hz, CH-3), 8.25 (2H, dd, *J* = 1.8, 1.7 Hz, CH-6), 12.48 (2H, s, OH-9)

^{13}C-NMR (600 MHz; d_6-DMSO) δ= 51.57, 116.5, 119.7, 121.018, 127.6, 132.335, 138.027, 144.42, 167.66, 168.226

IR (ATR): v= 2922.05, 1698.17, 1633.45, 1166.61, 854.52.

HR MS (ES) m/z = found 462.1321, requires 462.4480 $[M]^{+}$

MP= 293-295^{o}C

Methyl (E)-3-[10-[(E)-3-methoxy-3-oxo-prop-1-enyl]-9-anthryl]prop-2-enoate (60c)

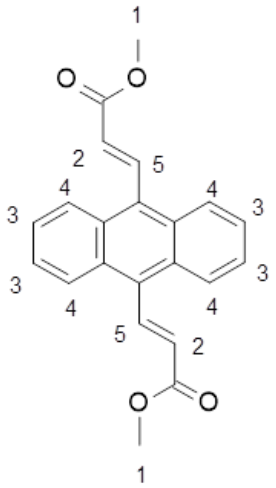

60c

Under a dry nitrogen atmosphere, triphenylphosphine (2.38 mmol, 624mg) and Pd $(OAc)_2$ (267mg) were added together in DMF (20 ml) in a Schlenk tube. After activation; 9,10-dibromoanthracene (2.0 g, 5.9 mmol), acrylamide (2.143ml, 2.38mmol) and triethylamine (3.317mL, 2.38mmol) were added to the mixture. The reaction was heated up to 90^{o}C and left to stir for 24 hrs. The completed reaction mixture was allowed to cool down to room temperature and diluted with HCl (15 ml, 2M). Dilution with HCl gave a green precipitate and then it was filtered. The filtrate was then washed with water (3x20ml) and diethyl ether (3x15ml). After this procedure, the green precipitate was recrystallised using methanol to give **60c** bright green crystals; yield: (0.62g, 33%).

^{1}H NMR (600 MHz; d_6-DMSO) δ= 3.8 (6H, s, CH-1), 6.4 (2H, d, *J* = 16.81 Hz, CH-2), 7.63 (4H, ddd, *J* = 6.94, 6.47, 3.70 Hz, CH-3), 8.22 (4H, ddd, *J* = 6.67, 6.18, 3.45 Hz, CH-4), 8.55 (2H, d, *J* = 16.25 Hz, CH-5)

^{13}C-NMR (600 MHz; d_6-DMSO) δ= 51.6, 116.7, 126.7, 126.8, 129.7, 130.8, 133.4, 167.7

IR (ATR): v= 2947.45, 1709.23, 1433.93, 997.69

HR MS (ES) m/z = found 346.1205, requires 346.3759 $[M]^{+}$

MP=219-221^{o}C

(*E*)-N-(1,3-benzodioxol-5-ylmethyl)-3-[10-[(E)-3-(1,3-benzodioxol-5-ylmethylamino)-3-oxo-prop-1-enyl]-9-anthryl]prop-2-enamide (52a)

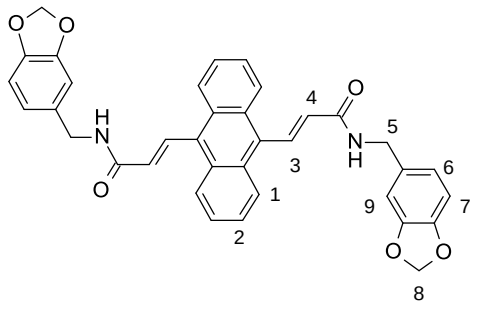

52a

(E)-3-[10-[(E)-2-carboxyvinyl]-9-anthryl]prop-2-enoicacid **60c** (140mg, 0.44mmol) and piperonylamine (103.6mg, 0.96mmol) were stirred in DCM (4ml) at room temperature under N_2.To this solution mixture EDCI.HCl (185.4mg, 0.96mmol) and HOBt (130mg, 0.96mmol) in DCM (6ml) was added dropwise at 0°C. Then, DIPEA (0.34ml, 1.93mmol) was added dropwise to the solution mixture and was left to stir and reflux for 24h. After completion of the reaction, the resulting precipitate was filtered and washed with water (3x 20 ml) and brine (20ml) and dried under vacuum to produce **52a** a green solid; yield: (141mg, 55%).

^{1}H NMR (400 MHz; d_6-DMSO) δ= 3.7 (4H, s, CH-5), 5.99 (4H, s, CH-8), 6.20 (2H,d, *J*= 16.21, CH-3)6.79 (2H, d, *J* = 2.53 Hz, CH-6),6.82 (2H,s, CH-9), 6.85 (2H,d, *J* = 1.41 Hz, CH-7),7.61 (4H, ddd, *J* = 6.65, 3.49, 3.18 Hz, CH-2), 8.24 (4H, ddd, *J* = 6.98, 3.42, 3.25 Hz, CH-1), 8.29 (2H, d, *J* = 16.37 Hz, CH-4)

^{13}C-NMR (400 MHz; d_6-DMSO) δ= 43.7,101.5,108.1,108.9,119.7,126.7,126.9,127.4,129.5 130.6,133.4,133.6,147.7,147.9,167.2

IR (ATR): v= 3272.15, 2920.37,

HR MS (ES) m/z = found 585.2025, requires 585.6313 $[M + H]^+$

MP=243-245^{o}C

(E)-3-[10-[(E)-3-oxo-4-(4-pyridylamino)but-1-enyl]-9-anthryl]-N-(4-pyridylmethyl)prop-2-enamide (52c)

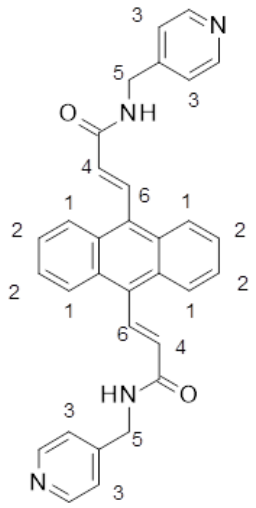

52c

(E)-3-[10-[(E)-2-carboxyvinyl]-9-anthryl]prop-2-enoic acid **60c** (140mg, 0.44mmol) and 4-(aminomethyl)pyridine (190.2mg, 1.76mmol) were stirred in DCM (4ml) at room temperature under N_2.To this solution mixture EDCI.HCl (337.4mg, 1.76mmol) and HOBt (238mg, 1.76mmol) in DCM (6ml) was added dropwise at 0°C. Then, DIPEA (0.612ml, 3.51mmol) was added dropwise to the solution mixture and was left to stir and reflux for 24h. After completion of the reaction, the resulting precipitate was filtered and washed with water (3x 20 ml) and brine (20ml) and dried under vacuum to produce **52c** a green solid; yield: (141.5mg, 65%).

^{1}H NMR (400 MHz; d_6-DMSO) δ= 3.8 (4H, s, CH-5), 6.2 (2H, d, *J* = 16.25 Hz, CH-4), 7.04 (4H, d, *J*= 1.23 Hz, CH-3), 7.61 (4H, dd, *J* = 6.85, 3.15 Hz, CH-2), 8.15 (4H, dd, *J* = 6.65, 3.33 Hz, CH-1), 8.24 (2H, d, *J* = 16.05 Hz, CH-6)

^{13}C-NMR (400 MHz; d_6-DMSO) δ= 40.73, 122.36, 123.41, 126.75, 127.31, 128.83, 131.05, 136.85, 149.44, 156.64

IR (ATR): v= 3285.03, 2971.91, 1624.16, 1650.77, 1605.86,1566.30

HR MS (ES) m/z = found 499.2131, requires 499.5814 $[M+H]^+$

MP=324-326^{o}C

(E)-3-[4-[3,5-bis[4-[(E)-2-carboxyvinyl]phenyl]phenyl]phenyl]prop-2-enoic acid (67a)

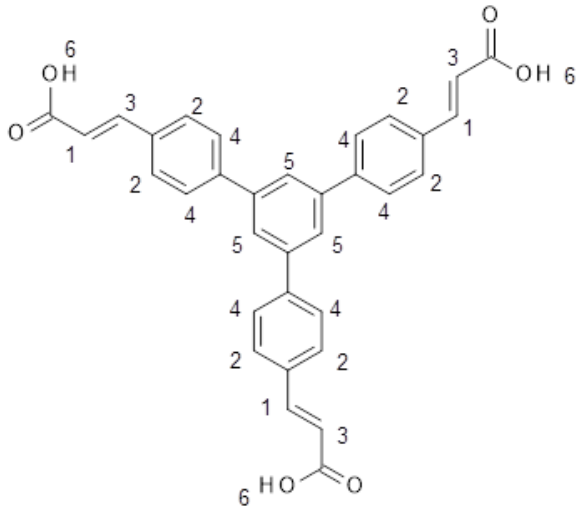

67a

A solution of ester (methyl (E)-3-[4-[3,5-bis[4-[(E)-3-methoxy-3-oxo-prop-1-enyl]phenyl]phenyl]phenyl]prop-2-enoate) **67** compound 285mg was dissolved in a mixture of THF (5ml) and distilled water (5ml). To this mixture, KOH (100mg) pellets were added. The reaction mixture was placed under reflux for 12hrs. The mixture was monitored *via* TLC using a 1:1 EtOAc and hexane solvent system. The resultant reaction mixture was diluted with 3M HCl and the white precipitate formed was filtered to produce **67a** a white solid (213mg, 81%). The mass after subsequent modifications of the resulted compound was unfortunately not high enough for Mass spec. analysis.

^{1}H NMR (400 MHz; d_6-DMSO) δ= 6.63 (3H, d, *J*=16.01 Hz, CH-1), 7.68 (3H, d, *J*=16.07, CH-3), 7.8 (6H , d, *J*=8.39, CH-2) 7.97 (6H, d, *J* =8.38, CH-4), 8.02(3H, s, CH-5), 12.43 (3H, s, OH-6)

^{13}C-NMR (400 MHz; d_6-DMSO) δ=127.162, 133.4, 141.00571, 142.31, 125.11, 139.05797, 127.05, 119.71464, 168.2265

IR (ATR): v= 2950.92, 1699.03, 1586.68, 1165.54.

(E)-3-[10-[(E)-2-carboxyvinyl]-9-anthryl]prop-2-enoic acid (60d)

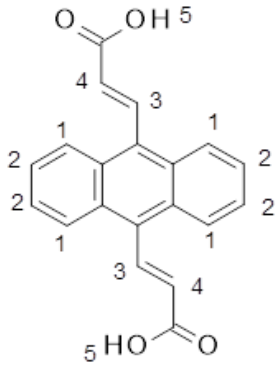

60d

A solution of methyl (E)-3-[10-[(E)-3-methoxy-3-oxo-prop-1-enyl]-9-anthryl]prop-2-enoate (**60c**) (285mg) was dissolved in a mixture of THF(5ml) and distilled water (5ml). To this mixture, KOH pellets (100mg) were added. The reaction mixture was placed under reflux for 12hrs. The mixture was monitored *via* TLC using a 1:1 EtoAc and hexane solvent system. The resultant reaction mixture was diluted with 3M HCl and the white precipitate formed was filtered to produce **60d** a white solid; yield: (0.11g, 42%).

^{1}H NMR (400 MHz; d_6-DMSO) δ=6.32 (2H, d, *J*= 16.06 Hz, CH-4), 7.64 (4H, dd, *J* = 6.83, 3.30 Hz, CH-2), 8.22 (4H, dd, *J* = 6.80, 3.34 Hz, CH-1), 8.48 (2H, d, *J*= 16.18 Hz, CH-3),12.86 (2H, s, OH-5)

^{13}C-NMR (400 MHz; d_6-DMSO) δ= 116.7, 126.7, 126.8, 129.7, 130.8, 133.4, 167.7

IR (ATR): v= 2971.63, 1683.00, 1628.15, 1441.91,1421.05

HR MS (ES) m/z = found 318.0891, requires 318.3227 $[M]^+$

MP=259-261^{o}C

anthracene-9,10-dicarboxylic acid (64)

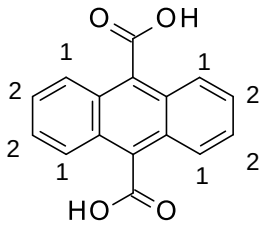

64

A solution of ester **60c** (15.5mg,0.045mmol) in dry DCM (4ml) was cooled to -78^{o}C followed by dropwise addition of diisobutylaluminum hydride (1.5 M in toluene, 33µL, 0.049mmol). Reaction was stirred at -78^{o}C for 30 minutes, then quenched with methanol (2ml) and saturated aqueous Rochelle's salt solution (5ml). The aqueous phase was then extracted by dichloromethane (3x5ml) and organic phases dried over sodium sulphate. *This procedure was used to oxidize ester compound **60c** to aldehyde **69** however the reaction was reduced to alcohol **70** yield: (11.5mg, 0.043mmol, 95%).

^{1}H NMR (400 MHz; d_6-$CDCl_3$) δ=7.40 (4H, dd, *J*=6.96, 3.29 Hz, CH-2), 8.24 (4H, dd, *J*= 6.67, 3.45 Hz, CH-1)

^{13}C-NMR (400 MHz; d_6-$CDCl_3$) δ= 126.8, 128.1, 129.6, 130.8, 170.1

IR (ATR): v= 3290.48, 2920.32, 1437.26, 1368.39

HR MS (ES) m/z = found 269.0967, requires 266.2692 $[M+3H]^{+}$

MP=175-177^{o}C

(E)-N-[2-(1-piperidyl)ethyl]-1-[10-[(E)-2-(1-piperidyl)ethyliminomethyl]-9-anthryl]methanimine (55c)

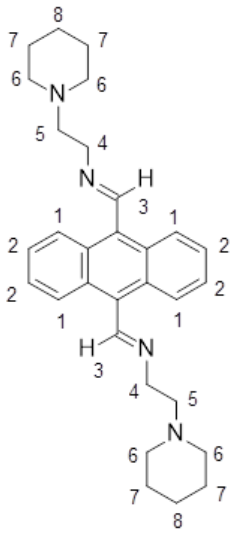

55c

1-(2-Aminoethyl) piperidine (0.35ml, 314mg, 0.0024mol) and 9-10dibromocarbaldehyde (250mg) were stirred in dry DCM (40ml) over molecular sieves. The reaction mixture was refluxed for 12 hrs under N_2 environment. The resulted mixture was monitored *via* TLC which showed the consumption of both starting materials. After TLC analysis, the crude mixture was left to cool down to room temperature. The solid imine product **55c** was filtered and it was dried under vacuum before being recrystallised from methanol to yield a yellow coloured **55c** solid (0.32g, 65% yield) and then it was stored in 0^{o}C.

^{1}H NMR (400 MHz; d_6-DMSO) δ= 9.3(2H, s, CH-3), 8.5(4H, ddd, *J*=6.90, 3.11, 1.90 Hz, CH-2), 7.52(4H, ddd, *J*=6.98, 3.22, 1.52, CH-1), 4.08(4H, t, *J*=6.96 Hz, CH-4), 2.86(4H, t, *J*=7.70 Hz, CH-5), 2.58(8H, broad, CH-6) 1.67(8H, quintet, *J*=5.46 Hz, CH-7) 1.5 (4H, t, *J*=6.32 Hz, CH-8)

^{13}C-NMR (400 MHz; d_6-DMSO) δ= 24.1, 26.3, 50.9, 54.9, 55, 126.7, 127.4, 130.7, 130.9, 159.9

IR (ATR): v= 2924.30, 2791.03, 2849.60, 1640.34, 1437.78, 754.18

HR MS (ES) m/z = found 455.3179, requires 456.6635 $[M+2H]^{+}$

MP=158-160^{o}C

(E)-N-[2-(1H-indol-3-yl)ethyl]-1-[10-[(E)-2-(1H-indol-3-yl)ethyliminomethyl]-9-anthryl]methanimine (55k)

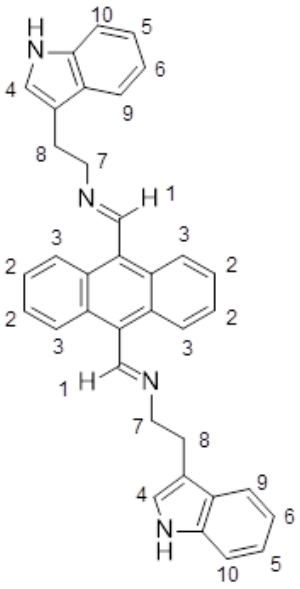

55k

Tryptamine (390mg, 0.00245mol) and 9-10dibromocarbaldehyde (250mg) were stirred in dry DCM (40ml) over molecular sieves. The reaction mixture was refluxed for 12hrs under N_2 environment. The resultant mixture was monitored *via* TLC which showed the consumption of both starting materials. After TLC analysis, the crude mixture was left to cool down to room temperature. The resulting yellow solid **55k** was filtered and it was dried under vacuum before being recrystallised from methanol to give (0.44g, 80%) yield.

^{1}H NMR (400 MHz; d_6-DMSO) δ= 3.68 (4H, t, *J*=6.65 Hz, CH-8) 4.26 (4H, t, *J*=8.66Hz, CH_2-7), 7.01 (2H, t, *J*=8.76Hz, CH-6), 7.10 (2H, t, *J*=8.78Hz, CH-5) 7.23(2H, s, CH-4),7.39 (2H, dddd, *J* = 8.0, 1.2, 0.5, 0.5 Hz*data book values, H-10), 7.424(4H, dd, *J*=6.63, 2.21 Hz, CH-3), 7.695 (2H, d, *J*= 7.74Hz, CH-9), 8.123 (4H, dd, *J*=6.97,2.68, CH-2)

*extensive overlap, leading to difficulty in assignment, therefore a nmr prediction package was used. (244)(247)(248).

^{13}C-NMR (600 MHz; d_6-DMSO) δ=22.5, 46.9, 111.6, 112, 118.7, 120.2, 121.7, 122.2, 126.7, 127.5, 127.6, 130.7, 130.8, 136.4, 159.9

IR (ATR): v=2843.46, 2922.6, 1652.99, 1621.80, 741.77,755.12

HR MS (ES) m/z = found 519.2541, requires 520.6642 $[M+2H]^+$

MP=237-239^{o}C

N-[3-[(E)-[10-[(E)-(3-acetamidophenyl)iminomethyl]-9

anthryl]methyleneamino]phenyl]acetamide (55l)

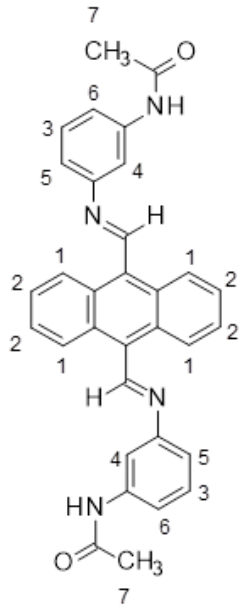

55l

3′-Aminoacetanilide (360 mg, 0.00245mol) and 9-10dibromocarbaldehyde (250mg) were stirred in dry DCM (40ml) over molecular sieves. The reaction mixture was refluxed for 12hrs under N_2 environment. The resultant mixture was monitored *via* TLC which showed the consumption of both starting materials. After TLC analysis, the crude mixture was left to cool down to room temperature. The resulting off white solid **55l** was filtered and it was dried under vacuum before being recrystallised from methanol to give (190mg,35%) yield.

^{1}H NMR (400 MHz; d_6-DMSO) δ= 2.09 (9H, s, CH-7), 7.245 (2H, d, *J*=6.34Hz, CH-6), 7.45 (2H, dd, *J*=8.42, 7.16 Hz, CH-5), 7.58 (2H, s , CH-4), 7.71 (4H, dd, *J*=6.97,2.68, CH-2), 7.74 (2H, ddd, *J* = 7.9, 7.4, 0.5 Hz*data booked values, CH-3) 8.73 (4H, dd, *J*=6.63, 2.21 Hz, CH-1)

*extensive overlap, leading to difficulty in assignment, therefore a nmr prediction package was used (244)(247)(248).

^{13}C-NMR (600 MHz; d_6-DMSO) δ= 24, 115, 119.1, 121.6, 126.7, 129.4, 130.7, 130.9, 137.5, 143.7, 159.9, 168.4

IR (ATR): v= 3279.68, 2864.19, 1620.19, 1653.88, 1442.34, 1000.36,1032.17

HR MS (ES) m/z = found 499.2130, requires 499.5814 $[M+H]^+$

MP=329-331^o

(E)-N-(5-methylthiazol-2-yl)-1-[10-[(E)-(5-methylthiazol-2-yl)iminomethyl]-9-anthryl]methanimine (55j)

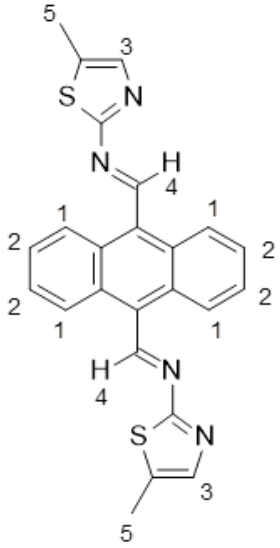

55j

2-Amino-5-methylthiazole (500 mg, 0.0048mol) and 9,10-dibromocarbaldehyde (250mg) were stirred in dry DCM (40ml) over molecular sieves. The reaction mixture was refluxed for 12hrs under N_2 environment. The resultant mixture was monitored *via* TLC which showed the consumption of both starting materials. After TLC analysis, the crude mixture was left to cool down to room temperature. The resulting red solid **55j** was filtered and it was dried under vacuum before being recrystallised from methanol to give (0.34g, 75%) yield.

^{1}H NMR (400 MHz; d_6-DMSO) δ= 1.23 (6H, s, CH_3-5), 7.6 (2H, d, *J*=1.20Hz, CH-3), 7.77 (4H, dd, *J*=6.85,3.24 Hz, CH-1), 8.78 (4H, dd, *J*=6.93,3.19Hz, CH-2), 10.22 (2H, s, CH-4)

^{13}C-NMR (400 MHz; d_6-DMSO) δ=12.495, 124.2714, 128.264, 128.341, 129.366, 129.423, 135.2327, 167.977, 196.115

IR (ATR): v= 2919.38, 1677.56, 1577.16, 1440.95, 751.59

HR MS (ES) m/z = found 427.1048 requires 427.5635 $[M+H]^+$

MP=264-266^{o}C

(E)-N-(3-morpholinopropyl)-1-[10-[(E)-3-morpholinopropyliminomethyl]-9-anthryl]methanimine (55m)

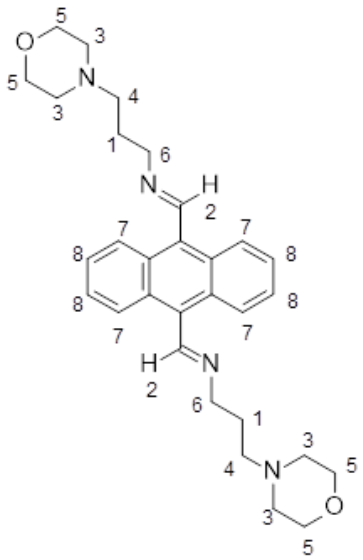

55m

3-Morpholinopropylamine (350 mg, 0.0024mol) and 9,10-dibromocarbaldehyde (250mg) were stirred in dry DCM (40ml) over molecular sieves. The reaction mixture was refluxed for 12hrs under N_2 environment. The resultant mixture was monitored *via* TLC which showed the consumption of both starting materials. After TLC analysis, the crude mixture was left to cool down to room temperature. The resulting off white solid **55m** was filtered and it was dried under vacuum before being recrystallised from methanol to give (0.31g, 60%) yield.

^{1}H NMR (600 MHz; d_6-DMSO) δ= 1.9 (4H, m(5), *J*=7.2Hz, CH-1), 2.29 (2H, s, *data booked values CH-2), 2.39 (4H, q, *J*=1.84Hz, CH-4), 2.52 (4H, t, *J*=1.90Hz, CH-3), 3.49 (4H, t, *J*=4.75Hz, CH-6), 3.62 (8H, t, *J*=4.69Hz, CH-5), 7.60 (4H, dd, *J*=6.69, 3.16 Hz, CH-7), 8.5(4H, dd, *J*=7.24,3.24 Hz, CH-8)

extensive overlap, leading to difficulty in assignment, therefore a nmr prediction package was used (244)(247)(248).

^{13}C-NMR (600 MHz; d_6-DMSO) δ= 23.1, 46.9, 50.9, 54.1, 66.3, 126.7, 126.9, 130.7, 130.8, 159.9

IR (ATR): v= 2807.34, 2854.18, 1630.97, 1238.90, 1116.07.

HR MS (ES) m/z = found 487.3073, requires 488.6623 $[M+2H]^+$

MP=160-162^{o}C

(E)-N-(1,3-benzodioxol-5-ylmethyl)-1-[10-[(E)-1,3-benzodioxol-5-ylmethyliminomethyl]-9-anthryl]methanimine (55a)

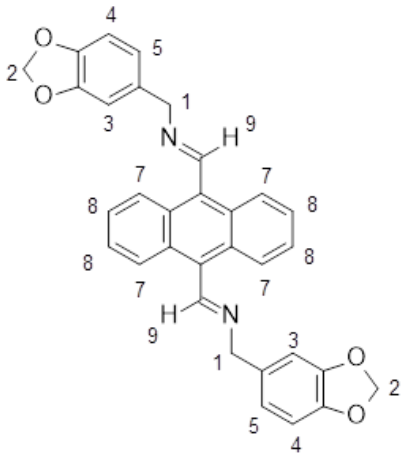

55a

Piperonylamine (370 mg, 0.00245mol) and 9,-10-dibromocarbaldehyde (250mg, moles) were stirred in dry DCM (40ml) over molecular sieves. The reaction mixture was refluxed for 12hrs under N_2 environment. The resultant mixture was monitored via TLC which showed the consumption of both starting materials. After TLC analysis, the crude mixture was left to cool down to room temperature. The resulting yellow solid **55a** was filtered and it was dried under vacuum before being recrystallised from methanol to give (0.42g, 78%) yield.

^{1}H NMR (600 MHz; d_6-DMSO) δ= 5.03 (4H, s, CH-1), 6.02 (4H, s, CH-2), 6.9 (2H, dd, *J*=7.98, 0.42 Hz, CH-4), 6.98 (2H, dd, *J*=7.76, 1.66 Hz, CH-5), 7.08 (2H, dd, *J*=1.42, 0.28 Hz, CH-3), 7.6(4H, dd, *J*=7.04, 3.31 Hz, CH-7), 8.54(4H, dd, *J*=7.01, 3.29 Hz, CH-8), 9.62(2H, t, *J*=1.30Hz, CH-9)

^{13}C-NMR (600 MHz; d_6-DMSO) δ= 65, 101.5, 108.1, 108.9, 125.42, 126.7, 127.6, 130.7, 130.8, 137.5, 147.7, 147.9, 159.9

IR (ATR): v= 2935.03, 1618.90, 1502.29,1488.79,765.11

HR MS (ES) m/z = found 501.1815, requires 501.5509 $[M+H]^+$

MP=235-237^{o}C

6.2 Cell Culture Methods

Incubation was carried out using Thermofisher Steri-Cycle CO_2 incubators and for plate reading Thermofisher Epoch Microplate Spectrophotometer was used. Centrifugation was carried out using aThermo Scientific Sorvall ST 40 Centrifuge Series.

6.2.1 Media Preparation

Commercially available DMEM (Dulbecco's Modified Eagle Medium- low glucose), including sodium pyruvate and α-glutamine, 500 mL, was obtained from Gibco, USA. All procedures carried out under sterile conditions, 94 mL of medium was taken and the required volume of supplements (10 % Fetal Bovine Serum (FBS), 2 mM/mL Glutamine, 100 U/mL penicillin and 100 µg/mL streptomycin.) were added.

6.2.2 Cell Line and Cell Culture Conditions

Human cervical cancer cell lines (HeLa) were obtained from the American Type Culture Collection (ATCC) (ATCC® CCL-2™).

HeLa cells were cultured in Dulbecco's Eagle Modified Medium low glucose (DMEM) containing 10 % Fetal Bovine Serum (FBS), 2 mM/mL Glutamine, 100 U/mL penicillin and 100 µg/mL streptomycin.

These cells were kept in media which was changed with fresh media every 2 days. All of the cells were cultured in a humidified incubator whose conditions are 37 ^{o}C, 5 % CO_2, 95 % air.

6.2.3 Cell Passaging

The cells were split when the cells reached 70 % confluency in the flask. First of all, the medium was removed from the flask and then cells were washed with DPBS (1X) (pH 7.4) containing 10 mM sodium dibasic phosphate, 2.7 mM KCI, 2 mM Potassium phosphate, 137 mM NaCI. After that, the cells were detached from the flask with 0.25 % (w/v) trypsin-5mM EDTA in PBS (Phosphate Buffered Saline) solution and incubated for 5 minutes in an incubator with conditions at 37 ^{o}C, 5 % CO_2, 95 % air. Dissociated cells were resuspended

with medium containing 10 % Fetal Bovine Serum (FBS) to inhibit the trypsin activity and then centrifuged at 1500rpm for 5 minutes. After centrifugation, the supernatant was discarded, and cells were resuspended with media and seeded into the flasks.

6.2.4 Cell Counting and Viability

In order to determine cell density a hemacytometer was used, with the following procedure. First of all, chamber and cover slip cleaned with 70 % IMS. After gentle drying, the coverslip was placed in position. 10 µL of the harvested cells in media (cell suspension) and a 10µl of a prepared 0.4% trypan blue in buffered isotonic salt solution (pH 7.2 – 7.3) were added to eppendorfs. 10µL of Eppendorf solution is then loaded into the hemacytometer. The chamber placed in the inverted microscope with 10x objective. Finally, the blue stained cells and total number of cells in the central gridded square were counted and the average number of cells per mL was estimated by applying this formula;

$$Concentration = \frac{Number\ of\ cells}{Number\ of\ squares}\ x\ 10000\ x\ sample\ dilution$$

With cell viability calculated with the following equation, where 95% viability was the target for cells;

$$\%viable\ cells = \left(1 - \left(\frac{Number\ of\ blue\ cells}{Number\ of\ total\ cells}\right)\right) x\ 100$$

6.2.5 Cell Freezing

Cells were trypsinized from the cell plate and then centrifuged as described previously in Section 3. After that, the supernatant was discarded and the pellet was resuspended with freezing medium, including 90% heat inactivated Fetal Bovine Serum (FBS) and 10 % Dimethyl Sulfoxide (DMSO). 1 ml of cell suspension were put into each cryovial and then frozen at -80 ^{o}C or kept in liquid nitrogen tank for long term preservation.

6.2.6 Cell Thawing

Cryovials were taken from the liquid nitrogen tank and thawed quickly at 37 ^{o}C. After that, the cell suspension was transferred to a 15 mL tube and 5 mL of the medium was added into the cell suspension drop by drop with gentle shaking. Centrifugation was done at 1500rpm for 5 min and then supernatant was discarded. After the pellet was resuspended with medium, they were seeded to T-25 flasks. Subsequent to 12 hours incubation, the media was removed and washed with DPBS (1X) (pH:7.4) containing 10 mM sodium dibasic phosphate, 2.7 mM KCl, 2 mM Potassium phosphate,137 mM NaCl. Fresh media was added to the cell monolayer a day later thawing.

6.2.7 Seeding plates

Assays were carried out using a 96 well plate. This 96-well plate contains one blank, 3 controls which contains cells including a negative control with media, one vehicle control which is DMSO and medium solutions, and a positive control of Doxorubicin (200µL) and media. Drugs were prepared in 100, 30, 10, 1 µM concentrations to make 8 seeded well plates in total which were done in triplicate. All drugs were prepared in DMSO and then diluted in media to give 5µL of DMSO max in 100µM treatments which is controlled by vehicle with a DMSO volume of 5µL.

6.2.8 Presto Blue Assay

Cell suspension (200µl) containing 5000 healthy HeLa cells was seeded in 96-well plates (BDFalcon, Franklin Lakes, NJ) and allowed to attach and stabilize overnight at 37 °C with 5% CO_2. Aspiration of media and rinsing solution was done through pipetting off liquid. Cell viability was then tested with PrestoBlue assay.

The presto blue assay was carried out in light sensitive conditions. 100µl of PrestoBlue solution (10% in medium) was added to each well and the plates were incubated at 37 °C for 1 hour. After incubation time, the change in florescence was measured at 570/600 nm using a Spectra Max fluorescence multi-well plate reader.

6.2.9 NMR intercalation procedure

NMR tubes used were Wilmad 5 mm, thin-walled tubes obtained from GPE Scientific (Product No: 502-7). NMR samples were spiked with Sodium d4-trimethylsilylpropionate (TSP) to a concentration of 10 mmol/L. All spectra were recorded in 0.6ml of H_2O-D_2O (90:10 v/v) solvent, with 25mM phosphate buffer, 150mM KCl and 1mM EDTA.

Oligonucleotide d(TTAGGGT)4 was purchased from Sigma Aldrich and made up to a concentration of 0.4mM in the solvent mix. This oligonucleotide solvent mix was then micro-pipetted at a volume of 0.6ml into NMR tubes. Stock solutions of drug compounds in DMSO were used to make up the molar ratios of 0.125:1, 0.25:1, 0.5:1 and 1:1 drug to oligomer. A non-active drug (**53a**) and DMSO on its own were added as controls to validate that the effects on the spectra were from cytotoxic elements of the drug compounds rather than the effects from DMSO or addition of compound, which could change environment, pH or shimming of NMR instrument.

Spectra were acquired at 300 K using a Bruker Avance III 600MHz FT-NMR. The WATERNOESY parameter set which executes the pulse sequence noesygppr1d (Bruker, size of fid 65536, 12335.526 Hz spectral width, 128 scans, d1 = 4 s) was used to acquire ^{1}H 1D experiments with a pre-saturation delay during relaxation and mixing time (experiment time: 14 min 44 sec). With this pulse sequence, all non-exchangeable protons are detected in the deuterated D_2O/H_2O buffer solution. T1 relaxation experiments were acquired for d1 calibration with a modified version of the zggpw5 pulse sequence. With a saturation recovery block (delays 0.01, 0.22, 0.54, 1.05, 1.84, 3.08, 5.01, 8.01, 12.69, 20.00 s) before the first 90° pulse and using water suppression (Bruker, size of fid 65536/11 F2/F1, 12335.526/5882.353 Hz spectral width in F2/F1, 64 scans, 0.1 s relaxation delay) (experimental time 1 h 4 min 6 sec).

Bruker Topspin 3.5 pl7 was used for assignment of peaks, manual phasing, baseline correction and manual integration. Manual integration was done to ensure bias and slope

was correct and that the integrals were all of the same width. Calculation of chemical shift change done through built in top spin distance measurements between peaks.

Chapter 7 – References

1. Rodriguez R, Miller KM, Forment JV, Bradshaw CR, Nikan M, Britton S, et al. Small-molecule–induced DNA damage identifies alternative DNA structures in human genes. Nature Chemical Biology. 2012;8(3):301–10.

2. Wright WE, Tesmer VM, Huffman KE, Levene SD, Shay JW. Normal human chromosomes have long G-rich telomeric overhangs at one end. Genes & development. 1997 Nov 1;11(21):2801–9.

3. Aisner DL, Wright WE, Shay JW. Telomerase regulation: not just flipping the switch. Current opinion in genetics & development. 2002 Feb 1;12(1):80–5.

4. van Doorn WG, Woltering EJ. Senescence and programmed cell death: substance or semantics? Journal of experimental botany. 2004 Oct 1;55(406):2147–53.

5. Biffi G, Tannahill D, McCafferty J, Balasubramanian S. Quantitative visualization of DNA G-quadruplex structures in human cells. Nature chemistry. 2013 Mar;5(3):182–6.

6. Blackburn EH. Telomeres and telomerase: their mechanisms of action and the effects of altering their functions. FEBS letters. 2005 Feb 7;579(4):859–62.

7. Bang I. Examination of the guanyle acid. Biochemische Zeitschrift. 1910;26:293–311.

8. Zhou J, Bourdoncle A, Rosu F, Gabelica V, Mergny J. Tri-G-Quadruplex: Controlled Assembly of a G-Quadruplex Structure from Three G-Rich Strands. Angewandte Chemie International Edition. 2012 Oct 29;51(44):11002–5.

9. Gellert M, Lipsett MN, Davies DR. Helix formation by guanylic acid. Proceedings of the National Academy of Sciences of the United States of America. 1962 Dec;48(12):2013.

10. Sen D, Gilbert W. A sodium-potassium switch in the formation of four-stranded G4-DNA. Nature. 1990 Mar;344(6265):410–4.

11. Hud NV, Plavec JA. The role of cations in determining quadruplex structure and stability. Quadruplex nucleic acids. 2006;100.

12. Neidle S, Parkinson G. Telomere maintenance as a target for anticancer drug discovery. Nature Reviews Drug Discovery. 2002 May;1(5):383–93.

13. Punchihewa C, Yang D. Therapeutic targets and drugs II: G-quadruplex and G-quadruplex inhibitors. In Telomeres and telomerase in cancer 2009 (pp. 251–280). Humana Press.

14. Neidle S. Quadruplex nucleic acids as novel therapeutic targets. Journal of medicinal chemistry. 2016 Jul 14;59(13):5987–6011.

15. Greider CW, Blackburn EH. Identification of a specific telomere terminal transferase activity in Tetrahymena extracts. cell. 1985 Dec 1;43(2):405–13.

16. Sun Z-Y, Wang X-N, Cheng S-Q, Su X-X, Ou T-M. Developing novel G-quadruplex ligands: From interaction with nucleic acids to interfering with nucleic acid–protein interaction. Molecules. 2019 Jan;24(3):396.

17. Harley CB, Futcher AB, Greider CW. Telomeres shorten during ageing of human fibroblasts. Nature. 1990 May;345(6274):458–60.

18. Mehle C, Ljungberg B, Roos G. Telomere shortening in renal cell carcinoma. Cancer research. 1994 Jan 1;54(1):236–41.

19. Kim NW, Piatyszek MA, Prowse KR, Harley CB, West MD, Ho PD, Coviello GM, Wright WE, Weinrich SL, Shay JW. Specific association of human telomerase activity with immortal cells and cancer. Science. 1994 Dec 23;266(5193):2011-5.

20. Wang Q, Liu J, Chen Z, Zheng K, Chen C, Hao Y, et al. G-quadruplex formation at the 3' end of telomere DNA inhibits its extension by telomerase, polymerase and unwinding by helicase. Nucleic Acids Research. 2011 Mar 25;39(14):6229–37.

21. Sun D, Thompson B, Cathers BE, Salazar M, Kerwin SM, Trent JO, Jenkins TC, Neidle S, Hurley LH. Inhibition of human telomerase by a G-quadruplex-interactive compound. Journal of medicinal chemistry. 1997 Jul 4;40(14):2113-6.

22. Monchaud D, Teulade-Fichou MP. A hitchhiker's guide to G-quadruplex ligands. Organic & biomolecular chemistry. 2008;6(4):627–36.

23. Burger AM, Dai F, Schultes CM, Reszka AP, Moore MJ, Double JA, Neidle S. The G-quadruplex-interactive molecule BRACO-19 inhibits tumor growth, consistent with telomere targeting and interference with telomerase function. Cancer research. 2005 Feb 15;65(4):1489-96.

24. Kim MY, Vankayalapati H, Shin-Ya K, Wierzba K, Hurley LH. Telomestatin, a potent telomerase inhibitor that interacts quite specifically with the human telomeric intramolecular G-quadruplex. Journal of the American Chemical Society. 2002 Mar 13;124(10):2098–9.

25. Lipps HJ, Rhodes D. G-quadruplex structures: in vivo evidence and function. Trends in cell biology. 2009 Aug 1;19(8):414–22.

26. Mergny JL, Lacroix L, Teulade-Fichou MP, Hounsou C, Guittat L, Hoarau M, Arimondo PB, Vigneron JP, Lehn JM, Riou JF, Garestier T. Telomerase inhibitors based on quadruplex ligands selected by a fluorescence assay. Proceedings of the National Academy of Sciences. 2001 Mar 13;98(6):3062-7.

27. Dixon IM, Lopez F, Tejera AM, Estève J-P, Blasco MA, Pratviel G, et al. A G-quadruplex ligand with 10000-fold selectivity over duplex DNA. Journal of the American Chemical Society. 2007;129(6):1502–3.

28. Saleh MM, Laughton CA, Bradshaw TD, Moody CJ. Development of a series of bis-triazoles as G-quadruplex ligands. RSC advances. 2017 Oct 6;7(75):47297–308.

29. Moorhouse AD, Haider S, Gunaratnam M, Munnur D, Neidle S, Moses JE. Targeting telomerase and telomeres: a click chemistry approach towards highly selective G-quadruplex ligands. Molecular BioSystems. 2008;4(6):629–42.

30. Garner TP, Williams HE, Gluszyk KI, Roe S, Oldham NJ, Stevens MF, Moses JE, Searle MS. Selectivity of small molecule ligands for parallel and anti-parallel DNA G-quadruplex structures. Organic & biomolecular chemistry. 2009;7(20):4194-200.

31. Campbell NH, Patel M, Tofa AB, Ghosh R, Parkinson GN, Neidle S. Selectivity in ligand recognition of G-quadruplex loops. Biochemistry. 2009 Mar 3;48(8):1675–80.

32. Luedtke NW. Targeting G-quadruplex DNA with small molecules. CHIMIA International Journal for Chemistry. 2009 Mar 25;63(3):134–9.

33. Li Q, Xiang JF, Yang QF, Sun HX, Guan AJ, Tang YL. G4LDB: a database for discovering and studying G-quadruplex ligands. Nucleic acids research. 2013 Jan 1;41(D1):D1115–23.

34. Sun D, Thompson B, Cathers BE, Salazar M, Kerwin SM, Trent JO, Jenkins TC, Neidle S, Hurley LH. Inhibition of human telomerase by a G-quadruplex-interactive compound. Journal of medicinal chemistry. 1997 Jul 4;40(14):2113-6.

35. Shin-ya K, Wierzba K, Matsuo KI, Ohtani T, Yamada Y, Furihata K, Hayakawa Y, Seto H. Telomestatin, a novel telomerase inhibitor from Streptomyces anulatus. Journal of the American Chemical Society. 2001 Feb 14;123(6):1262-3.

36. Kim MY, Vankayalapati H, Shin-Ya K, Wierzba K, Hurley LH. Telomestatin, a potent telomerase inhibitor that interacts quite specifically with the human telomeric intramolecular G-quadruplex. Journal of the American Chemical Society. 2002 Mar 13;124(10):2098-9.

37. Rodriguez R, Müller S, Yeoman JA, Trentesaux C, Riou J-F, Balasubramanian S. A novel small molecule that alters shelterin integrity and triggers a DNA-damage response at telomeres. Journal of the American Chemical Society. 2008 Nov 26;130(47):15758–9.

38. De Cian A, DeLemos E, Mergny JL, Teulade-Fichou MP, Monchaud D. Highly efficient G-quadruplex recognition by bisquinolinium compounds. Journal of the American Chemical Society. 2007 Feb 21;129(7):1856-7.

39. Tera M, Ishizuka H, Takagi M, Suganuma M, Shin-ya K, Nagasawa K. Macrocyclic hexaoxazoles as sequence-and mode-selective G-quadruplex binders. Angewandte Chemie International Edition. 2008 Jul 14;47(30):5557–60.

40. Tera M, Iida K, Ishizuka H, Takagi M, Suganuma M, Doi T, Shin-ya K, Nagasawa K. Synthesis of a potent G-quadruplex-binding macrocyclic heptaoxazole. ChemBioChem. 2009 Feb 13;10(3):431-5.

41. Lam EYN, Beraldi D, Tannahill D, Balasubramanian S. G-quadruplex structures are stable and detectable in human genomic DNA. Nature communications. 2013 Apr 30;4(1):1–8.

42. Ohnmacht SA, Marchetti C, Gunaratnam M, Besser RJ, Haider SM, Di Vita G, Lowe HL, Mellinas-Gomez M, Diocou S, Robson M, Šponer J. A G-quadruplex-binding compound showing anti-tumour activity in an in vivo model for pancreatic cancer. Scientific reports. 2015 Jun 16;5:11385.

43. Leonetti C, Scarsella M, Riggio G, Rizzo A, Salvati E, D'Incalci M, Staszewsky L, Frapolli R, Stevens MF, Stoppacciaro A, Mottolese M. G-quadruplex ligand RHPS4 potentiates the antitumor activity of camptothecins in preclinical models of solid tumors. Clinical Cancer Research. 2008 Nov 15;14(22):7284-91.

44. Gowan SM, Harrison JR, Patterson L, Valenti M, Neidle S, Kelland LR. A G-quadruplex-interactive potent small-molecule inhibitor of telomerase exhibiting in vitro and in vivo antitumor activity. Molecular pharmacology. 2002 May 1;61(5):1154-62.

45. Mergny JL, Hélène C. G-quadruplex DNA: A target for drug design. Nature Medicine. 1998 Dec;4(12):1366–7.

46. Siddiqui-Jain A, Grand CL, Bearss DJ, Hurley LH. Direct evidence for a G-quadruplex in a promoter region and its targeting with a small molecule to repress c-MYC transcription. Proceedings of the National Academy of Sciences. 2002 Sep 3;99(18):11593-8.

47. Rankin S, Reszka AP, Huppert J, Zloh M, Parkinson GN, Todd AK, Ladame Balasubramanian S, Neidle S. Putative DNA quadruplex formation within the human c-kit oncogene. Journal of the American Chemical Society. 2005 Aug 3;127(30):10584-9.

48. Dai J, Chen D, Jones RA, Hurley LH, Yang D. NMR solution structure of the major G-quadruplex structure formed in the human BCL2 promoter region. Nucleic Acids Research. 2006 Oct 1;34(18):5133–44.

49. Sun D, Guo K, Rusche JJ, Hurley LH. Facilitation of a structural transition in the polypurine/polypyrimidine tract within the proximal promoter region of the human VEGF gene by the presence of potassium and G-quadruplex-interactive agents. Nucleic Acids Research. 2005 Jan 1;33(18):6070–80.

50. De Armond R, Wood S, Sun D, Hurley LH, Ebbinghaus SW. Evidence for the Presence of a Guanine Quadruplex Forming Region within a Polypurine Tract of the Hypoxia Inducible Factor 1α Promoter.Biochemistry. 2005 Dec 13;44(49):16341–50.

51. Qin Y, Rezler EM, Gokhale V, Sun D, Hurley LH. Characterization of the G-quadruplexes in the duplex nuclease hypersensitive element of the PDGF-A promoter and modulation of PDGF-A promoter activity by TMPyP4. Nucleic Acids Research. 2007 Dec 1;35(22):7698–713.

52. Neidle S. Quadruplex nucleic acids as targets for anticancer therapeutics. Nature Reviews Chemistry. 2017 May 10;1(5):1-0.

53. Rigo R, Palumbo M, Sissi C. G-quadruplexes in human promoters: A challenge for therapeutic applications. Biochimica et Biophysica Acta (BBA)-General Subjects. 2017 May 1;1861(5):1399-413.

54. Balasubramanian S, Hurley LH, Neidle S. Targeting G-quadruplexes in gene promoters: a novel anticancer strategy?. Nature reviews Drug discovery. 2011 Apr;10(4):261-75.

55. Collie GW, Parkinson GN. The application of DNA and RNA G-quadruplexes to therapeutic medicines. Chemical Society Reviews. 2011;40(12):5867–92.

56. d'Auriol L, Mattei M-G, Andre C, Galibert F. Localization of the human c-kit protooncogene on the q11–q12 region of chromosome 4. Human Genetics. 1988 Apr 1;78(4):374–6.

57. Yarden Y, Kuang WJ, Yang-Feng T, Coussens L, Munemitsu S, Dull TJ, Chen E, Schlessinger J, Francke U, Ullrich A. Human proto-oncogene c-kit: a new cell surface receptor tyrosine kinase for an unidentified ligand. The EMBO journal. 1987 Nov;6(11):3341-51.

58. Yamamoto K, Tojo A, Aoki N, Shibuya M. Characterization of the Promoter Region of the Human c-kit proto-oncogene. Japanese Journal of Cancer Research. 1993 Nov;84(11):1136–44.

59. Metcalfe DD. Mast cells and mastocytosis. Blood. 2008 Aug 15;112(4):946–56.

60. Gregory-Bryson E, Bartlett E, Kiupel M, Hayes S, Yuzbasiyan-Gurkan V. Canine and human gastrointestinal stromal tumors display similar mutations in c-KIT exon 11. BMC Cancer. 2010 Dec 1;10(1):559.

61. Shaw TJ, Keszthelyi EJ, Tonary AM, Cada M, Vanderhyden BC. Cyclic AMP in ovarian cancer cells both inhibits proliferation and increases c-KIT expression. Experimental cell research. 2002 Feb 1;273(1):95-106.

62. Kitamura Y, Hirota S, Nishida T. A loss-of-function mutation of c-kit results in depletion of mast cells and interstitial cells of Cajal, while its gain-of-function mutation results in their oncogenesis. Mutation Research/Fundamental and Molecular Mechanisms of Mutagenesis. 2001 Jun 2;477(1):165–71.

63. Raiber EA, Kranaster R, Lam E, Nikan M, Balasubramanian S. A non-canonical DNA structure is a binding motif for the transcription factor SP1 in vitro. Nucleic acids research. 2011/10/22. 2012 Feb 1;40(4):1499–508.

64. Gunaratnam M, Swank S, Haider SM, Galesa K, Reszka AP, Beltran M, Cuenca F, Fletcher JA, Neidle S. Targeting human gastrointestinal stromal tumor cells with a quadruplex-binding small molecule. Journal of medicinal chemistry. 2009 Jun 25;52(12):3774-83.

65. McLuckie KI, Waller ZA, Sanders DA, Alves D, Rodriguez R, Dash J, McKenzie GJ, Venkitaraman AR, Balasubramanian S. G-quadruplex-binding benzo [a] phenoxazines down-regulate c-KIT expression in human gastric carcinoma cells. Journal of the American Chemical Society. 2011 Mar 2;133(8):2658-63.

66. Zorzan E, Da Ros S, Musetti C, Shahidian LZ, Coelho NF, Bonsembiante F, Létard S, Gelain ME, Palumbo M, Dubreuil P, Giantin M. Screening of candidate G-quadruplex ligands for the human c-KIT promotorial region and their effects in multiple in-vitro models. Oncotarget. 2016 Apr 19;7(16):21658.

67. Bejugam M, Gunaratnam M, Müller S, Sanders DA, Sewitz S, Fletcher JA, Neidle S, Balasubramanian S. Targeting the c-Kit promoter G-quadruplexes with 6-substituted indenoisoquinolines. ACS medicinal chemistry letters. 2010 Oct 14;1(7):306-10.

68. Bejugam M, Sewitz S, Shirude PS, Rodriguez R, Shahid R, Balasubramanian S. Trisubstituted isoalloxazines as a new class of G-quadruplex binding ligands: small molecule regulation of c-kit oncogene expression. Journal of the American Chemical Society. 2007 Oct 31;129(43):12926-7.

69. Wang X, Zhou CX, Yan JW, Hou JQ, Chen SB, Ou TM, Gu LQ, Huang ZS, Tan JH. Synthesis and evaluation of quinazolone derivatives as a new class of c-KIT G-quadruplex binding ligands. ACS medicinal chemistry letters. 2013 Oct 10;4(10):909-14.

70. Manaye S, Eritja R, Aviñó A, Jaumot J, Gargallo R. Porphyrin binding mechanism is altered by protonation at the loops in G-quadruplex DNA formed near the transcriptional activation site of the human c-kit gene. Biochimica et Biophysica Acta (BBA) - General Subjects. 2012 Dec 1;1820(12):1987–96.

71. Musso L, Mazzini S, Rossini A, Castagnoli L, Scaglioni L, Artali R, Di Nicola M, Zunino F, Dallavalle S. c-MYC G-quadruplex binding by the RNA polymerase I inhibitor BMH-21 and analogues revealed by a combined NMR and biochemical Approach. Biochimica et Biophysica Acta (BBA)-General Subjects. 2018 Mar 1;1862(3):615-29.

72. Palumbo SL, Ebbinghaus SW, Hurley LH. Formation of a Unique End-to-End Stacked Pair of G-Quadruplexes in the hTERT Core Promoter with Implications for Inhibition of Telomerase by G-Quadruplex-Interactive Ligands. Journal of the American Chemical Society. 2009 Aug 12;131(31):10878–91.

73. Cogoi S, Quadrifoglio F, Xodo LE. G-rich Oligonucleotide Inhibits the Binding of a Nuclear Protein to the Ki-ras Promoter and Strongly Reduces Cell Growth in Human Carcinoma Pancreatic Cells. Biochemistry. 2004 Mar 9;43(9):2512–23.

74. Morgan RK, Batra H, Gaerig VC, Hockings J, Brooks TA. Identification and characterization of a new G-quadruplex forming region within the kRAS promoter as a transcriptional regulator. Biochimica et Biophysica Acta (BBA) - Gene Regulatory Mechanisms. 2016 Feb 1;1859(2):235–45.

75. Dexheimer TS, Sun D, Hurley LH. Deconvoluting the structural and drug-recognition complexity of the G-quadruplex-forming region upstream of the bcl-2 P1 promoter. Journal of the American Chemical Society. 2006 Apr 26;128(16):5404-15.

76. Sun D, Guo K, Rusche JJ, Hurley LH. Facilitation of a structural transition in the polypurine/polypyrimidine tract within the proximal promoter region of the human VEGF gene by the presence of potassium and G-quadruplex-interactive agents. Nucleic Acids Research. 2005 Jan 1;33(18):6070–80.

77. Martiny-Baron G, Marmé D. VEGF-mediated tumour angiogenesis: a new target for cancer therapy. Current Opinion in Biotechnology. 1995 Jan 1;6(6):675–80.

78. Bikfalvi A, Bicknell R. Recent advances in angiogenesis, anti-angiogenesis and vascular targeting. Trends in Pharmacological Sciences. 2002 Dec 1;23(12):576–82.

79. Finkenzeller G, Sparacio A, Technau A, Marmé D, Siemeister G. Sp1 recognition sites in the proximal promoter of the human vascular endothelial growth factor gene are essential for platelet-derived growth factor-induced gene expression. Oncogene. 1997 Aug;15(6):669–76.

80. Shi Q, Le X, Abbruzzese JL, Peng Z, Qian CN, Tang H, Xiong Q, Wang B, Li XC, Xie K. Constitutive Sp1 activity is essential for differential constitutive expression of vascular endothelial growth factor in human pancreatic adenocarcinoma. Cancer research. 2001 May 15;61(10):4143-54.

81. Willett CG, Boucher Y, Di Tomaso E, Duda DG, Munn LL, Tong RT, Chung DC, Sahani DV, Kalva SP, Kozin SV, Mino M. Direct evidence that the VEGF-specific antibody bevacizumab has antivascular effects in human rectal cancer. Nature medicine. 2004 Feb;10(2):145-7.

82. Ferrara N, Hillan KJ, Gerber H-P, Novotny W. Discovery and development of bevacizumab, an anti-VEGF antibody for treating cancer. Nature Reviews Drug Discovery. 2004 May;3(5):391–400.

83. Sun D, Liu WJ, Guo K, Rusche JJ, Ebbinghaus S, Gokhale V, Hurley LH. The proximal promoter region of the human vascular endothelial growth factor gene has a G-quadruplex structure that can be targeted by G-quadruplex–interactive agents. Molecular cancer therapeutics. 2008 Apr 1;7(4):880-9.

84. Wheelhouse RT, Sun DK, Han HY, Han FXG, Hurley LH. Cationic porphyrins as telomerase inhibitors : the interaction of tetra-(N-methyl-4-pyridyl)porphine with quadruplex DNA. Journal of the American Chemical Society.1998 Apr;120(13):3261–2.

85. Lipps HJ, Rhodes D. G-quadruplex structures: in vivo evidence and function. Trends in Cell Biology. 2009 Aug 1;19(8):414–22.

86. Kang C, Zhang X, Ratliff R, Moyzis R, Rich A. Crystal structure of four-stranded Oxytricha telomeric DNA. Nature. 1992 Mar;356(6365):126–31.

87. Castor KJ, Liu Z, Fakhoury J, Hancock MA, Mittermaier A, Moitessier N, Sleiman HF. A Platinum (II) Phenylphenanthroimidazole with an Extended Side-Chain Exhibits Slow Dissociation from ac-Kit G-Quadruplex Motif. Chemistry–A European Journal. 2013 Dec 23;19(52):17836-45.

88. Adams JM, Cory S. The Bcl-2 Protein Family: Arbiters of Cell Survival. Science. 1998 Aug 28;281(5381):1322-6.

89. Young RL, Korsmeyer SJ. A negative regulatory element in the bcl-2 5'-untranslated region inhibits expression from an upstream promoter. Molecular and cellular biology. 1993 Jun 1;13(6):3686-97.

90. Dexheimer TS, Sun D, Hurley LH. Deconvoluting the Structural and Drug-Recognition Complexity of the G-Quadruplex-Forming Region Upstream of the bcl-2 P1 Promoter. Journal of the American Chemical Society. 2006 Apr 26;128(16):5404–15.

91. Dai J, Dexheimer TS, Chen D, Carver M, Ambrus A, Jones RA, Yang D. An intramolecular G-quadruplex structure with mixed parallel/antiparallel G-strands formed in the human BCL-2 promoter region in solution. Journal of the American Chemical Society. 2006 Feb 1;128(4):1096-8.

92. del Toro M, Bucek P, Aviñó A, Jaumot J, González C, Eritja R, Gargallo R. Targeting the G-quadruplex-forming region near the P1 promoter in the human BCL-2 gene with the cationic porphyrin TMPyP4 and with the complementary C-rich strand. Biochimie. 2009 Jul 1;91(7):894-902.

93. Douarre C, Gomez D, Morjani H, Zahm JM, O'Donohue MF, Eddabra L, Mailliet P, Riou JF, Trentesaux C. Overexpression of Bcl-2 is associated with apoptotic resistance to the G-quadruplex ligand 12459 but is not sufficient to confer resistance to long-term senescence. Nucleic acids research. 2005 Jan 1;33(7):2192-203.

94. Ramsay RG, Gonda TJ. MYB function in normal and cancer cells. Nature Reviews Cancer. 2008 Jul;8(7):523–34.

95. Klempnauer KH, Gonda TJ, Bishop JM. Nucleotide sequence of the retroviral leukemia gene v-myb and its cellular progenitor c-myb: the architecture of a transduced oncogene. Cell. 1982 Dec 1;31(2):453-63.

96. Greig KT, Carotta S, Nutt SL. Critical roles for c-Myb in hematopoietic progenitor cells. InSeminars in immunology 2008 Aug 1 (Vol. 20, No. 4, pp. 247-256). Academic Press.

97. Zuber J, Rappaport AR, Luo W, Wang E, Chen C, Vaseva AV, Shi J, Weissmueller S, Fellman C, Taylor MJ, Weissenboeck M. An integrated approach to dissecting oncogene addiction implicates a Myb-coordinated self-renewal program as essential for leukemia maintenance. Genes & development. 2011 Aug 1;25(15):1628-40.

98. Biroccio A, Benassi B, D'Agnano I, D'Angelo C, Buglioni S, Mottolese M, Ricciotti A, Citro G, Cosimelli M, Ramsay RG, Calabretta B. c-Myb and Bcl-x overexpression predicts poor prognosis in colorectal cancer: clinical and experimental findings. The American journal of pathology. 2001 Apr 1;158(4):1289-99.

99. Miao RY, Drabsch Y, Cross RS, Cheasley D, Carpinteri S, Pereira L, Malaterre J, Gonda TJ, Anderson RL, Ramsay RG. MYB is essential for mammary tumorigenesis. Cancer research. 2011 Nov 15;71(22):7029-37.

100. Persson M, Andrén Y, Moskaluk CA, Frierson Jr HF, Cooke SL, Futreal PA, Kling T, Nelander S, Nordkvist A, Persson F, Stenman G. Clinically significant copy number alterations and complex rearrangements of MYB and NFIB in head and neck adenoid cystic carcinoma. Genes, Chromosomes and Cancer. 2012 Aug;51(8):805-17.

101. Guerra J, Withers DA, Boxer LM. Myb binding sites mediate negative regulation of c-myb expression in T-cell lines.

102. McCann S, Sullivan J, Guerra J, Arcinas M, Boxer LM. Repression of the c-myb gene by WT1 protein in T and B cell lines. The Journal of biological chemistry 1995 Oct 6;270(40):23785—23789.

103. Perrotti D, Melotti P, Skorski T, Casella I, Peschle C, Calabretta B. Overexpression of the zinc finger protein MZF1 inhibits hematopoietic development from embryonic stem cells: correlation with negative regulation of CD34 and c-myb promoter activity. Molecular and Cellular Biology. 1995 Nov 1;15(11):6075-87.

104. Bellon T, Perrotti D, Calabretta B. Granulocytic Differentiation of Normal Hematopoietic Precursor Cells Induced by Transcription Factor PU.1 Correlates With Negative Regulation of the c-myb Promoter. Blood. 1997 Sep 1;90(5):1828–39.

105. Palumbo SL, Memmott RM, Uribe DJ, Krotova-Khan Y, Hurley LH, Ebbinghaus SW. A novel G-quadruplex-forming GGA repeat region in the c-myb promoter is a critical regulator of promoter activity. Nucleic acids research. 2008 Apr 1;36(6):1755–69.

106. Estus S, Zaks WJ, Freeman RS, Gruda M, Bravo R, Johnson EM. Altered gene expression in neurons during programmed cell death: identification of c-jun as necessary for neuronal apoptosis. The Journal of cell biology. 1994 Dec 15;127(6):1717-27.

107. Matsugami A, Ouhashi K, Kanagawa M, Liu H, Kanagawa S, Uesugi S, Katahira M. An intramolecular quadruplex of (GGA) 4 triplet repeat DNA with a G: G: G: G tetrad and a G (: A): G (: A): G (: A): G heptad, and its dimeric interaction. Journal of molecular biology. 2001 Oct 19;313(2):255-69.

108. Matsugami A, Okuizumi T, Uesugi S, Katahira M. Intramolecular higher order packing of parallel quadruplexes comprising a G:G:G:G tetrad and a G(:A):G(:A):G(:A):G heptad of GGA triplet repeat DNA. The Journal of biological chemistry. 2003 Jul 25;278(30):28147-53.

109. Drygin D, Siddiqui-Jain A, O'Brien S, Schwaebe M, Lin A, Bliesath J, Ho CB, Proffitt C, Trent K, Whitten JP, Lim JK. Anticancer activity of CX-3543: a direct inhibitor of rRNA biogenesis. Cancer research. 2009 Oct 1;69(19):7653-61.

110. Yang D, Okamoto K. Structural insights into G-quadruplexes: towards new anticancer drugs. Future medicinal chemistry. 2010 Apr;2(4):619–46.

111. Kelland LR. Overcoming the immortality of tumour cells by telomere and telomerase based cancer therapeutics – current status and future prospects. European journal of cancer. 2005 May 1;41(7):971–9.

112. Perry PJ, Reszka AP, Wood AA, Read MA, Gowan SM, Dosanjh HS, Trent JO, Jenkins TC, Kelland LR, Neidle S. Human telomerase inhibition by regioisomeric disubstituted amidoanthracene-9, 10-diones. Journal of medicinal chemistry. 1998 Nov 19;41(24):4873-84.

113. Read MA, Wood AA, Harrison JR, Gowan SM, Kelland LR, Dosanjh HS, Neidle S. Molecular modeling studies on G-quadruplex complexes of telomerase inhibitors: structure− activity relationships. Journal of medicinal chemistry. 1999 Nov 4;42(22):4538-46.

114. Harrison RJ, Gowan SM, Kelland LR, Neidle S. Human telomerase inhibition by substituted acridine derivatives. Bioorganic & medicinal chemistry letters. 1999 Sep 6;9(17):2463-8.

115. Read M, Harrison RJ, Romagnoli B, Tanious FA, Gowan SH, Reszka AP, Wilson WD, Kelland LR, Neidle S. Structure-based design of selective and potent G quadruplex-mediated telomerase inhibitors. Proceedings of the National Academy of Sciences. 2001 Apr 24;98(9):4844-9.

116. Harrison RJ, Cuesta J, Chessari G, Read MA, Basra SK, Reszka AP, Morrell J, Gowan SM, Incles CM, Tanious FA, Wilson WD. Trisubstituted acridine derivatives as potent and selective telomerase inhibitors. Journal of medicinal chemistry. 2003 Oct 9;46(21):4463-76.

117. Parkinson GN, Ghosh R, Neidle S. Structural basis for binding of porphyrin to human telomeres. Biochemistry. 2007 Mar 6;46(9):2390-7.

118. Ou TM, Lu YJ, Tan JH, Huang ZS, Wong KY, Gu LQ. G-quadruplexes: targets in anticancer drug design. ChemMedChem: Chemistry Enabling Drug Discovery. 2008 May 19;3(5):690-713.

119. Han FX, Wheelhouse RT, Hurley LH. Interactions of TMPyP4 and TMPyP2 with quadruplex DNA. Structural basis for the differential effects on telomerase inhibition. Journal of the American Chemical Society. 1999 Apr 21;121(15):3561-70.

120. Wheelhouse RT, Sun DK, Han HY, Han FXG, Hurley LH. Cationic porphyrins as telomerase inhibitors : the interaction of tetra-(N-methyl-4-pyridyl)porphine with quadruplex DNA. Journal of the American Chemical Society. 1998 Apr 8;120(13):3261–2.

121. Izbicka E, Wheelhouse RT, Raymond E, Davidson KK, Lawrence RA, Sun D, Windle BE, Hurley LH, Von Hoff DD. Effects of cationic porphyrins as G-quadruplex interactive agents in human tumor cells. Cancer research. 1999 Feb 1;59(3):639-44.

122. Grand CL, Han H, Muñoz RM, Weitman S, Von Hoff DD, Hurley LH, Bearss DJ. The Cationic Porphyrin TMPyP4 Down-Regulates c-MYC and Human Telomerase Reverse Transcriptase Expression and Inhibits Tumor Growth in Vivo 1 This research was supported by grants from the NIH and the Arizona Disease Control Research Commission. 1. Molecular cancer therapeutics. 2002 Jun 1;1(8):565-73.

123. Samudrala R, Zhang X, Wadkins RM, Mattern DL. Synthesis of a non-cationic, water-soluble perylenetetracarboxylic diimide and its interactions with G-quadruplex-forming DNA. Bioorganic & Medicinal Chemistry. 2007 Jan 1;15(1):186–93.

124. Parrotta L, Ortuso F, Moraca F, Rocca R, Costa G, Alcaro S, Artese A. Targeting unimolecular G-quadruplex nucleic acids: a new paradigm for the drug discovery?. Expert opinion on drug discovery. 2014 Oct 1;9(10):1167-87.

125. Fedoroff OY, Salazar M, Han H, Chemeris VV, Kerwin SM, Hurley LH. NMR-based model of a telomerase-inhibiting compound bound to G-quadruplex DNA. Biochemistry. 1998 Sep 8;37(36):12367-74.

126. Taka T, Huang L, Wongnoppavich A, Tam-Chang S-W, Lee TR, Tuntiwechapikul W. Telomere shortening, and cell senescence induced by perylene derivatives in A549 human lung cancer cells. Bioorganic & Medicinal Chemistry. 2013 Feb 15;21(4):883–90.

127. Sissi C, Lucatello L, Krapcho AP, Maloney DJ, Boxer MB, Camarasa MV, Pezzoni G, Menta E, Palumbo M. Tri-, tetra-and heptacyclic perylene analogues as new potential antineoplastic agents based on DNA telomerase inhibition. Bioorganic & Medicinal Chemistry. 2007 Jan 1;15(1):555-62.

128. Cuenca F, Greciano O, Gunaratnam M, Haider S, Munnur D, Nanjunda R, Wilson WD, Neidle S. Tri-and tetra-substituted naphthalene diimides as potent G-quadruplex ligands. Bioorganic & medicinal chemistry letters. 2008 Mar 1;18(5):1668-73.

129. Doria F, Richter SN, Nadai M, Colloredo-Mels S, Mella M, Palumbo M, Freccero M. BINOL− Amino Acid Conjugates as Triggerable Carriers of DNA-Targeted Potent Photocytotoxic Agents. Journal of medicinal chemistry. 2007 Dec 27;50(26):6570-9.

130. Richter SN, Maggi S, Mels SC, Palumbo M, Freccero M. Binol quinone methides as bisalkylating and DNA cross-linking agents. Journal of the American Chemical Society. 2004 Nov 3;126(43):13973-9.

131. Di Antonio M, Doria F, Richter SN, Bertipaglia C, Mella M, Sissi C, Palumbo M, Freccero M. Quinone methides tethered to naphthalene diimides as selective G-quadruplex alkylating agents. Journal of the American Chemical Society. 2009 Sep 16;131(36):13132-41.

132. Doria F, Nadai M, Folini M, Di Antonio M, Germani L, Percivalle C, Sissi C, Zaffaroni N, Alcaro S, Artese A, Richter SN. Hybrid ligand–alkylating agents targeting telomeric G-quadruplex structures. Organic & biomolecular chemistry. 2012;10(14):2798-806.

133. Doria F, Nadai M, Folini M, Scalabrin M, Germani L, Sattin G, Mella M, Palumbo M, Zaffaroni N, Fabris D, Freccero M. Targeting loop adenines in G-quadruplex by a selective oxirane. Chemistry (Weinheim an der Bergstrasse, Germany). 2013 Jan 2;19(1).

134. Nadai M, Doria F, Di Antonio M, Sattin G, Germani L, Percivalle C, Palumbo M, Richter SN, Freccero M. Naphthalene diimide scaffolds with dual reversible and covalent interaction properties towards G-quadruplex. Biochimie. 2011 Aug 1;93(8):1328-40.

135. Collie GW, Promontorio R, Hampel SM, Micco M, Neidle S, Parkinson GN. Structural basis for telomeric G-quadruplex targeting by naphthalene diimide ligands. Journal of the American Chemical Society. 2012 Feb 8;134(5):2723-31.

136. Micco M, Collie GW, Dale AG, Ohnmacht SA, Pazitna I, Gunaratnam M, Reszka AP, Neidle S. Structure-based design and evaluation of naphthalene diimide G-quadruplex ligands as telomere targeting agents in pancreatic cancer cells. Journal of medicinal chemistry. 2013 Apr 11;56(7):2959-74.

137. Marchetti C, Zyner KG, Ohnmacht SA, Robson M, Haider SM, Morton JP, Marsico G, Vo T, Laughlin-Toth S, Ahmed AA, Di Vita G. Targeting multiple effector pathways in pancreatic ductal adenocarcinoma with a G-quadruplex-binding small molecule. Journal of medicinal chemistry. 2018 Jan 22;61(6):2500-17.

138. Tanious FA, Jenkins TC, Neidle S, Wilson WD. Substituent position dictates the intercalative DNA-binding mode for anthracene-9,10-dione antitumor drugs. Biochemistry. 1992 Nov 1;31(46):11632–40.

139. Weisman-Shomer P, Cohen E, Hershco I, Khateb S, Wolfovitz-Barchad O, Hurley LH, Fry M. The cationic porphyrin TMPyP4 destabilizes the tetraplex form of the fragile X syndrome expanded sequence d (CGG) n. Nucleic acids research. 2003 Jul 15;31(14):3963-70.

140. Morris MJ, Wingate KL, Silwal J, Leeper TC, Basu S. The porphyrin TmPyP4 unfolds the extremely stable G-quadruplex in MT3-MMP mRNA and alleviates its repressive effect to enhance translation in eukaryotic cells. Nucleic Acids Research. 2012 May 1;40(9):4137–45.

141. Waller ZA, Sewitz SA, Hsu ST, Balasubramanian S. A small molecule that disrupts G-quadruplex DNA structure and enhances gene expression. Journal of the American Chemical Society. 2009 Sep 9;131(35):12628-33.

142. Waller ZAE, Shirude PS, Rodriguez R, Balasubramanian S. Triarylpyridines: a versatile small molecule scaffold for G-quadruplex recognition. Chemical communications (Cambridge, England). 2008(12):1467-9.

143. Ilyinsky NS, Varizhuk AM, Beniaminov AD, Puzanov MA, Shchyolkina AK, Kaluzhny DN. G-quadruplex ligands: Mechanisms of anticancer action and target binding. Molecular Biology. 2014 Nov 1;48(6):778–94.

144. O'Hagan M, Peñalver P, Fisher R, Morales JC, Galan MC. Stiff-Stilbene Ligands Target G-Quadruplex DNA and Exhibit Selective Anticancer and Antiparasitic Activity. Chemistry–A European Journal. 2020 Feb 6.

145. Métifiot M, Amrane S, Litvak S, Andreola ML. G-quadruplexes in viruses: function and potential therapeutic applications. Nucleic Acids Research. 2014 Nov 10;42(20):12352–66.

146. Artusi S, Nadai M, Perrone R, Biasolo MA, Palu G, Flamand L, Calistri A, Richter SN. The Herpes Simplex Virus-1 genome contains multiple clusters of repeated G-quadruplex:

Implications for the antiviral activity of a G-quadruplex ligand. Antiviral research. 2015 Jun 1;118:123-31.

147. Perrone R, Butovskaya E, Daelemans D, Palu G, Pannecouque C, Richter SN. Anti-HIV-1 activity of the G-quadruplex ligand BRACO-19. Journal of Antimicrobial Chemotherapy. 2014 Dec 1;69(12):3248-58.

148. Shum KT, Zhou J, Rossi JJ. Aptamer-based therapeutics: new approaches to combat human viral diseases. Pharmaceuticals. 2013 Dec;6(12):1507-42.

149. Jing N. Developing G-quartet oligonucleotides as novel anti-HIV agents: focus on anti-HIV drug design. Expert Opinion on Investigational Drugs. 2000 Aug 1;9(8):1777–85.

150. Held DM, Kissel JD, Patterson JT, Nickens DG, Burke DH. HIV-1 inactivation by nucleic acid aptamers. Front Biosci. 2006 Jan 1;11:89-112.

151. Tluckova K, Marusic M, Tothova P, Bauer L, Šket P, Plavec J, Viglasky V. Human papillomavirus G-quadruplexes. Biochemistry. 2013 Oct 15;52(41):7207-16.

152. Topalis D, Andrei G, Snoeck R. The large tumor antigen: A “Swiss Army knife” protein possessing the functions required for the polyomavirus life cycle. Antiviral Research. 2013 Feb 1;97(2):122–36.

153. Perrone R, Nadai M, Frasson I, Poe JA, Butovskaya E, Smithgall TE, Palumbo M, Palù G, Richter SN. A dynamic G-quadruplex region regulates the HIV-1 long terminal repeat promoter. Journal of medicinal chemistry. 2013 Aug 22;56(16):6521-30.

154. Perrone R, Nadai M, Poe JA, Frasson I, Palumbo M, Palu G, Smithgall TE, Richter SN. Formation of a unique cluster of G-quadruplex structures in the HIV-1 Nef coding region: implications for antiviral activity. PloS one. 2013 Aug 27;8(8):e73121.

155. Piekna-Przybylska D, Sharma G, Maggirwar SB, Bambara RA. Deficiency in DNA damage response, a new characteristic of cells infected with latent HIV-1. Cell Cycle. 2017 May 19;16(10):968–78.

156. Norseen J, Johnson FB, Lieberman PM. Role for G-quadruplex RNA binding by Epstein-Barr virus nuclear antigen 1 in DNA replication and metaphase chromosome attachment. Journal of virology. 2009 Oct 15;83(20):10336-46.

157. Gilbert-Girard S, Gravel A, Artusi S, Richter SN, Wallaschek N, Kaufer BB, Flamand L. Stabilization of telomere G-quadruplexes interferes with human herpesvirus 6A chromosomal integration. Journal of virology. 2017 Jul 15;91(14).

158. Taetz S, Baldes C, Mürdter TE, Kleideiter E, Piotrowska K, Bock U, Haltner-Ukomadu E, Mueller J, Huwer H, Schaefer UF, Klotz U. Biopharmaceutical characterization of the telomerase inhibitor BRACO19. Pharmaceutical research. 2006 May 1;23(5):1031-7.

159. Biswas B, Kandpal M, Vivekanandan P. A G-quadruplex motif in an envelope gene promoter regulates transcription and virion secretion in HBV genotype B. Nucleic Acids Research. 2017 Nov 2;45(19):11268–80.

160. Wang SR, Min YQ, Wang JQ, Liu CX, Fu BS, Wu F, Wu LY, Qiao ZX, Song YY, Xu GH, Wu ZG. A highly conserved G-rich consensus sequence in hepatitis C virus core gene represents a new anti–hepatitis C target. Science advances. 2016 Apr 1;2(4):e1501535.

161. Dicenzo GC, Benedict AB, Fondi M, Walker GC, Finan TM, Mengoni A, Griffitts JS. Robustness encoded across essential and accessory replicons of the ecologically versatile bacterium Sinorhizobium meliloti. PLoS genetics. 2018 Apr 19;14(4):e1007357.

162. Yadav VK, Abraham JK, Mani P, Kulshrestha R, Chowdhury S. QuadBase: genome-wide database of G4 DNA—occurrence and conservation in human, chimpanzee, mouse and rat promoters and 146 microbes. Nucleic acids research. 2007 Oct 25;36(suppl_1):D381-5.

163. König SLB, Huppert JL, Sigel RKO, Evans AC. Distance-dependent duplex DNA destabilization proximal to G-quadruplex/ i -motif sequences. Nucleic Acids Research. 2013 Aug 1;41(15):7453–61.

164. Mishra SK, Jain N, Shankar U, Tawani A, Sharma TK, Kumar A. Characterization of highly conserved G-quadruplex motifs as potential drug targets in Streptococcus pneumoniae. Scientific Reports. 2019 Feb 11;9(1):1-3.

165. Rawal P, Kummarasetti VB, Ravindran J, Kumar N, Halder K, Sharma R, Mukerji M, Das SK, Chowdhury S. Genome-wide prediction of G4 DNA as regulatory motifs: role in Escherichia coli global regulation. Genome research. 2006 May 1;16(5):644-55.

166. Saranathan N, Vivekanandan P. G-quadruplexes: more than just a kink in microbial genomes. Trends in microbiology. 2019 Feb 1;27(2):148-63.

167. Neidle S. The structures of quadruplex nucleic acids and their drug complexes. Current opinion in structural biology. 2009 Jun 1;19(3):239-50.

168. Kaplan OI, Berber B, Hekim N, Doluca O. G-quadruplex prediction in E. coli genome reveals a conserved putative G-quadruplex-Hairpin-Duplex switch. Nucleic Acids Research. 2016 Nov 2;44(19):9083–95.

169. Brocchieri L. The GC content of bacterial genomes. Journal of Phylogenetics & Evolutionary Biology. 2013 Apr 10:1-3.

170. Ding Y, Fleming AM, Burrows CJ. Case studies on potential G-quadruplex-forming sequences from the bacterial orders Deinococcales and Thermales derived from a survey of published genomes. Scientific Reports. 2018;8(1):15679.

171. Brumm PJ, Monsma S, Keough B, Jasinovica S, Ferguson E, Schoenfeld T, Lodes M, Mead DA. Complete genome sequence of thermus aquaticus Y51MC23. PloS one. 2015 Oct 14;10(10):e0138674.

172. Waller ZA, Pinchbeck BJ, Buguth BS, Meadows TG, Richardson DJ, Gates AJ. Control of bacterial nitrate assimilation by stabilization of G-quadruplex DNA. Chemical Communications. 2016;52(92):13511-4.

173. Bedrat A, Lacroix L, Mergny JL. Re-evaluation of G-quadruplex propensity with G4Hunter. Nucleic acids research. 2016 Feb 29;44(4):1746-59.

174. Čechová J, Lýsek J, Bartas M, Brázda V. Complex analyses of inverted repeats in mitochondrial genomes revealed their importance and variability. Bioinformatics. 2018 Apr 1;34(7):1081–5.

175. Brázda V, Kolomazník J, Lýsek J, Hároníková L, Coufal J, Št'astný J. Palindrome analyser–A new web-based server for predicting and evaluating inverted repeats in nucleotide sequences. Biochemical and biophysical research communications. 2016 Sep 30;478(4):1739-45.

176. Brázda V, Lýsek J, Bartas M, Fojta M. Complex analyses of short inverted repeats in all sequenced chloroplast DNAs. BioMed research international. 2018 Jul 24;2018.

177. Huang HS, Chen IB, Huang KF, Lu WC, Shieh FY, Huang YY, Huang FC, Lin JJ. Synthesis and human telomerase inhibition of a series of regioisomeric disubstituted amidoanthraquinones. Chemical and pharmaceutical bulletin. 2007;55(2):284-92.

178. Harrison RJ, Gowan SM, Kelland LR, Neidle S. Human telomerase inhibition by substituted acridine derivatives. Bioorganic & Medicinal Chemistry Letters. 1999 Sep;9(17):2463–8.

179. Seenisamy J, Bashyam S, Gokhale V, Vankayalapati H, Sun D, Siddiqui-Jain A, Streiner N, Shin-ya K, White E, Wilson WD, Hurley LH. Design and synthesis of an expanded porphyrin that has selectivity for the c-MYC G-quadruplex structure. Journal of the American Chemical Society. 2005 Mar 9;127(9):2944-59.

180. Gowan SM, Harrison JR, Patterson L, Valenti M, Neidle S, Kelland LR. A G-quadruplex-interactive potent small-molecule inhibitor of telomerase exhibiting in vitro and in vivo antitumor activity. Molecular pharmacology. 2002 May 1;61(5):1154-62.

181. Redman JE, Granadino-Roldan JM, Schouten JA, Ladame S, Reszka AP, Neidle S, Balasubramanian S. Recognition and discrimination of DNA quadruplexes by acridine-peptide conjugates. Organic & biomolecular chemistry. 2009;7(1):76-84.

182. Franceschin M. G-Quadruplex DNA Structures and Organic Chemistry: More Than One Connection. European Journal of Organic Chemistry. 2009 May;2009(14):2225–38.

183. Naasani I, Seimiya H, Yamori T, Tsuruo T. FJ5002: A Potent Telomerase Inhibitor Identified by Exploiting the Disease-oriented Screening Program with COMPARE Analysis. Cancer Research. 1999 Aug 15;59(16):4004.

184. Kim MY, Vankayalapati H, Shin-Ya K, Wierzba K, Hurley LH. Telomestatin, a potent telomerase inhibitor that interacts quite specifically with the human telomeric intramolecular G-quadruplex. Journal of the American Chemical Society. 2002 Mar 13;124(10):2098-9.

185. Shin-ya K, Wierzba K, Matsuo KI, Ohtani T, Yamada Y, Furihata K, Hayakawa Y, Seto H. Telomestatin, a novel telomerase inhibitor from Streptomyces anulatus. Journal of the American Chemical Society. 2001 Feb 14;123(6):1262-3.

186. Doi T, Yoshida M, Shin-ya K, Takahashi T. Total Synthesis of (R)-Telomestatin. Organic Letters. 2006 Aug 31;8(18):4165-7.

187. Binz N, Shalaby T, Rivera P, Shin-Ya K, Grotzer MA. Telomerase inhibition, telomere shortening, cell growth suppression and induction of apoptosis by telomestatin in childhood neuroblastoma cells. European journal of cancer. 2005 Dec 1;41(18):2873-81.

188. Tauchi T, Shin-Ya K, Sashida G, Sumi M, Okabe S, Ohyashiki JH, Ohyashiki K. Telomerase inhibition with a novel G-quadruplex-interactive agent, telomestatin: in vitro and in vivo studies in acute leukemia. Oncogene. 2006 Sep;25(42):5719-25.

189. Shammas MA, Reis RJ, Li C, Koley H, Hurley LH, Anderson KC, Munshi NC. Telomerase inhibition and cell growth arrest after telomestatin treatment in multiple myeloma. Clinical Cancer Research. 2004 Jan 15;10(2):770-6.

190. Franceschin M, Rossetti L, D'Ambrosio A, Schirripa S, Bianco A, Ortaggi G, Savino M, Schultes C, Neidle S. Natural and synthetic G-quadruplex interactive berberine derivatives. Bioorganic & Medicinal Chemistry Letters. 2006 Mar 15;16(6):1707-11.

191. Liu ZR, Rill RL. N, N'-bis [3, 3'-(dimethylamino) propylamine]-3, 4, 9, 10-perylenetetracarboxylic diimide, a dicationic perylene dye for rapid precipitation and quantitation of trace amounts of DNA. Analytical biochemistry. 1996 Apr 5;236(1):139-45.

192. Whitten JP, Pierre F, Regan C, Schwaebe M, Yiannikouros GP, Jung M, inventors; Cylene Pharmaceuticals Inc, assignee. Methods for converting quinolone esters into quinolone amides. United States patent US 7,652,134. 2010 Jan 26.

193. Le Gresley A, Abdullah A, Chawla D, Desai P, Ghosh U, Gollapalli U, Kiran M, Lafon S, Sinclair A. Diacrylamides as selective G-quadruplex ligands in in vitro and in vivo assays. MedChemComm. 2011;2(6):466-70.

194. Whitcombe NJ, Hii KK, Gibson SE. Advances in the Heck chemistry of aryl bromides and chlorides. Tetrahedron. 2001;35(57):7449-76.

195. Bhanage BM, Fujita SI, Arai M. Heck reactions with various types of palladium complex catalysts: application of multiphase catalysis and supercritical carbon dioxide. Journal of organometallic chemistry. 2003 Dec 7;687(2):211-8.

196. Seenisamy J, Rezler EM, Powell TJ, Tye D, Gokhale V, Joshi CS, Siddiqui-Jain A, Hurley LH. The dynamic character of the G-quadruplex element in the c-MYC promoter and modification by TMPyP4. Journal of the American Chemical Society. 2004 Jul 21;126(28):8702-9.

197. Phan AT, Modi YS, Patel DJ. Propeller-type parallel-stranded G-quadruplexes in the human c-myc promoter. Journal of the American Chemical Society. 2004 Jul 21;126(28):8710-6.

198. Kelly JA, Feigon J, Yeates TO. Reconciliation of the X-ray and NMR structures of the thrombin-binding aptamer d (GGTTGGTGTGGTTGG).

199. Đapić V, Abdomerović V, Marrington R, Peberdy J, Rodger A, Trent JO, Bates PJ. Biophysical and biological properties of quadruplex oligodeoxyribonucleotides. Nucleic acids research. 2003 Apr 15;31(8):2097-107.

200. Xu Y, Noguchi Y, Sugiyama H. The new models of the human telomere d [AGGG (TTAGGG) 3] in K+ solution. Bioorganic & medicinal chemistry. 2006 Aug 15;14(16):5584-91.

201. Mergny JL, Phan AT, Lacroix L. Following G-quartet formation by UV-spectroscopy. FEBS Letters. 1998 Sep 11;435(1):74–8.

202. Balagurumoorthy P, Brahmachari SK. Structure and stability of human telomeric sequence. Journal of Biological Chemistry. 1994 Aug 26;269(34):21858-69.

203. Li W, Wu P, Ohmichi T, Sugimoto N. Characterization and thermodynamic properties of quadruplex/duplex competition. FEBS letters. 2002 Aug 28;526(1-3):77-81.

204. Scaglioni L, Mondelli R, Artali R, Sirtori FR, Mazzini S. Nemorubicin and doxorubicin bind the G-quadruplex sequences of the human telomeres and of the c-MYC promoter element Pu22. Biochimica et Biophysica Acta (BBA)-General Subjects. 2016 Jun 1;1860(6):1129-38.

205. Jin RZ, Breslauer KJ, Jones RA, Gaffney BL. Tetraplex formation of a guanine-containing nonameric DNA fragment. Science. 1990 Oct 26;250(4980):543-6.

206. Wang Y, de los Santos C, Gao X, Greene K, Live D, Patel DJ. Multinuclear nuclear magnetic resonance studies of Na cation-stabilized complex formed by d(G-G-T-T-T-T-C-G-G) in solution: Implications for G-tetrad structures. Journal of Molecular Biology. 1991 Dec 5;222(3):819–32.

207. Sundquist WI, Klug A. Telomeric DNA dimerizes by formation of guanine tetrads between hairpin loops. nature. 1989 Dec;342(6251):825–9.

208. Williamson JR, Raghuraman MK, Cech TR. Monovalent cation-induced structure of telomeric DNA: The G-quartet model. Cell. 1989 Dec 1;59(5):871–80.

209. Hardin CC, Henderson E, Watson T, Prosser JK. Monovalent cation induced structural transitions in telomeric DNAs: G-DNA folding intermediates. Biochemistry. 1991 May 1;30(18):4460–72

210. Smith FW, Feigon J. Quadruplex structure of Oxytricha telomeric DNA oligonucleotides. nature. 1992 Mar;356(6365):164–8.

211. Smith FW, Feigon J. Strand orientation in the DNA quadruplex formed from the Oxytricha telomere repeat oligonucleotide d (G4T4G4) in solution. Biochemistry. 1993 Aug 1;32(33):8682-92.

212. Kim J, Cheong C, Moore PB. Tetramerization of an RNA oligonucleotide containing a GGGG sequence. Nature. 1991 May;351(6324):331–2.

213. Neidle S, Read MA. G-quadruplexes as therapeutic targets. Biopolymers: Original Research on Biomolecules. 2000;56(3):195-208.

214. Reed J, Gunaratnam M, Beltran M, Reszka AP, Vilar R, Neidle S. TRAP–LIG, a modified telomere repeat amplification protocol assay to quantitate telomerase inhibition by small molecules. Analytical biochemistry. 2008 Sep 1;380(1):99-105.

215. Corbett PT, Leclaire J, Vial L, West KR, Wietor JL, Sanders JK, Otto S. Dynamic combinatorial chemistry. Chemical reviews. 2006 Sep 13;106(9):3652-711.

216. Lin C, Dickerhoff J, Yang D. NMR studies of G-quadruplex structures and G-quadruplex-interactive compounds. InG-Quadruplex Nucleic Acids 2019 (pp. 157-176). Humana, New York, NY.

217. Zhou Q, Li L, Xiang J, Tang Y, Zhang H, Yang S, Li Q, Yang Q, Xu G. Screening Potential Antitumor Agents from Natural Plant Extracts by G-Quadruplex Recognition and NMR Methods. Angewandte Chemie International Edition. 2008 Jul 14;47(30):5590-2.

218. Damião MC, Pasqualoto KF, Ferreira AK, Teixeira SF, Azevedo RA, Barbuto JA, Palace-Berl F, Franchi-Junior GC, Nowill AE, Tavares MT, Parise-Filho R. Novel capsaicin analogues as potential anticancer agents: synthesis, biological evaluation, and in silico approach. Archiv der Pharmazie. 2014 Dec;347(12):885-95.

219. Nikolova EN, Kim E, Wise AA, O'Brien PJ, Andricioaei I, Al-Hashimi HM. Transient Hoogsteen base pairs in canonical duplex DNA. Nature. 2011 Feb;470(7335):498-502.

220. Del Rosso PG, Almassio MF, Bruno M, Garay RO. Mild persubstitution of di-and tetrabrominated arenes with arylthiolate nucleophiles. Tetrahedron Letters. 2010 Dec 22;51(51):6730-3.

221. Singh M, Argade NP. Synthetic Studies towards NG-121: Diastereoselective synthesis of NG-121 methyl ether. Synthesis. 2012 Dec;44(24):3797-804.

222. Bunin BA. The combinatorial index. Elsevier; 1998 Apr 15.

223. Boncler M, Różalski M, Krajewska U, Podsędek A, Watala C. Comparison of PrestoBlue and MTT assays of cellular viability in the assessment of anti-proliferative effects of plant extracts on human endothelial cells. Journal of pharmacological and toxicological methods. 2014 Jan 1;69(1):9-16.

224. Aboul-ela F, Murchie AI, Norman DG, Lilley DM. Solution structure of a parallel-stranded tetraplex formed by d (TG4T) in the presence of sodium ions by nuclear magnetic resonance spectroscopy. Journal of molecular biology. 1994 Oct 27;243(3):458-71.

225. Moyzis RK, Buckingham JM, Cram LS, Dani M, Deaven LL, Jones MD, Meyne J, Ratliff RL, Wu JR. A highly conserved repetitive DNA sequence,(TTAGGG) n, present at the telomeres of human chromosomes. Proceedings of the National Academy of Sciences. 1988 Sep 1;85(18):6622-6.

226. Bulatov TM, Pugachev MV, Shtyrlin NV, Shtyrlin YG. Novel approach to 6-alkenyl-substituted pyridoxine derivatives based on the Heck reaction. Tetrahedron Letters. 2018 Aug 15;59(33):3220-2.

227. Chandra BP, Wu Z, Ntim SA, Rao GN, Mitra S. The effect of functional group polarity in palladium immobilized multiwalled carbon nanotube catalysis: Application in carbon–carbon coupling reaction. Applied Sciences. 2018 Sep;8(9):1511.

228. Smalley AP, Gaunt MJ. Mechanistic insights into the palladium-catalyzed aziridination of aliphatic amines by C–H activation. Journal of the American Chemical Society. 2015 Aug 26;137(33):10632-41.

229. Carpino LA, Imazumi H, Foxman BM, Vela MJ, Henklein P, El-Faham A, Klose J, Bienert M. Comparison of the Effects of 5-and 6-HOAt on Model Peptide Coupling Reactions Relative to the Cases for the 4-and 7-Isomers. Organic letters. 2000 Jul 27;2(15):2253-6.

230. Islam MS, Nahra F, Tzouras NV, Barakat A, Cazin CS, Nolan SP, Al-Majid AM. Mizoroki–Heck Cross-Coupling of Acrylate Derivatives with Aryl Halides Catalyzed by Palladate Pre-Catalysts. European Journal of Inorganic Chemistry. 2019 Nov 24;2019(43):4695-9.

231. Zhao M, Ou S, Wu CD. Improvement of the CO2 capture capability of a metal–organic framework by encapsulating dye molecules inside the mesopore space. Crystal Growth & Design. 2017 May 3;17(5):2688-93.

232. Leiro V, Parreira P, Freitas SC, Martins MC, Pêgo AP. Conjugation Chemistry Principles and Surface Functionalization of Nanomaterials. InBiomedical Applications of Functionalized Nanomaterials 2018 Jan 1 (pp. 35-66). Elsevier.

233. Das S, da Silva CJ, Silva MD, Dantas MD, de Fátima Â, Ruiz AL, da Silva CM, de Carvalho JE, Santos JC, Figueiredo IM, da Silva-Júnior EF. Highly functionalized piperidines: Free radical scavenging, anticancer activity, DNA interaction and correlation with biological activity. Journal of advanced research. 2018 Jan 1;9:51-61.

234. Ou A, Guédin A, Skelton BW, Amrane S, Evans CW, Norret M, Iyer KS, Mergny JL, Smith NM. Multicarbazole scaffolds for selective G-quadruplex binding. Chemical Communications. 2018;54(69):9647-50.

235. Nichols WK, Mehta R, Skordos K, Macé K, Pfeifer AM, Carr BA, Minko T, Burchiel SW, Yost GS. 3-methylindole-induced toxicity to human bronchial epithelial cell lines. Toxicological Sciences. 2003 Feb 1;71(2):229-36.

236. Rajanarendar E, Reddy KG, Ramakrishna S, Reddy MN, Shireesha B, Durgaiah G, Reddy YN. Synthesis and in vitro and in vivo anticancer activity of novel 3-methyl-5H-isoxazolo [5′, 4′: 5, 6] pyrido [2, 3-b] indoles. Bioorganic & medicinal chemistry letters. 2012 Nov 1;22(21):6677-80.

237. Gupta SD, Rao GB, Bommaka MK, Raghavendra NM, Aleti S. Eco-sustainable synthesis and biological evaluation of 2-phenyl 1, 3-benzodioxole derivatives as anticancer, DNA binding and antibacterial agents. Arabian Journal of Chemistry. 2016 Nov 1;9:S1875-83.

238. Baginski M, Serbakowska K. In silico design of telomerase inhibitors. Drug Discovery Today. 2020 May 6.

239. Nygren J, Svanvik N, Kubista M. The interactions between the fluorescent dye thiazole orange and DNA. Biopolymers: Original Research on Biomolecules. 1998 Jul;46(1):39-51.

240. Lubitz I, Zikich D, Kotlyar A. Specific high-affinity binding of thiazole orange to triplex and G-quadruplex DNA. Biochemistry. 2010 May 4;49(17):3567-74.

241. Ou Z, Li Z, Gao Y, Xing W, Jia H, Zhang H, Yi N. Novel triazole and morpholine substituted bisnaphthalimide: Synthesis, photophysical and G-quadruplex binding properties. Journal of Molecular Structure. 2019 Jun 5;1185:27-37.

242. Whitney AM, Ladame S, Balasubramanian S. Templated ligand assembly by using G-quadruplex DNA and dynamic covalent chemistry. Angewandte Chemie International Edition. 2004 Feb 20;43(9):1143-6.

243. Mazzitelli CL, Wang J, Smith SI, Brodbelt JS. Gas-phase stability of G-quadruplex DNA determined by electrospray ionization tandem mass spectrometry and molecular dynamics simulations. Journal of the American Society for Mass Spectrometry. 2007 Oct 1;18(10):1760-73.

244. Banfi D, Patiny L. www. nmrdb. org: Resurrecting and processing NMR spectra on-line. Chimia International Journal for Chemistry. 2008 Apr 30;62(4):280-1.

245. Harner MJ, Frank AO, Fesik SW. Fragment-based drug discovery using NMR spectroscopy. Journal of Biomolecular NMR. 2013 Jun 1;56(2):65-75.

246. Lepre CA. Practical aspects of NMR-based fragment screening. In Methods in Enzymology 2011 Jan 1 (Vol. 493, pp. 219-239). Academic Press.

247. Castillo AM, Patiny L, Wist J. Fast and accurate algorithm for the simulation of NMR spectra of large spin systems. Journal of Magnetic Resonance. 2011 Apr 1;209(2):123-30.

248. Aires-de-Sousa J, Hemmer MC, Gasteiger J. Prediction of 1H NMR chemical shifts using neural networks. Analytical Chemistry. 2002 Jan 1;74(1):80-90.